GEORGIA INSTITUTE OF TECHNOLOGY — OFFICE OF CONTRACT ADMINISTRATION

PROJECT ADMINISTRATION DATA SHEET

[x] ORIGINAL [ ] REVISION NO. _____

Project No. E-26-B03 (cont. of E-26-B02) DATE 4/28/82

Project Director: J. M. Kallfelz School/~~Lab~~: Nuclear Eng.

Sponsor: Union Carbide Corp., Nuclear Div., Oak Ridge, TN

Type Agreement: Proj. Auth. X01 under Basic Agmt. 7802, S.A. No. 4 (Prime D.O.E.)

Award Period: From 3/15/82 To ~~9/30/82~~ 6/30/83 9/30/83 (Performance) _____ (Reports)

Sponsor Amount: $10,227* Contracted through:

Cost Sharing: None GTRI/~~GIT~~

Title: Analytic Reactor Physics and Design Investigations

ADMINISTRATIVE DATA OCA Contact William F. Brown x4820

1) Sponsor Technical Contact:

Dr. F. C. Maienschein, Director
Engineering Physics Division
Oak Ridge National Laboratory
P. O. Box X
Oak Ridge, TN

2) Sponsor Admin/Contractual Matters:

Ms. I. K. Gentry
Union Carbide Corp.
Purchasing Div.
P. O. Box M
Oak Ridge, TN 37830
(615) 576-1448

Defense Priority Rating: NA Security Classification: NA

RESTRICTIONS

See Attached _____ Supplemental Information Sheet for Additional Requirements.

Travel: Foreign travel must have prior approval — Contact OCA in each case. Domestic travel requires sponsor approval where total will exceed greater of $500 or 125% of approved proposal budget category.

Equipment: Title vests with None proposed or anticipated

COMMENTS:

Supplemental Agreement No. 4 adds $10,227 for additional three months effort through 9/30/82.

*Revised total amount of subcontract (including previous project numbers) is $222,951.

New project number assigned because of change in overhead base.

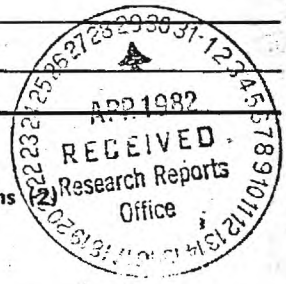

COPIES TO: RAN

~~Administrative Coordinator~~
Research Property Management
Accounting
Procurement/EES Supply Services

Research ~~Security~~ Services
Reports Coordinator (OCA)
Legal Services (OCA)
Library

EES Public Relations (2)
Computer Input
Project File
Other _____

FORM OCA 4:781

GEORGIA INSTITUTE OF TECHNOLOGY OFFICE OF CONTRACT ADMINISTRATION

N-F&B 2-1
SR410

SPONSORED PROJECT TERMINATION/CLOSEOUT SHEET

Date January 4, 1984

Project No. E-26-B03 School/~~Lab~~ NE

Includes Subproject No.(s)

Project Director(s) J.M. Kallfelz GTRI / ~~GIT~~

Sponsor Union Carbide Corp., (under DOE Prime)

Title Analytic Reactor Physics and Design Investigation

Effective Completion Date: 9/30/83 (Performance) 9/30/83 (Reports)

Grant/Contract Closeout Actions Remaining:

- [x] None (No Final Report required on E-26-B03)
- [ ] Final Invoice or Final Fiscal Report
- [ ] Closing Documents
- [ ] Final Report of Inventions
- [ ] Govt. Property Inventory & Related Certificate
- [ ] Classified Material Certificate
- [ ] Other

Continues Project No. ~~E~~-26-B02 Continued by Project No. E-26-B04

COPIES TO:

Project Director
Research Administrative Network
Research Property Management
Accounting
Procurement/EES Supply Services
Research Security Services
Reports Coordinator (OCA)
Legal Services

Library
GTRI
Research Communications (2)
Project File
Other

Form OCA 60:1028

E-26-803

Georgia Institute of Technology
A UNIT OF THE UNIVERSITY SYSTEM OF GEORGIA
SCHOOL OF NUCLEAR ENGINEERING AND HEALTH PHYSICS
ATLANTA, GEORGIA 30332
(404) 894-3720

May 12, 1982

MEMORANDUM

TO: D. G. Cacuci, J. H. Marable, and C. R. Weisbin (ORNL)

FROM: J. M. Kallfelz and L. A. Belblidia

SUBJECT: Progress Report for ORNL Subcontract 7802
Month of April 1982

Accomplishments During Report Period

- The first draft of a joint journal paper on "Generalized Peturbation Theory with Derivative Operators for Power Density Investigations"[1] was completed.
- Further details concerning XY and RZ models for power density sensitivities[2] were investigated with Charlie Cowan.

Plans for Work in May

We will continue work on the joint journal paper[1] mentioned above. Dan Cacuci will visit Georgia Tech on 13 and 14 May to discuss topics covered in the first draft of this paper.

References

1. J. M. Kallfelz and L. A. Belblidia, "Progress Report for ORNL Subcontract 7802, Months of January, February and March, 1982," Memorandum to C. R. Weisbin, J. H. Marable and D. G. Cacuci, dated April 23, 1982.
2. J. M. Kallfelz, "XY and RZ Models for Power Density (PD) Sensitivities," Memorandum to C. L. Cowan (GE-ARSD), dated January 6, 1982.

E-26-1303

Georgia Institute of Technology
A UNIT OF THE UNIVERSITY SYSTEM OF GEORGIA
SCHOOL OF NUCLEAR ENGINEERING AND HEALTH PHYSICS
ATLANTA, GEORGIA 30332
(404) 894-3720

June 11, 1982

MEMORANDUM

TO: D. G. Cacuci, J. H. Marable, and C. R. Weisbin (ORNL)

FROM: J. M. Kallfelz and L. A. Belblidia

SUBJECT: Progress Report for ORNL Subcontract 7802
Month of May 1982

Accomplishments During Report Period

- The second draft of a joint journal paper on "Generalized Perturbation Theory with Derivative Operators for Power Density Investigations"[1] was completed. Dan Cacuci visited Georgia Tech on 13 and 14 May to discuss topics covered in the first draft of this paper.

Plans for Work in June

We will complete work on the joint journal paper[1] mentioned above.

References

1. J. M. Kallfelz and L. A. Belblidia, "Progress Report for ORNL Subcontract 7802, Months of January, February and March, 1982," Memorandum to C. R. Weisbin, J. H. Marable and D. G. Cacuci, dated April 23, 1982.

JMK/lm

E-26-B03

Georgia Institute of Technology
A UNIT OF THE UNIVERSITY SYSTEM OF GEORGIA
SCHOOL OF NUCLEAR ENGINEERING AND HEALTH PHYSICS
ATLANTA, GEORGIA 30332
(404) 894-3720

July 12, 1982

MEMORANDUM

TO: D.G. Cacuci, J.H. Marable, and C.R. Weisbin (ORNL)

FROM: L.A. Belblidia and J.M. Kallfelz

SUBJECT: Progress Report for ORNL Subcontract 7802
Month of June 1982

Accomplishments During Report Period

The last draft of a joint journal paper on "Generalized Perturbation Theory with Derivative Operators for Power Density Investigations"[1] was completed during Dan Cacuci's visit to Georgia Tech on June 30 and July 1.

Plans for Work in July

We will complete work on the joint journal paper[1] mentioned above, and will submit this paper to Nuclear Science and Engineering for publication.

References

1. J.M. Kallfelz and L.A. Belblidia, "Progress Report for ORNL Subcontract 7802, Months of January, February and March, 1982," Memorandum to C.R. Weisbin, J.H. Marable and D.G. Cacuci, dated April 23, 1982.

E26-B03

Georgia Institute of Technology
A UNIT OF THE UNIVERSITY SYSTEM OF GEORGIA
SCHOOL OF NUCLEAR ENGINEERING AND HEALTH PHYSICS
ATLANTA, GEORGIA 30332
(404) 894-3720

December 20, 1982

MEMORANDUM

TO: C. R. Weisbin and D. G. Cacuci (ORNL)

FROM: J. M. Kallfelz and L. A. Belblidia

SUBJECT: Progress Report for ORNL Subcontract 7802
Months of August and September 1982

The level of activity for this period was relatively low due to staffing problems.

Accomplishments During Report Period

- Revisions of NSE paper[1] to include Jim Marable suggestions and redrawing of figures in order that they conform to NSE publication standards (See Attachment).

- We looked into potential extension of the GPT-Taylor method to 2D models and thermal reactor power distributions. At this point we still have not conducted any calculations to reach any conclusion.

Reference

1. L. A. Belblidia, J. M. Kallfelz and D. G. Cacuci, "Generalized Perturbation Theory with Derivative Operators for Power Density Investigations," to be published in Nucl. Sci. Eng.

ATTACHMENT

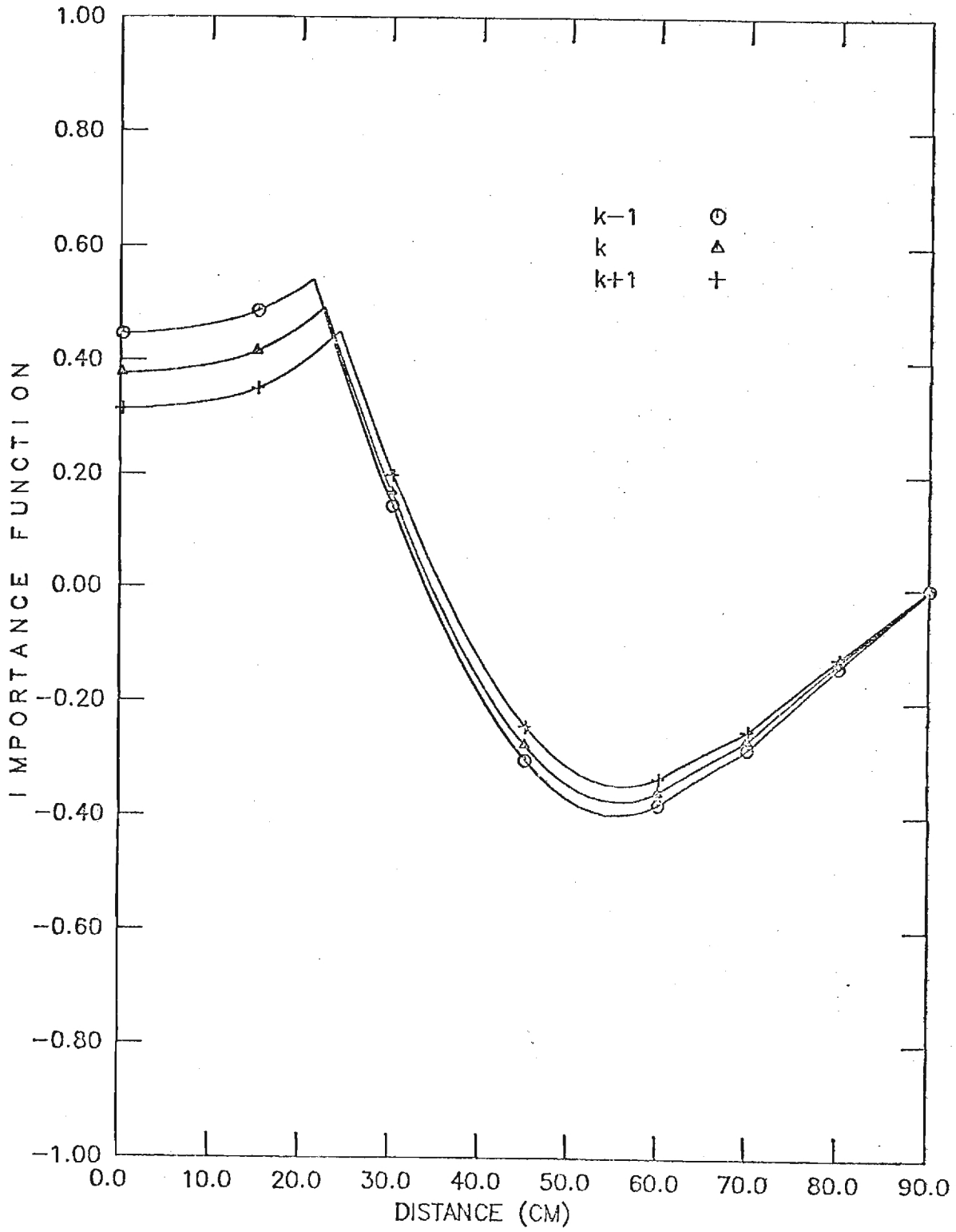
1.00
0.80
0.60
0.40
0.20
0.00
−0.20
−0.40
−0.60
−0.80
−1.00
IMPORTANCE FUNCTION
k−1
k
k+1
0.0
10.0
20.0
30.0
40.0
50.0
60.0
70.0
80.0
90.0
DISTANCE (CM)

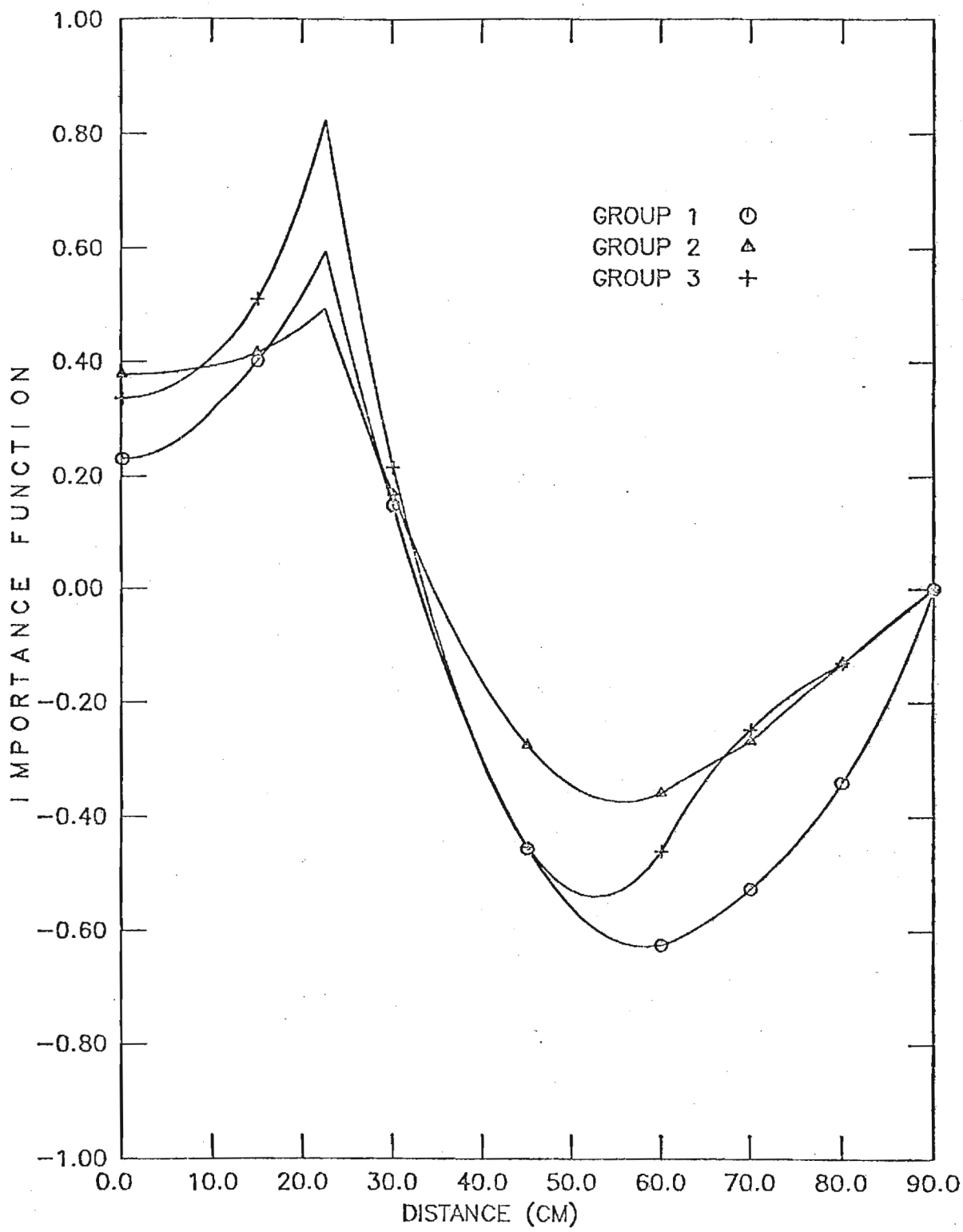
1.00
0.80
0.60
0.40
0.20
0.00
−0.20
−0.40
−0.60
−0.80
−1.00
IMPORTANCE FUNCTION
GROUP 1
GROUP 2
GROUP 3
0.0
10.0
20.0
30.0
40.0
50.0
60.0
70.0
80.0
90.0
DISTANCE (CM)

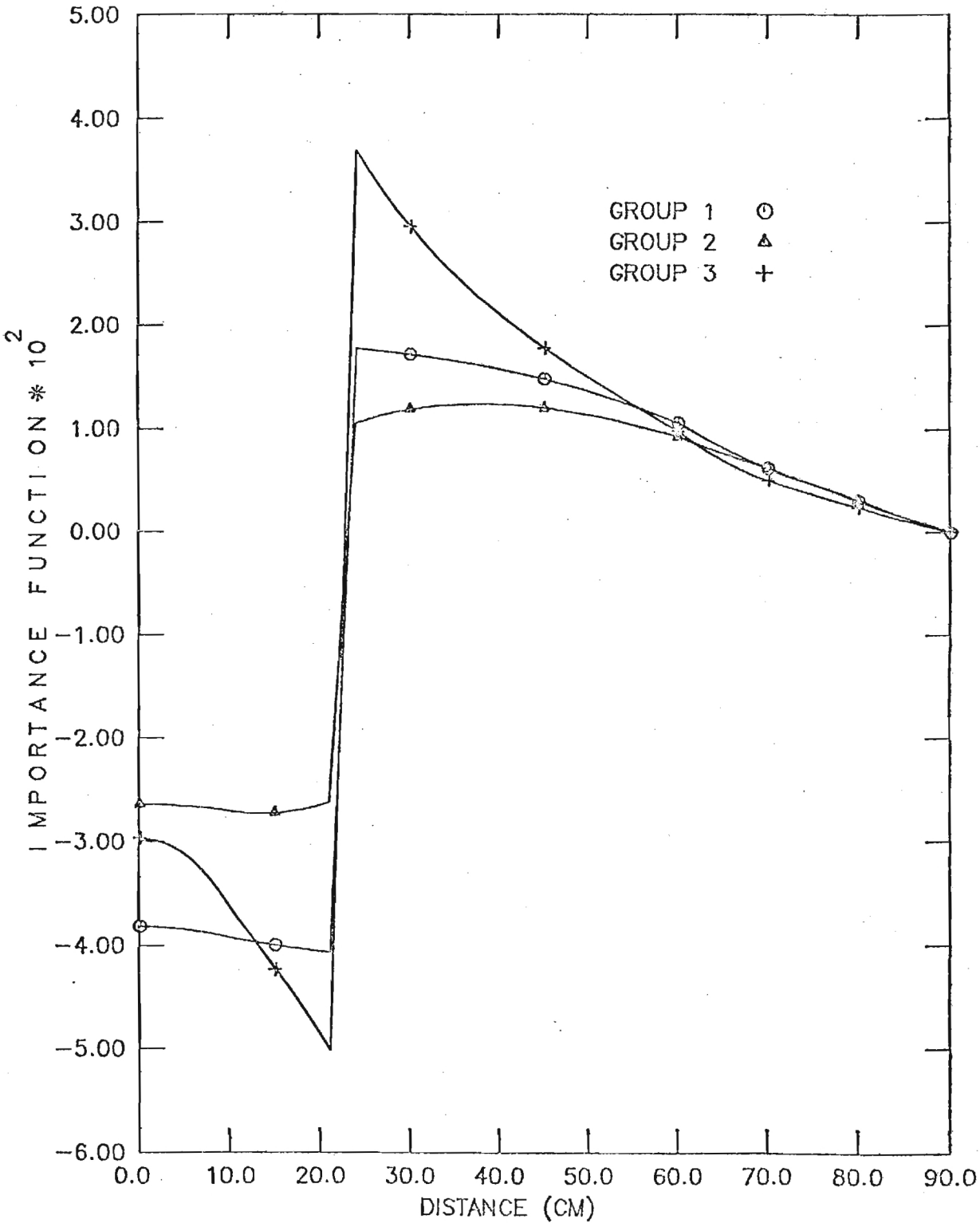
5.00
4.00
3.00
2.00
1.00
0.00
−1.00
−2.00
−3.00
−4.00
−5.00
−6.00
IMPORTANCE FUNCTION * 10^2
0.0
10.0
20.0
30.0
40.0
50.0
60.0
70.0
80.0
90.0
DISTANCE (CM)
GROUP 1
GROUP 2
GROUP 3

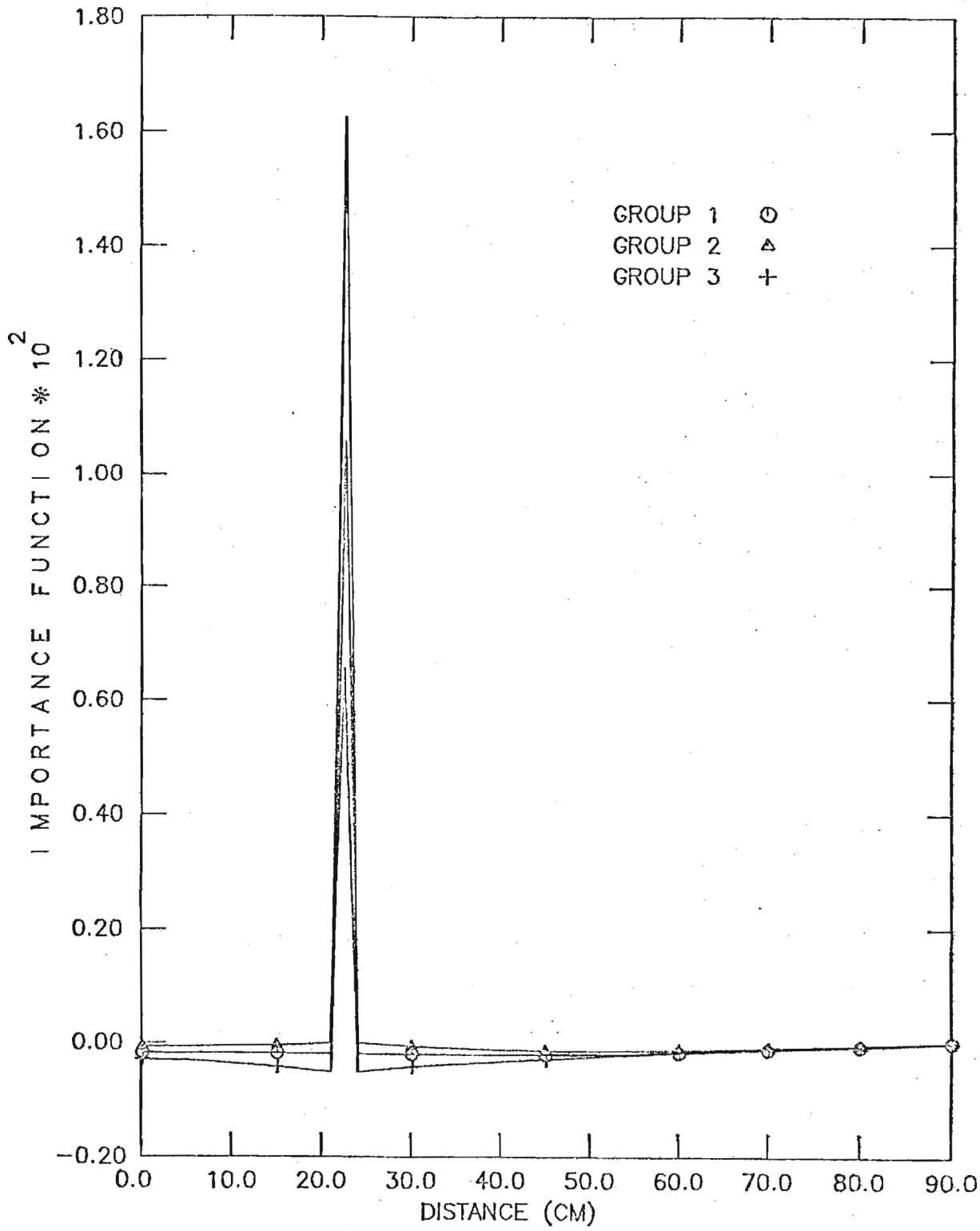
1.80
1.60
1.40
1.20
1.00
0.80
0.60
0.40
0.20
0.00
−0.20
IMPORTANCE FUNCTION * 10^2
GROUP 1
GROUP 2
GROUP 3
0.0
10.0
20.0
30.0
40.0
50.0
60.0
70.0
80.0
90.0
DISTANCE (CM)

E-26-B03

Georgia Institute of Technology

A UNIT OF THE UNIVERSITY SYSTEM OF GEORGIA

SCHOOL OF NUCLEAR ENGINEERING AND HEALTH PHYSICS

ATLANTA, GEORGIA 30332

(404) 894-3720

August 4, 1982

MEMORANDUM

TO: D.G. Cacuci, J.H. Marable, and C.R. Weisbin (ORNL)

FROM: L.A. Belblidia and J.M. Kallfelz

SUBJECT: Progress Report for ORNL Subcontract 7802
Month of July 1982

Accomplishments During Report Period

The final draft of a joint journal paper on "Generalized Perturbation Theory with Derivative Operators for Power Density Investigations"[1] was completed, and is ready for submission to Nuclear Science and Engineering.

References

1. J.M. Kallfelz and L.A. Belblidia, "Progress Report for ORNL Subcontract 7802, Months of January, February and March, 1982," Memorandum to C.R. Weisbin, J.H. Marable and D.G. Cacuci, dated April 23, 1982.

F26-B03

Georgia Institute of Technology
A UNIT OF THE UNIVERSITY SYSTEM OF GEORGIA
SCHOOL OF NUCLEAR ENGINEERING AND HEALTH PHYSICS
ATLANTA, GEORGIA 30332
(404) 894-3720

December 20, 1982

MEMORANDUM

TO: C. R. Weisbin and D. G. Cacuci (ORNL)

FROM: J. M. Kallfelz and L. A. Belblidia

SUBJECT: Progress Report for ORNL Subcontract 7802
Months of October, November and December 1982

The subcontract and performance period was extended for the above months with no additional funding. No activity on the project is reported for this period because of staffing problems.

JMK/vw
LAB/vw

E-26-803

Georgia Institute of Technology
A UNIT OF THE UNIVERSITY SYSTEM OF GEORGIA
SCHOOL OF NUCLEAR ENGINEERING AND HEALTH PHYSICS
ATLANTA, GEORGIA 30332
(404) 894-3720

April 5, 1983

MEMORANDUM

TO: C. R. Weisbin and D. G. Cacuci (ORNL)

FROM: J. M. Kallfelz and L. A. Belblidia

SUBJECT: Progress Report for ORNL Subcontract 7802 Months of January, February, and March 1983

The level of activity for this period was relatively low due to staffing problems.

Accomplishments During Report Period

Dan Cacuci visited Georgia Tech from January 13 to Janauary 15, 1983 to discuss and revise our joint paper[1] which was accepted for publication in NSE. Changes were made in the manuscript resolve all the questions raised by the reviewers, and to enhance the readability of the paper. A copy of the revised article is attached to this report.

Reference

1. L. A. Belblidia, J. A. Kallfelz, and D. G. Cacuci, "Generalized Perturbation Theory with Derivative Operators for Power Density Investigations in Nuclear Reactors," to be published in Nucl. Sci. Eng.

JMK/vw
LAB/vw

Attachment

GENERALIZED PERTURBATION THEORY WITH DERIVATIVE OPERATORS FOR POWER DENSITY INVESTIGATIONS IN NUCLEAR REACTORS

L.A. Belblidia and J.M. Kallfelz*
School of Nuclear Engineering and Health Physics
Georgia Institute of Technology
Atlanta, Georgia 30332

and

D.G. Cacuci
Engineering Physics Division
Oak Ridge National Laboratory
P.O. Box X
Oak Ridge, TN 37830

Send proofs to:
Dan G. Cacuci
Engineering Physics Division
Oak Ridge National Laboratory
P.O. Box X
Oak Ridge, TN 37830

55 pages

6 figures

12 tables

*Present address: Kernforschungszentrum Karlsruhe,
D-7500 Karlsruhe 1, Germany

Acknowledgments

Stimulating discussions with A. Gandini and V. Perone are gratefully acknowledged. We thank Jim Marable for his critical review of the manuscript which led to some modifications in the presentation. Special thanks are due to Lynne Messenger and Sharon Reeves for their expert typing of this manuscript.

This research was performed under Subcontract No. 7802(X01) with the Georgia Institute of Technology under Union Carbide Corporation contract W-7405-eng-26 with the U.S. Department of Energy.

Abstract

This work presents an efficient method to analyze variations that nuclear data perturbations induce in one-dimensional power-density distributions. This method is called the Taylor-GPT method since it is based on: (a) use of a Taylor-series expansion of the response variation, and (b) use of generalized perturbation theory (GPT) to evaluate the derivative operators that appear as coefficients in this Taylor-series. Equations satisfied by the importance functions for the derivatives of the response variations are derived and solved with existing GPT codes. The characteristics of these functions are highlighted analytically.

Particular attention is focused on the numerical value and location of the maximum power density. This is because perturbations in system parameters affect not only the value at the maximum, but also affect the location of this maximum. The Taylor-GPT method can efficiently assess such effects.

The practical usefulness of the Taylor-GPT method is illustrated by considering test cases involving a simplified heterogeneous LMFBR model. The results indicate that this method is as accurate as the GPT method, yet requires fewer calculations when investigating space-dependent power density variations.

I. INTRODUCTION

Generalized perturbation theory (GPT)[1-4] has been used for many years to investigate[2-6] the influence of cross section perturbations and design changes on integral performance parameters (customarily called responses) in reactors. The successful application of GPT to analysis of the power density response[5,6] provided a strong motivation to study in detail the effects of parameter perturbations on such space-dependent responses. Thus, this paper presents an application of first-order GPT to efficiently evaluate the space derivatives of the response that appear as coefficients in a Taylor-series expansion technique. This technique will henceforth be referred to as the "Taylor-GPT" method, and will be used to investigate the space-dependent characteristics of variations in the power density response. The shift in the location of the maximum of this response is of particular interest.[5, 7-10]

I. A. Generalized Perturbation Theory

In reactor design studies, "sensitivities" $\delta P/\delta\alpha$ of a response P to input data α (typically nuclide densities or cross sections) are of interest.[2-6] In particular, P can denote a ratio of linear functionals of the real flux $\underline{\phi}(\underline{r})$. For such a P, the use of GPT to calculate sensitivities requires that the following adjoint inhomogeneous Boltzmann equation be solved for $\underline{\Gamma}^*$:

$$(A^* - \lambda B^*)\,\underline{\Gamma}^* = \underline{S}^*. \qquad (1)$$

In Eq. (1), A^* is the adjoint loss and scattering operator, B^* is the adjoint fission operator, and λ is the system eigenvalue.

In multigroup formalism, $\underline{\Gamma}^*(\underline{r})$ is the generalized adjoint function, whose component $\Gamma_j^*(\underline{r})$ gives the importance of neutrons at $\underline{r}$ in energy group j to the ratio P. Thus, Γ_j^* satisfies the following equation that, except for the S^* term,[2] is formally identical to the "normal" adjoint equation[11] for ϕ_j^*:

$$-D_j \nabla^2 \Gamma_j^*(\underline{r}) + \Sigma_{rem,j} \Gamma_j^*(\underline{r}) =$$

$$\sum_h \Sigma_{j \to h} \Gamma_h^*(\underline{r}) + \lambda \nu \Sigma_{f,j} \sum_h \chi_h \Gamma_h^*(\underline{r}) + S_j^*(\underline{r}). \qquad (2)$$

In Eq. (2), all cross sections are functions of $\underline{r}$. The boundary conditions associated with Eq. (2) are formally identical to those for the ϕ_j^* equation, e.g., $\Gamma_j^* = 0$ at the outer reactor boundary (or extrapolated boundary).

Consider a ratio P of functionals of the real flux defined as

$$P = \frac{a_1}{a_2} = \frac{\int_{V_1} \sum_j \sigma_{1,j}(\underline{r}) \phi_j(\underline{r}) \, d\underline{r}}{\int_{V_2} \sum_j \sigma_{2,j}(\underline{r}) \phi_j(\underline{r}) \, d\underline{r}}, \qquad (3)$$

where V_1 and V_2 specify the volumes associated with the space integration over $\underline{r}$. (In the sequel, lack of such specification implies integration over the entire reactor volume.) For P defined by Eq. (3), there corresponds the following fixed source for Eq. (2):

$$S_j^*(\underline{r}) = \frac{\sigma_{1,j}}{a_1} - \frac{\sigma_{1,j}}{a_2}. \qquad (4)$$

Typically, $\sigma_{i,j}$ is some microscopic or macroscopic cross section.

In previous works[3,4] that used the concepts of GPT, the expression for the fixed source $\underline{S}^*$ was generally written as

$$\underline{S}^* = \frac{1}{P} \frac{\partial P}{\partial \underline{\Phi}} . \tag{5}$$

The expression $\partial P/\partial \underline{\Phi}$, though, was used in a formal sense and did not have a precise mathematical meaning. Based on the rigorous and comprehensive sensitivity theory[7,8] for nonlinear systems that has recently been developed, it can be shown that $\partial P/\partial \underline{\Phi}$ is in fact the partial Gateaux-derivative of P with respect to $\underline{\Phi}$, i.e., $\partial P/\partial \underline{\Phi}$ is the operator defined via the relationship

$$\frac{d}{d\varepsilon} \left[P(\underline{\Phi} + \varepsilon \underline{h}) \right]_{\varepsilon=0} = \frac{\partial P}{\partial \underline{\Phi}} \underline{h}, \tag{6}$$

where ε is a real scalar and $\underline{h}$ is an arbitrary vector of "increments" around $\underline{\Phi}$. Having thus specified its precise mathematical meaning, the notation $\partial P/\partial \underline{\Phi}$ will be retained, for convenience, in the sequel.

In the first-order GPT method, the relative response variation is given by[4]

$$\frac{\delta P}{P} = \int \underline{\Phi} \, \underline{\delta G} \, d\underline{r} + \int \underline{\Gamma}^* \, \delta L \, \underline{\Phi} \, d\underline{r}, \tag{7}$$

where $\underline{\Phi}$ and $\underline{\Gamma}^*$ are, respectively, the real flux and generalized adjoint function, δL represents the perturbation in the Boltzmann operator, and the component of $\underline{\delta G}$ for energy group j is defined as

$$\delta G_j(\underline{r}) = \frac{\delta\sigma_{1,j}(\underline{r})}{a_1} - \frac{\delta\sigma_{2,j}(\underline{r})}{a_2} . \qquad (8)$$

The first term on the right side of Eq. (7) arises from changes in the cross sections that appear explicitly in Eq. (3), and is customarily referred to as the "direct-effect" term. The second term on the right side of Eq. (7) is customarily referred to as the "indirect-effect" term, and arises from the change in the flux corresponding to the perturbation $\delta \mathbf{L}$ of the Boltzmann operator.

I. B. Power Density and Related Spatial Shifts

In studies of uncertainties in calculated responses, P, for the heterogeneous core of a large LMFBR,[5,6] GPT has been employed to determine the sensitivities $\delta P/\delta\sigma$ to variations in the cross sections. The responses studied included, for each driver zone, the ratio $R_M(\underline{r}_m)$ of the zonal maximum power density to the total reactor power, defined as

$$R_M(\underline{r}_m) = \frac{Q_1(\underline{r}_m)}{Q_2} , \qquad (9)$$

where $\underline{r}_m$ is the location at which the zonal maximum power density occurs in the unperturbed case (i.e., the "base case"). The terms in the above equation are defined by the following expressions:

$$Q_1(\underline{r}_m) = \int \sum_j \Sigma_{1,j}(\underline{r}') \, \phi_j(\underline{r}') \, \delta(\underline{r}'-\underline{r}_m) \, d\underline{r}', \qquad (10)$$

and

$$Q_2 = \int \sum_j \Sigma_{2,j}(\underline{r}) \, \phi_j(\underline{r}) \, d\underline{r}. \qquad (11)$$

The quantities $\Sigma_{i,j}$ have identical forms for i = 1 and i = 2; considering only fission energy and assuming localized energy deposit, their explicit expression is

$$\Sigma_{i,j}(\underline{r}) = \sum_k p^k \Sigma^k_{f,j}(\underline{r}), \tag{12}$$

where p^k is the total recoverable energy release per fission in the k-th isotope.

The power density $R(\underline{r})$ is defined as in Eq. (9), except that $\underline{r}$ is not necessarily the location where a maximum occurs. Furthermore, to facilitate the subsequent presentation of the Taylor-GPT method, and to clearly highlight its most important characteristics, a one-dimensional (x) model is henceforth considered, with the power density defined as

$$R(x) = \frac{Q_1(x)}{Q_2} . \tag{13}$$

Such one dimensional models are frequently used for scoping calculations; of course, detailed power-density studies require the use of multi-dimensional models.

Reference 5 discussed "far-range" shifts in the location of the reactor peak (i.e., maximum) of the power density (e.g., shifts between driver zones) and "near-range" shifts around the location of the initial maximum R in a particular driver zone. There, the influence of near-range shifts in the location of the zonal peak power density on the sensitivities $\delta R_M/R_M$ was estimated to be small. Note, though, that the nature of these spatial shifts was not rigorously analyzed.

The theory of Cacuci[7,8], which uses Gateaux-differentials, can be applied to problems involving such maxima. This theory has successfully

been applied[12] to obtain sensitivities for the numerical values of the maximum power response and the maximum fuel temperature response, and for the sensitivities of the phase-space locations for these maxima, for a reactor safety problem describing a protected transient with scram on high power level in the Fast Flux Test Facility.

Recently, Gandini suggested the application of GPT to functionals involving derivative operators (see footnote 26 of Ref. 13). References 9 and 10 reported preliminary investigations that used GPT in conjunction with a Taylor-series expansion for a simple response function. These investigations indicated that this method appears promising for explicitly investigating near-range, or localized, spatial shifts.

The purpose of this work is to present new developments and results regarding response variations that involve localized spatial shifts. Included are first examples in reactor physics of importance functions associated with derivative operators,[14] and a detailed discussion of the characteristics of these functions. To analyze both direct and indirect effects caused by cross-section perturbations, this work considers a more general response than previously considered in Refs. 9 and 10. The basics of the Taylor-GPT method are described in Sec. II, and the application of GPT to space derivatives of the response R(x) is discussed in Sec. III. A theoretical analysis that highlights the main characteristics of the importance functions for these derivatives is presented in Sec. IV. Section V describes the use of the Taylor-GPT method for predicting effects of cross-section variations on the power density and on the spatial shifts in the maximum power density. In addition, this section discusses several indicators that can be used to assess the accuracy of the Taylor-GPT method. Comparison of results given by exact calculations, GPT, and

Taylor-GPT have been performed for several test cases involving a simplified model of a heterogeneous LMFBR core. These test cases are described in Sec. VI, and the numerical results and specific comparisons are presented in Sec. VII. Finally, the summary and conclusions presented in Sec. VIII highlight the usefulness of the Taylor-GPT method for assessing effects of variations in nuclide densities and/or nuclear data on the maximum of the power density and on the spatial location of this maximum.

II. TAYLOR-SERIES EXPANSION WITH GENERALIZED PERTURBATION THEORY (TAYLOR-GPT)

II. A. Taylor-Series Expansion for Response Variation

The variation $\delta R(x)$ in the power density $R(x)$, caused by perturbations in cross sections, can be determined by using a Taylor-series expansion about an arbitrary spatial point x_k. Retaining the first three terms only, this Taylor series is

$$\delta R(x) = \delta R(x_k) + (x - x_k)\, \delta R^{(1)}(x_k) + \frac{1}{2}(x - x_k)^2\, \delta R^{(2)}(x_k), \quad (14)$$

where $\delta R^{(i)}(x_k)$ denotes the i-th spatial derivative of the response variation $\delta R(x)$, evaluated at x_k.

Two alternative approaches can be used to calculate the derivatives $\delta R^{(i)}$. One approach is to use the finite-difference approximations of the derivatives $\delta R^{(i)}$ at x_k, while an alternative approach is to use the adjoint solution that corresponds to $\delta R^{(i)}/R^{(i)}$ at x_k. As subsequent developments will show, either of these approaches can be implemented by using existing GPT codes,[16-18] thereby avoiding any additional programming. This inherent implemental expendiency enhances the practical usefulness of the Taylor-GPT method.

II. B. Finite-Difference Implementation of the Taylor-GPT Method

The values of the derivatives $\delta R^{(1)}(x)$ and $\delta R^{(2)}(x)$ can be approximated at $x = x_k$ by using the finite-difference expressions

$$\delta R_k^{(1)} = \frac{\delta R_{k+1} - \delta R_{k-1}}{2\Delta} , \tag{15}$$

and

$$\delta R_k^{(2)} = \frac{\delta R_{k+1} - 2\ \delta R_k + \delta R_{k-1}}{\Delta^2} . \tag{16}$$

In Eq. (15) and (16), Δ denotes the mesh spacing, and subscripts k-1, k, k+1 refer to values at x_{k-1}, x_k, x_{k+1}, respectively; for example, $\delta R_k = \delta R(x_k)$.

III. GENERALIZED PERTURBATION THEORY FOR RESPONSES INVOLVING DERIVATIVE OPERATORS

Equation (1) represents a "fixed-source" problem, and, due to linearity, such problems are known to possess the so-called "additivity" property. That is, if $\underline{\Gamma}_1^*$ is a solution of Eq. (1) with source $\underline{S}_1^*$, and $\underline{\Gamma}_2^*$ is a solution with $\underline{S}_2^*$, then $(\underline{\Gamma}_1^*+\underline{\Gamma}_2^*)$ is a solution corresponding to $(\underline{S}_1^* + \underline{S}_2^*)$. In the finite-difference approximation, the derivatives $\delta R^{(i)}$ are linear combinations of δR evaluated at x_k and at its neighboring mesh points. Therefore, it is possible, in principle, to find a source $\underline{S}^{*(i)}$ so that the corresponding adjoint equation and boundary conditions would yield the $\underline{\Gamma}^{*(i)}$ necessary to calculate $\delta R^{(i)}$. The actual procedure is detailed below.

III. A. Adjoint Functions for Calculating Spatial Derivatives of Response Variations

The ratio $\delta R^{(i)}/R^{(i)}$ at $x = x_k$ can be computed most efficiently by using adjoint functions. These adjoint functions, denoted by $\underline{\Gamma}_k^{*(i)}$, are solutions of

$$(A^* - \lambda B^*)\, \underline{\Gamma}_k^{*(i)} = \underline{S}_k^{*(i)}, \tag{17}$$

where, by analogy with Eq. (5), the adjoint source is

$$\underline{S}_k^{*(i)} = \frac{1}{R_k^{(i)}} \frac{\partial R_k^{(i)}}{\partial \underline{\Phi}}. \tag{18}$$

In the above equations, the operator $\partial R_k^{(i)}/\partial \underline{\Phi}$ is defined in the same way as $\partial R_k/\partial \underline{\Phi}$ [see Eq. (6)], $\underline{\Gamma}_k^{*(i)}$ is subject to the same boundary conditions as $\underline{\Gamma}_k^*$, and $R_k^{(i)}$ denotes the i-th derivative at x_k, of R(x) with respect to x.

Changing the order of differentiation, Eq. (18) becomes

$$\underline{S}_k^{*(i)} = \frac{1}{R_k^{(i)}} \left[\frac{\partial R}{\partial \underline{\Phi}} \right]_{x=x_k}^{(i)} . \tag{19}$$

Recalling Eq. (5), Eq. (19) is finite-differenced for i=1 and i=2 to obtain

$$\underline{S}_k^{*(1)} = \frac{1}{R_k^{(1)}} \frac{R_{k+1}\underline{S}_{k+1}^* - R_{k-1}\underline{S}_{k-1}^*}{2\Delta} , \tag{20}$$

and

$$\underline{S}_k^{*(2)} = \frac{1}{R_k^{(2)}} \frac{R_{k+1}\underline{S}_{k+1}^* - 2R_k\underline{S}_k^* + R_{k-1}\underline{S}_{k-1}^*}{\Delta^2} , \tag{21}$$

respectively.

For calculational purposes, Eqs. (20) and (21) can be further simplified by using the expression

$$R_k = \frac{Q_{1,k}}{Q_2} = \frac{Q_1(x_k)}{Q_2} , \tag{22}$$

and using similar expressions for R_{k-1} and R_{k+1}. Replacing these expressions in Eqs. (20) and (21), and using Eq. (5) yields, for energy group j,

$$S^{*(1)}_{k,j} = \frac{\Sigma_{1,j}(x)\,\delta(x - x_{k+1}) - \Sigma_{1,j}(x)\,\delta(x - x_{k-1})}{Q_{1,k+1} - Q_{1,k-1}} - \frac{\Sigma_{2,j}(x)}{Q_2}, \quad (23)$$

and

$$S^{*(2)}_{k,j} = \frac{\Sigma_{1,j}(x)\,\delta(x - x_{k+1}) - 2\,\Sigma_{1,j}(x)\,\delta(x - x_k) + \Sigma_{1,j}(x)\,\delta(x - x_{k-1})}{Q_{1,k+1} - 2Q_{1,k} + Q_{1,k-1}}$$

$$- \frac{\Sigma_{2,j}(x)}{Q_2}, \quad (24)$$

respectively. Equations (23) and (24) can be used with existing GPT codes to calculate the corresponding $\underline{\Gamma}^{*(i)}_k$, thereby avoiding any additional programming. The procedure is described in Appendix A for the Italian GPT package.[16-18]

For the finite-difference approximations given by Eqs. (20) and (21), the functions $\underline{\Gamma}^{*(i)}_k$ can be related to the generalized adjoint fluxes (i.e., importances) for the response sensitivities at x_{k-1}, x_k, and x_{k+1} by making use of the previously mentioned additivity property of fixed-source problems. For the sources given by Eqs. (20) and (21), the use of this property gives, for i=1 and i=2,

$$\underline{\Gamma}^{*(1)}_k = \frac{1}{R^{(1)}_k} \frac{R_{k+1}\,\underline{\Gamma}^{*}_{k+1} - R_{k-1}\,\underline{\Gamma}^{*}_{k-1}}{2\,\Delta}, \quad (25)$$

and

$$\underline{\Gamma}_k^{*(2)} = \frac{1}{R_k^{(2)}} \frac{R_{k+1}\,\underline{\Gamma}_{k+1}^{*} - 2R_k\,\underline{\Gamma}_k^{*} + R_{k-1}\,\underline{\Gamma}_{k-1}^{*}}{\Delta^2}, \qquad (26)$$

respectively. The adjoint functions $\underline{\Gamma}_k^{*(1)}$ and $\underline{\Gamma}_k^{*(2)}$ are used to determine the values of $\delta R^{(1)}/R^{(1)}$ and $\delta R^{(2)}/R^{(2)}$ at x_k, respectively.

III. B. Calculation of Direct Effects

From the definition of the power density at x_k, the expression giving the direct-effect component of the response sensitivity is obtained as

$$\frac{\delta R_{k,D}}{R_k} = \frac{\sum_j \delta\Sigma_{1,j}(x_k)\,\phi_j(x_k)}{Q_{1,k}} - \frac{\int \sum_j \delta\Sigma_{2,j}(x)\,\phi_j(x)dx}{Q_2}. \qquad (27)$$

Multiplying Eq. (27) by R_k gives

$$\delta R_{k,D} = \frac{1}{Q_2}\left[\sum_j \delta\Sigma_{1,j}(x_k)\,\phi_j(x_k) - R_k Q_3\right], \qquad (28)$$

where

$$Q_3 = \int \sum_j \delta\Sigma_{2,j}(x)\;\phi_j(x)dx. \qquad (29)$$

Using a uniform mesh spacing about x_k, the first spatial derivative at x_k of the direct-effect component can be approximated as

$$\delta R^{(1)}_{k,D} = \frac{1}{2\Delta}\frac{1}{Q_2}\left[\sum_j \delta\Sigma_{1,j}(x_{k+1})\,\phi_j(x_{k+1}) - R_{k+1}Q_3 - \sum_j \delta\Sigma_{1,j}(x_{k-1})\,\phi_j(x_{k-1}) + R_{k-1}Q_3\right] . \tag{30}$$

Dividing Eq. (30) by $R^{(1)}_k$, and simplifying the resulting expression gives

$$\frac{\delta R^{(1)}_{k,D}}{R^{(1)}_k} = \frac{1}{Q_2}\frac{1}{R_{k+1} - R_{k-1}}\sum_j\left[\delta\Sigma_{1,j}(x_{k+1})\,\phi_j(x_{k+1}) - \delta\Sigma_{1,j}(x_{k-1})\,\phi_j(x_{k-1})\right] - \frac{Q_3}{Q_2} . \tag{31}$$

Using the fact that

$$Q_2(R_{k+1} - R_{k-1}) = \sum_j\left[\Sigma_{i,j}(x_{k+1})\,\phi_j(x_{k+1}) - \Sigma_{i,j}(x_{k-1})\,\phi_j(x_{k-1})\right] ,$$

and replacing Q_2 and Q_3 by their respective expressions, Eq. (31) becomes

$$\frac{\delta R^{(1)}_{k,D}}{R^{(1)}_k} = \frac{\sum_j\left[\delta\Sigma_{1,j}(x_{k+1})\,\phi_j(x_{k+1}) - \delta\Sigma_{1,j}(x_{k-1})\,\phi_j(x_{k-1})\right]}{\sum_j\left[\Sigma_{1,j}(x_{k+1})\,\phi_j(x_{k+1}) - \Sigma_{1,j}(x_{k-1})\,\phi_j(x_{k-1})\right]} - \frac{\int\sum_j \delta\Sigma_{2,j}(x)\,\phi_j(x)\,dx}{\int\sum_j \Sigma_{2,j}(x)\,\phi_j(x)\,dx} . \tag{32}$$

The procedure that has led to Eq. (32) is repeated to derive the expression for the second spatial derivative at x_k of the direct-effect component. The final result is

$$\frac{\delta R^{(2)}_{k,D}}{R^{(2)}_{k}} = \frac{\sum_j \left[\delta\Sigma_{1,j}(x_{k+1})\phi_j(x_{k+1}) - 2\delta\Sigma_{1,j}(x_k)\phi_j(x_k) + \delta\Sigma_{1,j}(x_{k-1})\phi_j(x_{k-1})\right]}{\sum_j \left[\Sigma_{1,j}(x_{k+1})\phi_j(x_{k+1}) - 2\Sigma_{1,j}(x_k)\phi_j(x_k) + \Sigma_{1,j}(x_{k-1})\phi_j(x_{k-1})\right]}$$

$$- \frac{\int \sum_j \delta\Sigma_{2,j}(x)\phi_j(x)\,dx}{\int \sum_j \Sigma_{2,j}(x)\phi_j(x)\,dx} \quad . \tag{33}$$

The expressions given by Eqs. (32) and (33) can be calculated with existing GPT codes[18] as described in Appendix A.

IV. THE FUNCTIONS $\underline{\Gamma}^*$ and $\underline{\Gamma}^{*(i)}$: A THEORETICAL ANALYSIS OF THEIR PROPERTIES

For each i = 0, 1, ..., the adjoint functions $\Gamma_k^{(i)}$ satisfy Eq. (17), and thus are functions of both x and x_k, i.e. $\Gamma_k^{*(i)} = \Gamma^{*i}(x, x_k)$. The responses $R_k^{(i)} \equiv R^{(i)}(x_k)$, though, depend on x_k only. Therefore, the equations and boundary conditions satisfied by the adjoint functions $\underline{\Gamma}_k^*$ and $\underline{\Gamma}_k^{*(i)}$ are recast in the form

$$\left.\begin{aligned} &\mathbf{A}^*(R_k\,\underline{\Gamma}_k^*) - \lambda \mathbf{B}^*(R_k\,\underline{\Gamma}_k^*) = R_k\,\underline{S}_k^*\,, \\ &(R_k\,\underline{\Gamma}_k^*) = 0 \quad \text{at } x = L\,, \\ &d(R_k\,\underline{\Gamma}_k^*)/dx = 0 \quad \text{at } x = 0\,, \end{aligned}\right\} \tag{34}$$

and

$$\left.\begin{aligned} &\mathbf{A}^*\left[R_k^{(i)}\,\underline{\Gamma}_k^{*(i)}\right] - \lambda \mathbf{B}^*\left[R_k^{(i)}\,\underline{\Gamma}_k^{*(i)}\right] = R_k^{(i)}\,\underline{S}_k^{*(i)}\,, \\ &\left[R_k^{(i)}\,\underline{\Gamma}_k^{*(i)}\right] = 0 \quad \text{at } x = L\,, \\ &d\left[R_k^{(i)}\,\underline{\Gamma}_k^{*(i)}\right]/dx = 0 \quad \text{at } x = 0\,, \end{aligned}\right\} \tag{35}$$

where L denotes the outer (or the extrapolated) boundary of the reactor system, and all other quantities have the same meanings as before.

Eqs. (34) and (35) are the basis for establishing and analyzing relationships among the adjoint functions $\underline{\Gamma}_k^{*(i)}$, i = 1,2, ..., and $\underline{\Gamma}_k^*$. Of course, the functions $\underline{\Gamma}_k^{*(0)}$ and $\underline{\Gamma}_k$ are identical, since Eq. (35) reduces to Eq. (34) when i=0.

Differentiating Eq. (35) with respect to x_k gives

$$\left.\begin{aligned}
&\partial\, \mathbf{A}^*\left[\partial(R_k^{(i)}\ \underline{\Gamma}_k^{*(i)})/\partial x_k\right] - \lambda \mathbf{B}^*\left[\partial(R_k^{(i)}\ \underline{\Gamma}_k^{*(i)})/\partial x_k\right] = \\
&\qquad \partial\left[R^{(i)}\ \ \underline{S}^{*(i)}\right]/\partial x_k\ , \\
&\partial\left[R_k^{(i)}\ \underline{\Gamma}_k^{*(i)}\right]/\partial x_k \quad = 0 \quad \text{at } x = L, \\
&d\left\{\partial\left[R_k^{(i)}\ \underline{\Gamma}_k^{*(i)}\right]/\partial x_k\right\}/dx = 0 \quad \text{at } x = 0\ .
\end{aligned}\right\} \tag{36}$$

Using the definition of $\underline{S}_k^{*(i)}$ [i.e., Eq. (19)], the quantity $R_k^{(i)}\ \underline{S}_k^{*(i)}$ can be expressed as

$$R_k^{(i)}\ \underline{S}_k^{*(i)} = \int \left\{d^i\left[\partial R/\partial \underline{\phi}\right]/dx^i\right\}\ \delta(x-x_k)dx. \tag{37}$$

Differentiating Eq. (37) with respect to x_k, and using the definition[21] of the δ'-functional, i.e.

$$\int f(x)\ \delta'(x-a)\ dx \ = \ - \int f'(x)\ \delta(x-a)\ dx, \tag{38}$$

leads to

$$\partial\left[R_k^{(i)}\ \underline{S}_k^{*(i)}\right]/\partial x_k = -\int\left\{d^i\ \left[\partial R/\partial\underline{\Phi}\right]/dx^i\right\}\delta'(x-x_k)dx$$

$$=\int\left\{d^{i+1}\left[\partial R/\partial\underline{\Phi}\right]/dx^{i+1}\right\}\ \delta(x-x_k)dx\ . \qquad (39)$$

Writing Eq. (37) for i+1, and comparing the result with Eq. (39) shows that

$$\partial\left[R_k^{(i)}\ \underline{S}_k^{*(i)}\right]/\partial x_k = R_k^{(i+1)}\ \underline{S}_k^{*(i+1)}. \qquad (40)$$

Using Eq. (40) to replace the corresponding source term in Eq. (36), and comparing the resulting system of equations to the system obtained by writing Eq. (35) for i+1 leads to the conclusion that

$$\partial\left[R_k^{(i)}\ \underline{\Gamma}_k^{*(i)}\right]/\partial x_k = R_k^{(i+1)}\ \underline{\Gamma}_k^{*(i+1)},\ i = 0,\ 1,\ 2,... \qquad (41)$$

A simple inductive reasoning can now be used in conjunction with Eq. (41) to conclude that

$$R_k^{(i)}\ \underline{\Gamma}_k^{*(i)} = \partial^i\left[R_k\ \underline{\Gamma}_k^*\right]/\partial x_k^i. \qquad (42)$$

The qualitative behavior of $\underline{\Gamma}_k^*$, $\underline{\Gamma}_k^{*(1)}$, and $\underline{\Gamma}_k^{*(2)}$ as functions of x can be studied analytically by considering a one-group, one-region representation[19] of the adjoint diffusion equations given by Eqs. (34) and (35). For clarity, the functions satisfying the corresponding simplified adjoint diffusion equations are denoted by Γ_1^*, $\Gamma_1^{*(1)}$, and $\Gamma_1^{*(2)}$, where the subscript 1 now refers to the one-

group model rather than to the location of x_k. The respective equations can be written explicitly as follows:

$$\left.\begin{aligned} &d^2\Gamma_1^*/dx^2 + B^2\Gamma_1^* = -S^*/D \ , \\ &\Gamma_1^* = 0 \quad \text{at } x = L \ , \\ &d\Gamma_1^*/dx = 0 \quad \text{at } x = 0 \ , \end{aligned}\right\} \tag{43}$$

$$\left.\begin{aligned} &d^2\Gamma_1^{*(1)}/dx^2 + B^2\,\Gamma_1^{*(1)} = -\,S^{*(1)}/D \ , \\ &\Gamma_1^{*(1)} = 0 \quad \text{at } x = L \ , \\ &d\Gamma_1^{*(1)}/dx = 0 \quad \text{at } x = 0 \ , \end{aligned}\right\} \tag{44}$$

and

$$\left.\begin{aligned} &d^2\Gamma_1^{*(2)}/dx^2 + B^2\Gamma_1^{*(2)} = -\,S^{*(2)}/D \ , \\ &\Gamma_1^{*(2)} = 0 \quad \text{at } x = L \ , \\ &d\Gamma_1^{*(2)}/dx = 0 \quad \text{at } x = 0 \ . \end{aligned}\right\} \tag{45}$$

In Eqs. (43) through (45), B^2 and D represent the customary one-group, one-region buckling and diffusion coefficient, respectively. The analytical expressions for S^*, $S^{*(1)}$, and $S^{*(2)}$ are obtained by using Eqs. (9) through (11) in conjunction with Eq. (19) and with the definitions[21] of the δ'- and

δ''-functionals. Also, for simplicity, the constants $\Sigma_{i,j}$ [see Eq. (12)] are arbitrarily set to unity. Under these conditions, the following analytical expressions are obtained:

$$R_k = Q_{1,0}/Q_2 \ , \tag{46}$$

$$R_k^{(1)} = Q_{1,1}/Q_2 \ , \tag{47}$$

$$R_k^{(2)} = Q_{1,2}/Q_2 \ , \tag{48}$$

$$S^* = \frac{\delta(x-x_k)}{Q_{1,0}} - \frac{1}{Q_2} \ , \tag{49}$$

$$S^{*(1)} = -\frac{\delta'(x-x_k)}{Q_{1,1}} - \frac{1}{Q_2} \ , \tag{50}$$

$$S^{*(2)} = \frac{\delta''(x-x_k)}{Q_{1,2}} - \frac{1}{Q_2} \ , \tag{51}$$

where

$$Q_{1,0} = \phi(x_k), \tag{52}$$

$$Q_{1,1} = \left\{ d\phi/dx \right\}_{x=x_k}, \tag{53}$$

$$Q_{1,2} = \left\{ d^2\phi/dx^2 \right\}_{x=x_k}, \tag{54}$$

and

$$Q_2 = \int \phi(x)\, dx. \tag{55}$$

The adjoint diffusion equations given by Eqs. (43) through (45), with the source terms given by Eqs. (49) through (51), respectively, can be solved analytically to determine Γ_1^*, $\Gamma_1^{*(1)}$, and $\Gamma_1^{*(2)}$. For this purpose, it is convenient to use the Laplace-transform method, as illustrated in Appendix B where Eq. (45) is solved in detail. The following analytical expressions for the solutions of Eqs. (43) through (45) are thus obtained:

$$\Gamma_1^* = \frac{1}{B^2 DQ_2} + \left[\frac{1}{BDQ_{1,0}} \left(\frac{\cos Bx_k}{BL} - \frac{L - x_k}{L} \sin Bx_k \right) - \frac{2}{LB^3 DQ_2} \right] \cos Bx$$

$$- \frac{1}{BDQ_{1,0}} H(x-x_k) \sin B(x-x_k), \tag{56}$$

$$\Gamma_1^{*(1)} = \frac{1}{B^2 DQ_2} - \left(\frac{L - x_k}{DLQ_{1,1}} \cos Bx_k + \frac{2}{LB^3 DQ_2} \right) \cos Bx$$

$$+ \frac{1}{DQ_{1,1}} H(x-x_k) \cos B(x-x_k), \tag{57}$$

$$\Gamma_1^{*(2)} = \frac{1}{B^2 DQ_2} + \left[\frac{\cos Bx_k + B(L-x_k) \sin Bx_k}{LDQ_{1,2}} - \frac{2}{DB^3 LQ_2} \right] \cos Bx$$

$$+ \frac{B}{DQ_{1,2}} H(x-x_k) \sin B(x-x_k) - \frac{\delta(x-x_k)}{DQ_{1,2}}, \qquad (58)$$

where $H(x)$ represents the customary[21] Heaviside (unit-step) functional.

In view of Eqs. (56) through (58), the behavior of the functions Γ_1^*, $\Gamma_1^{*(1)}$, and $\Gamma_1^{*(2)}$ as x approaches x_k becomes of particular interest. Thus, Γ_1^* is continuous at x_k, where

$$\Gamma_1^*(x_k) = \frac{1}{B^2 DQ_2} + \left[\frac{1}{BDQ_{1,0}} \left(\frac{\cos Bx_k}{BL} - \frac{L - x_k}{L} \sin Bx_k \right) \right.$$

$$\left. - \frac{2}{LB^3 DQ_2} \right] \cos Bx_k, \qquad (59)$$

but the first- and second-derivatives of Γ_1^* with respect to x have a Heaviside- and a Dirac delta-type discontinuity, respectively, at $x = x_k$, since

$$\left\{ d\Gamma_1^*/dx \right\}_{x=x_k} = \left[\frac{2}{LB^2 DQ_2} - \frac{1}{DQ_{1,0}} \left(\frac{\cos Bx_k}{BL} - \frac{L - x_k}{L} \sin Bx_k \right) \right] \sin Bx_k$$

$$- \frac{1}{DQ_{1,0}} H(x-x_k), \qquad (60)$$

and

$$\left\{d^2\Gamma_1^*/dx^2\right\}_{x=x_k} = \left[\frac{2}{LBDQ_2} - \frac{B}{DQ_{1,0}}\left(\frac{\cos Bx_k}{BL} - \frac{L - x_k}{L}\sin Bx_k\right)\right]\cos Bx_k - \frac{\delta(x-x_k)}{DQ_{1,0}} . \tag{61}$$

At $x = x_k$, the function $\Gamma_1^{*(1)}$ has a Heaviside-type discontinuity, since

$$\left\{\Gamma_1^{*(1)}\right\}_{x=x_k} = \frac{1}{B^2DQ_2} - \left(\frac{L - x_k}{DLQ_{1,1}}\cos Bx_k + \frac{2}{LB^3DQ_2}\right)\cos Bx_k + \frac{1}{DQ_{1,1}} H(x-x_k), \tag{62}$$

while the first derivative of $\Gamma_1^{*(1)}$ with respect to x has a Dirac delta-discontinuity, since

$$\left\{d\Gamma_1^{*(1)}/dx\right\}_{x=x_k} = \left[\frac{B(L-x_k)}{DLQ_{1,1}}\cos Bx_k + \frac{2}{LB^2DQ_2}\right]\sin Bx_k + \frac{\delta(x-x_k)}{DQ_{1,1}} . \tag{63}$$

Finally, $\Gamma_1^{*(2)}$ has a Dirac delta-type discontinuity at $x = x_k$, since

$$\left\{\Gamma_1^{*(2)}\right\}_{x=x_k} = \frac{1}{B^2 DQ_2} + \left[\frac{\cos Bx_k + B(L-x_k)\sin Bx_k}{LDQ_{1,2}} - \frac{2}{DB^3 LQ_2}\right]\cos Bx_k - \frac{\delta(x-x_k)}{DQ_{1,2}} . \tag{64}$$

When x_k is close to the exact location x_m of the maximum, but such that $x_k < x_m$, $Q_{1,0}$ and $Q_{1,1}$ are positive, while $Q_{1,2}$ is negative. In this case, Eqs. (59) through (64) indicate that:

1. The functions $\Gamma_1^{*(1)}$ and $d\Gamma_1^*/dx$ both undergo step-jumps at $x = x_k$, but the former function undergoes a positive step jump, while the latter undergoes a negative step jump, and
2. The functions $\Gamma_1^{*(2)}$, $d\Gamma_1^{*(1)}/dx$, and $d^2\Gamma_1^*/dx^2$ all display "spikes", i.e. Dirac delta-type discontinuities at $x = x_k$. These delta-functionals cause positive spikes in $\Gamma_1^{*(2)}$ and $d\Gamma_1^{*(1)}/dx$, but cause a negative spike in $d^2\Gamma_1^*/dx^2$.

Since Eqs. (43) through (45) are particular forms of Eqs. (34) through (36), respectively, the functions Γ_1^*, $\Gamma_1^{*(1)}$, and $\Gamma_1^{*(2)}$ should also satisfy the relationships given by Eqs. (41) and (42). This fact can readily be verified by using Eqs. (56) through (58) and Eqs. (46) through (48) to show that

$$\partial(R_k \Gamma_1^*)/\partial x_k = R_k^{(1)} \Gamma_1^{*(1)}, \tag{65}$$

and

$$\partial^2(R_k \Gamma_1^*)/\partial x_k^2 = \partial\left[R_k^{(1)} \Gamma_1^{*(1)}\right]/\partial x_k = R_k^{(2)} \Gamma_1^{*(2)}. \tag{66}$$

V. RESPONSE VARIATIONS AND SPATIAL SHIFTS: CALCULATIONAL PROCEDURES AND ACCURACY OF PREDICTIONS

V. A. Response Variations and Accuracy of Predictions

The effects on the power density of variations in the macroscopic cross sections can be evaluated by three methods:

(1) direct calculations;

(2) use of generalized perturbation theory (GPT);

(3) use of Taylor-series expansion method with GPT (Taylor-GPT).

The first method consists of calculating the response (in this case, the point-power density) for the unperturbed case (denoted by the subscript 0), the response for the perturbed case (denoted by the subscript 1), and substracting the two to determine the change. The result of this process gives

$$\Delta R_e(x) = R_1(x) - R_0(x). \tag{67}$$

This method will henceforth be called "exact".

For the first-order GPT method, the response variation, denoted by $R_p(x)$, is considered to be given by

$$\delta R_p(x) = R(x) \left.\frac{\delta R}{R}\right|_x , \tag{68}$$

where $\delta R/R$ has the same expression as $\delta P/P$ in Eq. (7), except that P is replaced by the particular response R(x) defined by Eq. (13).

For the Taylor-GPT method, the response variation at x, denoted by $\delta R_{tp}(x)$, is considered to be given by the following three-term Taylor-series expansion about x:

$$\delta R_{tp}(x) = \delta R_p(x_k) + (x-x_k)\, \delta R_p^{(1)}(x_k) + \frac{1}{2}\,(x-x_k)^2\, \delta R_p^{(2)}(x_k). \qquad (69)$$

In Eq. (69), the variation in the power density at x_k and its first two derivatives at x_k are determined from GPT calculations.

The accuracy of the Taylor-GPT method can be assessed by comparing the left side of Eq. (69) to the result of a GPT sensitivity calculation at x, i.e., Eq. (68). A relative error, denoted by TAP and defined as

$$TAP = \frac{\delta R_{tp}(x) - \delta R_p(x)}{\delta R_p(x)} . \qquad (70)$$

can be used to assess this accuracy.

On the other hand, the relative error that results from:

a. the inaccuracy of GPT, and

b. the differences between Eq. (68) and the Taylor-series expansion of $\delta R(x)$ about x_k

is found by taking the direct calculations as the basis for comparison. This relative error is henceforth denoted by TAE, and is defined as

$$TAE = \frac{\delta R_{tp}(x) - \Delta R_e(x)}{\Delta R_e(x)} . \qquad (71)$$

V. B. Spatial Shifts in the Maximum Power Density

Numerically, a discrete set $R_i = R_0(x_i)$, $i=1,2, \ldots, N$ is obtained when the unperturbed power density $R_0(x)$ is calculated as a function of x. Consider now that x_k represents the discrete point at which the largest discrete value R_k is obtained. In general, x_k does not coincide with the spatial location, denoted by x_{m0}, at which $R_0(x)$ attains its actual maximum. The location x_{m0} can approximately be determined by expanding $R_0(x)$ in a Taylor series around x_k, i.e.,

$$R_0(x) = R_0(x_k) + (x-x_k)\, R_0^{(1)}(x_k) + \frac{1}{2}(x-x_k)^2\, R_0^{(2)}(x_k) + \ldots \quad (72)$$

and by evaluating the first spatial derivative of this expansion at x_{m0}. Retaining only terms up to $O[(x-x_k)^3]$ in Eq. (72), and noting that $dR_0(x)/dx$ vanishes at x_{m0} [since $R_0(x)$ attains its maximum there] gives

$$x_{m0} - x_k = - \frac{R_0^{(1)}(x_k)}{R_0^{(2)}(x_k)} . \quad (73)$$

When the system parameters are perturbed, the perturbed response, denoted by $R_1(x)$, attains its actual maximum at a location x_{m1} which, in general, will not coincide with x_{m0}. The location x_{m1} can be determined by expanding the perturbed response $R_1(x)$ in a Taylor series analogous to Eq. (72), and following the same procedure as that leading to Eq. (73). This gives

$$x_{m1} - x_k = - \frac{R_1^{(1)}(x_k)}{R_1^{(2)}(x_k)} . \quad (74)$$

The spatial shift $(x_{m1} - x_{m0})$ in the peak power density can now be estimated by subtracting Eq. (72) from Eq. (74). This gives

$$x_{m1} - x_{m0} = - \frac{R_0^{(1)} + \delta R^{(1)}}{R_0^{(2)} + \delta R^{(2)}} + \frac{R_0^{(1)}}{R_0^{(2)}} , \tag{75}$$

where all $R^{(i)}$ and $\delta R^{(i)}$, i=1,2, are understood as being evaluated at $x = x_k$. When $\delta R^{(2)}/R^{(2)}$ is much less than unity, Eq. (75) reduces to

$$x_{m1} - x_{m0} \simeq - \frac{\delta R^{(1)}}{R_0^{(2)}} . \tag{76}$$

Within the framework of first-order GPT, the perturbed response can be written as the sum of the unperturbed response and the response variation δR_p, where the latter term consists of a direct-effect component, δR_d, and an indirect-effect component, δR_i, i.e.,

$$\begin{aligned} R_1 &= R_0 + \delta R_p \\ &= R_0 + \delta R_d + \delta R_i . \end{aligned} \tag{77}$$

Similar expressions can be written for the spatial derivatives of the perturbed response:

$$\left.\begin{aligned} R_1^{(1)} &= R_0^{(1)} + \delta R_d^{(1)} + \delta R_i^{(1)} , \\ R_1^{(2)} &= R_0^{(2)} + \delta R_d^{(2)} + \delta R_i^{(2)} . \end{aligned}\right\} \tag{78}$$

If, on the one hand, the direct-effect components vanish, then Eqs. (74) and (78) give

$$(x_{m1} - x_k)_i = - \frac{R_0^{(1)} + \delta R_i^{(1)}}{R_0^{(2)} + \delta R_i^{(2)}} . \tag{79}$$

If, on the other hand, the indirect-effect components vanish, then Eqs. (74) and (78) give

$$(x_{m1} - x_k)_d = - \frac{R_0^{(1)} + \delta R_d^{(1)}}{R_0^{(2)} + \delta R_d^{(2)}} . \tag{80}$$

Adding Eqs. (79) and (80), and neglecting second-order terms of the form $\delta R_d^{(i)} \delta R_i^{(j)}$, gives

$$(x_{m1} - x_k)_d + (x_{m1} - x_k)_i = - \frac{R_0^{(1)} + \delta R_d^{(1)} + \delta R_i^{(1)}}{R_0^{(2)} + \delta R_i^{(2)} + \delta R_i^{(2)}} - \frac{R_0^{(1)}}{R_0^{(2)}} . \tag{81}$$

In view of Eqs. (74) and (78), the first term on the right side of Eq. (81) is the expression for $(x_{m1} - x_k)$ when both direct and indirect effects are present. The second term on the right side of Eq. (81) corresponds to the unperturbed case, i.e., to $(x_{m0} - x_k)$ as given by Eq. (72). Therefore, Eq. (81) becomes

$$(x_{m1} - x_k)_d + (x_{m1} - x_k)_i = (x_{m1} - x_k) + (x_{m0} - x_k). \tag{82}$$

Noting that x_k is a fixed point, and subtracting twice the quantity $(x_{m0} - x_k)$ from Eq. (82) gives

$$(x_{m1} - x_{m0})_d + (x_{m1} - x_{m0})_i = x_{m1} - x_{m0}. \tag{83}$$

Equation (83) shows that the spatial shift in the peak location can be expressed as the sum of a spatial shift due solely to direct effects and a spatial shift due solely to indirect effects.

V. C. Influence of the Spatial Shift on the Sensitivity of the Peak-Power Density

When a macroscopic cross section is perturbed, the resulting variation in peak power density is given by

$$\Delta R_{es} = R_1(x_{m1}) - R_0(x_{m0}). \tag{84}$$

Note that Eq. (84) is exact, i.e., it contains no approximations.

If the shift in the location of the peak is neglected, the variation in the response is given by Eq. (67) evaluated at x_{m0}, that is,

$$\Delta R_{e0} = R_1(x_{m0}) - R_0(x_{m0}). \tag{85}$$

In view of Eqs. (84) and (85), the effect of the spatial shift on the sensitivity of the peak power density can be assessed by using the expression

$$SE = \frac{\Delta R_{es} - \Delta R_{e0}}{\Delta R_{e0}} . \tag{86}$$

Since Cacuci[8] has shown that

$$\left| R_1(x_{m1}) - R_1(x_{m0}) \right| = O[(\delta\sigma)^2] , \tag{87}$$

where $\delta\sigma$ represents variations in the system parameters, it follows that the numerator of Eq. (86) is also of second order in these variations. Figure 1 illustrates the near-range spatial shift and its influence on the sensitivity of the extremum.

VI. DESCRIPTION OF TEST CASES

VI. A. Model and Cross Sections

A simplified three-region model, which has some of the significant characteristics[10] of a heterogeneous LMFBR, has been chosen to test the theoretical developments outlined in the previous sections. This model consists of an infinite slab, finite in the x-direction, with internal blanket (IB), driver (D), and external blanket (EB). The concentrations of Na, U-238, and Pu-239 are given in Table I, and are the same as for the beginning-of-life LMFBR model considered in Ref. 22. The three-group cross sections used are from the CITATION test case.[23]

The outer boundaries of regions IB, D, and EB are located at 10.5 cm, 60 cm, and 90.0 cm from the reactor center (x = 0), respectively. A driver zone mesh spacing of 1.5 cm is used for all reported results; however, this spacing was varied in some of the test calculations discussed in Sec. VII.B.

VI. B. Selection of Perturbations

Perturbations of nuclide densities or microscopic cross sections cause changes in the macroscopic cross sections, Σ , and thus in the Boltzmann operator, L. To choose perturbations appropriate for testing the proposed method, several desirable, and sometimes conflicting, conditions should be considered:

(i) To test the Taylor series method, $\delta\Sigma$ should cause a response variation $\delta R(x)$ that appreciably depends on x. This implies that the change in at least one of the derivatives $\delta R^{(i)}(x_k)$ should be appreciable.

(ii) To check the GPT method [see Eq. (7)], the indirect-effect component of the total perturbation $\delta R^{(i)}(x)$ should be appreciable.

(iii) To allow useful comparisons with "exact" (i.e., direct calculation) results, the perturbation $\delta\Sigma$ should not be so large that second- and higher-order terms in $\delta\Sigma$, which are ignored in the first-order GPT applied herein, become overwhelmingly large.

In view of the conditions described above, four test cases, as described in Table II, have been devised. In general, these cases meet the above conditions adequately, but the following exceptions should be noted:

(a) Case 1 does not satisfy condition (i) well, but is a good test for predicting a small spatial shift in the peak power density.

(b) Case 3 does not satisfy condition (iii) well, but is an interesting example of a very large perturbation that effectively transforms the heterogeneous core into a homogeneous one.

VII. RESULTS FOR TEST CASES

VII. A. $\underline{\Gamma}_k^{*(i)}$ Results

Various characteristics of the functions $\underline{\Gamma}_k^{*(i)}$ are illustrated by the results presented in Figs. 2 through 5. All numerical results discussed in this and the following sections are for x_k=22.5 cm, the mesh point at which the maximum value of R_k occurred in the unperturbed (i.e., "base-case") calculation of the power density R(x). The spatial shape of $\underline{\Gamma}_k^*$ is illustrated in Figs. 2 and 3. The neutron importance to $R(x_k)$ is greatest near x_k; there, a neutron is more likely to contribute to the numerator rather than the denominator of Eq. (13). As a function of x, $\underline{\Gamma}_k^*(x)$ is negative over a wide range due to the neutron contributions to the denominator of Eq. (13).

The shape of the curves for $\underline{\Gamma}_k^{*(1)}$ and $\underline{\Gamma}_k^{*(2)}$ can be discussed in terms of the expressions derived in Sec. IV. For this purpose, recall that $\underline{\Gamma}_k^*$ depends both on x_k and x, and that the associated response $R_k \equiv R(x_k)$ depends on x_k but not on x. In the following, the dependence of $\underline{\Gamma}^{*(i)}(x,x_k) \equiv \underline{\Gamma}_k^{*(i)}(x)$ on each of the two independent variables x and x_k will be addressed separately.

As functions of x_k, the relationships between the $\Gamma_{k,j}^{*(i)}$ for the j-th energy group have been generally given, in vector form, by Eq. (42), i.e.,

$$R_k^{(i)} \underline{\Gamma}_k^{*(i)} = \partial^i \left[R_k \underline{\Gamma}_k^* \right] / \partial x_k^i. \qquad [(42)]$$

Qualitatively, this behavior is illustrated in Fig. 4, which presents $\underline{\Gamma}_k^{*(1)}(x)$ as a function of x. For group 2, for example, given the fact that

$R_k^{(1)}$ is positive, the shape shown in Fig. 4 can be obtained by considering various fixed, but successively larger, values of x on the set of curves for $\underline{\Gamma}^*(x,x_k)$ shown in Fig. 2.

As functions of x, the qualitative behavior of $\Gamma_{k,j}^{*(i)}$, shown in Figs. 2 through 5, can be supported by considering the analytic results for Γ_1^*, $\Gamma_1^{*(1)}$ and $\Gamma_1^{*(2)}$ obtained in Sec. IV for a simple one-group, one-region case. Although the results shown in Figs. 2 through 5 are for a multi-region, multigroup case, the predominant features of these results near x_k are expected to be similar to those of the simpler one-group, one-region model. This is because:

(i) the fixed point x_k is well within the interior of the driver region, and hence is neutronically "far" (several mean free paths) from other regions;

(ii) the x-dependence of $\Gamma_{k,j}^{*(i)}(x)$ is strongly influenced by the spatial form of the fixed sources, $\underline{S}_k^{*(i)}(x)$; for our test cases, these sources are space-energy separable in the driver region;

(iii) coupling between groups for the multigroup case does not change the predominant features of the x-dependence of $\Gamma_{k,j}^{*(i)}(x)$, since this dependence is similar for all groups. This similarity, illustrated in Fig. 3, is principally due to (ii), above.

The discussion that followed Eqs. (59) through (64), and that focused on the predominant features of the x-dependence of the functions $\Gamma_1^{*(1)}$ and $\Gamma_1^{*(2)}$, also provides a good description of the predominant features of the x-dependence of the derivative importance functions shown in Figs. 4 and 5.

The values of $\Gamma_k^{*(2)}$ for $x \neq x_k$ are significantly smaller than the value at x_k, and are sensitive to the "fundamental harmonic correc-

tion"[2,4,24] that must be used to eliminate fundamental harmonic contamination when calculating $\underline{\Gamma}^{*(i)}$. Although the CIAP-INO version of CIAP-1D[17] that was employed to calculate the adjoint functions performs this correction, the correction was numerically inadequate to determine $\underline{\Gamma}_k^{*(2)}$. This situation was resolved by noting that the functions $\underline{\Gamma}_k^{*(i)}$ satisfy the orthogonality property

$$\langle \underline{\Gamma}_k^{*(i)}, B\, \underline{\Phi} \rangle = 0, \tag{88}$$

where B is the fission operator. As a result of applying this orthogonality property to eliminate fundamental harmonic contamination, the values for $\underline{\Gamma}_k^{*(2)}$ obtained by using the fixed source $\underline{S}_k^{*(2)}$ [see Eq. (24)] agreed well with the corresponding values obtained by using Eq. (26).

The numerical accuracy of calculating $\underline{\Gamma}_k^{*(1)}$ was verified in a similar manner: on the one hand, $\underline{\Gamma}_k^{*(1)}$ was calculated by using the fixed source $S_k^{*(1)}$ [see Eq. (23)] and, on the other hand, $\underline{\Gamma}_k^{*(1)}$ was calculated by using Eq. (25). These calculations gave essentially identical results.

A mesh spacing of 1.5 cm, which is a typical value specified for benchmark calculations of critical assemblies with LMFBR characteristics (e.g., ZPR-3-48),[25] was initially chosen for both forward and adjoint calculations. The results for the functions $\underline{\Gamma}_k^{*(i)}$ were obtained by using this mesh spacing. The sharp variations displayed by these functions provided a strong motivation to investigate whether this mesh spacing, which is adequate for calculating the comparatively smooth forward fluxes, is indeed adequate for accurately calculating the adjoint functions. This adequacy was investigated by performing several calculations with a finer mesh, obtained by reducing the 1.5 cm mesh spacing to 0.5 cm in a region around x_k. Although the shapes of $\underline{\Gamma}_k^{*(i)}$ changed slightly due to the

additional mesh points (an expected outcome considering the sharp variations involved), the use of the two meshes yielded essentially identical results for $\delta R_k^{(i)}$. This gives confidence that the 1.5 cm mesh spacing is indeed adequate. All numerical results reported in this work were obtained by using the 1.5 cm mesh-spacing.

VII. B. Comparison of Results for $\delta R^{(i)}(x_k)$ Obtained from GPT and Direct Calculations

The accuracy of values for $\delta R_k^{(i)}$ obtained from GPT calculations was verified by performing two direct TAIM[16] calculations. As discussed in Sec. V.A, the results of these direct calculations are termed "exact". The convergence criteria for these direct calculations were adequately stringent to insure that the exact results retained sufficient significant figures for comparisons with perturbation-theory results. As indicated in Tables III through VI, the exact and GPT results for $\delta R_k^{(i)}$ generally agreed within about 5%. Note that for all four cases, the indirect component of $\delta R_k^{(i)}$ is greater than the direct component for at least two of the three i values. Thus, condition (ii) of Sec. VI.B is largely satisfied.

The results shown in the last columns of Tables IV and V indicate that GPT and exact results do not agree well for $\delta R_k^{(2)}$ of Case 2, and for Case 3, respectively. For Case 3, the disagreement between GPT and exact results indicates that the nonlinear terms disregarded by first-order GPT are not small. This is not surprising, since, as discussed in Sec. VI.B, Case 3 represents a very large perturbation. The disagreement between GPT and exact results for $\delta R_k^{(2)}$ of Case 2 can be analyzed by comparing the results for $\delta R_k^{(2)}/R_k^{(2)}$ presented in the fourth columns of Tables III through VI. This comparison shows that $\delta R_k^{(2)}/R_k^{(2)}$ is smallest for Case 2, being about

an order of magnitude smaller than for Case 1 and about two orders of magnitude smaller than for Cases 3 and 4. Note now that the effects of the nonlinear terms disregarded by first-order GPT are measured by $\varepsilon(x)$ defined as

$$\varepsilon(x) = \delta R_p(x) - \Delta R_e(x), \tag{89}$$

where ΔR_e and δR_p are given by Eqs. (67) and (68), respectively. Recalling that $\delta R_k^{(2)}$ for Case 2 is a very small quantity that is calculated by using Eq. (16), it is expected that even a weak dependence of $\varepsilon(x)$ on x would cause appreciable differences between exact and GPT results. Calculations of $\varepsilon(x)$ have indicated that this is indeed true for Case 2. Note, though, that if $\delta R_k^{(2)}$ is small compared to δR_k and/or $\delta R_k^{(1)}$, then inaccuracies in $\delta R_k^{(2)}$ will influence results for $\delta R(x)$ appreciably only if $(x - x_k)$ is large. This follows from the use of Eq. (14).

VII. C. Comparison of Taylor-GPT, GPT, and Exact Results for $\delta R(x)$

The use of the Taylor-GPT method raises questions concerning the accuracy of both the GPT and Taylor-series features. To investigate these questions, two series of comparisons were performed:

(a) First, results obtained for $\delta R_{tp}(x)$ were compared to exact values $\Delta R_e(x)$ [see Eqs. (69) and (67), respectively]. As discussed in Sec. V.A, this comparison assesses the composite accuracy of both features (i.e., second-order Taylor expansion around x_k, and use of first-order GPT) of the Taylor-GPT method.

(b) Second, results for $\delta R_{tp}(x)$ were compared to results for $\delta R_p(x)$ [see Eqs. (69) and (68), respectively]. As discussed in Sec.

V.A, this comparison assesses the accuracy of solely the Taylor series expansion feature of the Taylor-GPT method. (The inaccuracies due to the use of GPT are eliminated in this comparison.)

Tables VII through IX present the comparisons mentioned in item (a) above. These comparisons show that for values of $x - x_k$ varying from −10 cm to 20 cm, $\delta R_{tp}(x)$ and $\Delta R_e(x)$ agree within about 5%. This generally good agreement worsens only when $x - x_k$ becomes large (in absolute value), or when $\delta R(x)$ is about to change sign while going smoothly through a zero (e.g., Case 4, x = 10.5 cm, in Table IX).

Although Case 1 does not generally satisfy condition (i) of Sec. VI.B, the values of $\delta R_{tp}(x)$ obtained by using all three terms in Eq. (69) agree well, within 5%, with the exact values $\Delta R_e(x)$. Notably, this good agreement persists even at distances $x - x_k$ as large as 30 cm. As will be discussed in Sec. VII.D, the perturbation considered in Case 1 causes only a small spatial shift in the location of the maximum power density. Thus, the good overall agreement between $\delta R_{tp}(x)$ and $\Delta R_e(x)$ obtained in this case represents an additional positive verification of the adequacy of the numerical methods used in this work.

The results presented in the last two columns of Tables VII through IX also indicate that the use of only the first two terms in the Taylor expansion given by Eq. (69) is adequate when x is not very far from x_k. The generally good agreement between $\Delta R_e(x)$ and the values of $\delta R_{tp}(x)$ obtained by using this two-term expansion indicates that, in certain cases, the number of adjoint calculations may be reduced; for example, calculation of $\underline{\Gamma}_k^{*(2)}$ may not be necessary if only small to moderately large distances $x - x_k$ are of interest. Of course, the adequacy of using a two-term expan-

sion for calculating $\delta R_{tp}(x)$ also depends on the size of the perturbation. Cases 1 and 2 involve small perturbations, but Cases 3 and 4 involve larger ones. For the latter cases, the importance of the term containing $\delta R_k^{(2)}$ in Eq. (69) is illustrated in Fig. 6.

Results for the second set of comparisons, i.e., those mentioned in item (b) at the beginning of this section, are presented in Table X. For completeness, this table presents not only comparisons of $\delta R_{tp}(x)$ vs. $\delta R_p(x)$, but also includes comparisons with the exact values $\Delta R_e(x)$. Note the selection of particular combinations of perturbation cases (i.e., Cases 3 and 4 of Table II) and values of x: each combination simultaneously involves a large perturbation and a large absolute value of $x - x_k$. The reason for selecting such combinations is to deliberately accentuate the space-dependent inaccuracies, expressed by $\varepsilon(x)$ defined by Eq. (89), of using first-order GPT.

The outcome of comparing $\delta R_{tp}(x)$, $\delta R_p(x)$, and $\Delta R_e(x)$ is concisely expressed in Table X by presenting the values for TAP and TAE obtained from Eqs. (70) and (71), respectively. As expected, the nonlinear effects ignored by the Taylor-GPT method are important in these cases; this importance is clearly indicated by the large values obtained for the quantity TAE. The main contribution to these nonlinear effects, though, arises from the GPT component of the Taylor-GPT method. This fact is indicated by the small values obtained for the quantity TAP, which show that the Taylor-GPT results agree closely with the GPT results. These characteristics are further highlighted in Fig. 6, which shows that, even though the GPT results differ from the exact ones by as much as 50%, the Taylor-GPT and GPT results agree within 4% for a large range of distances x. This indicates that whenever the GPT method is sufficiently accurate, the use of

the Taylor-GPT method could substantially reduce the number of calculations for investigations of space-dependent response variations.

VII. D. Spatial Shifts, and Their Influence on Peak Power Density Sensitivities

Perturbations in nuclear data alter not only the maximum value taken on by the power density, but also cause spatial shifts in the location of this maximum. To calculate these shifts by using the Taylor-GPT method, it is convenient to rewrite Eq. (75) as

$$x_{m1} - x_{m0} = - \frac{R_0^{(1)}}{R_0^{(2)}} \cdot \frac{\delta R^{(1)}/R^{(1)} - \delta R^{(2)}/R^{(2)}}{1 + \delta R^{(2)}/R^{(2)}} . \qquad (90)$$

Table XI presents numerical values for the spatial shifts (i.e., $x_{m1} - x_{m0}$) caused by the perturbations described in Cases 1 through 4. "Direct," "indirect," and "total" contributions were calculated by using the Taylor-GPT method. The respective contributions are denoted in Table XI by $S_{tp,D}$, $S_{tp,I}$, and $S_{tp,T}$, and were obtained by replacing the quantity $\delta R^{(i)}$ in Eq. (90) with $\delta R_D^{(i)}$, $\delta R_I^{(i)}$, and $(\delta R_D^{(i)} + \delta R_I^{(i)})$, respectively.

Recall that Eq. (90) has inaccuracies stemming from the use of both first-order GPT and second-order Taylor expansion in x. Inaccuracies due to the use of first-order GPT in Eq. (90) can be assessed by using perturbed data to recalculate the response $R_1(x)$. The numerical values of $R_1(x)$ thus obtained have been examined to determine the grid location x_{k1} at which the largest discrete value of $R_1(x)$ occured. Except for very small shifts, x_{k1} is not generally expected to coincide with x_k. (Recall that x_k denotes the location where the largest discrete value of the

unperturbed response occured.)

Using now the same procedure as that leading to Eq. (74) but with x_{k1} replacing x_k gives

$$x_{m1}-x_{k1} = -\frac{R_1^{(1)}(x_{k1})}{R_1^{(2)}(x_{k1})} . \tag{91}$$

Equation (91), rather than Eq. (74), is now used to determine x_{m1}; this is because, although, both equations stem from Taylor series truncated at the third order terms, the truncation errors in Eq. (91) are smaller than those in Eq. (74) since, in general, $|x_{m1}-x_{k1}| < |x_{m1}-x_k|$. Furthermore, it is expected that this procedure will in general allow determination of x_{m1} within an accuracy comparable to that of determining x_{m0} from Eq. (73).

The results shown in Table XI in the row labeled $S_{e,T}$ are the numerical values of $(x_{m1}-x_{m0})$ where x_{m1} and x_{m0} are obtained from Eqs. (91) and (73), respectively. A comparison between these results and the corresponsing results shown in the row labelled $S_{tp,T}$ indicates the magnitude of effects arising fron the use of firt-order GPT in Eq. (90).

The indirect contributions (i.e., $S_{tp,I}$) are generally preponderant; the direct contributions $S_{tp,D}$ are zero for Cases 3 and 4, and are still much smaller than $S_{tp,I}$ for Case 2. Only for Case 1, which involves a very small shift, are the values of $S_{tp,I}$ and $S_{tp,D}$ comparable.

The results presented in the last row of Table XI show that shifts predicted by the Taylor-GPT method agree well with the exact ones for distances between approximately 0.15 cm and 5 cm. For Case 3, which represents a perturbation so large that it effectively transforms the heterogeneous core into a homogeneous one, the shift predicted by the

Taylor-GPT method substantially overestimates the actual shift. This highlights the importance of the nonlinear terms that are neglected by first-order GPT.

The influence of spatial shifts on the sensitivity of peak-power density has been discussed in Sec. V.C. This influence is characterized by the quantity SE defined by Eq. (86). Note that the results for SE are subject to inaccuracies associated with Eqs. (73) and (91) which are used to determine the locations x_{m0} and x_{m1}, respectively. Table XII shows that the error caused by the shift in the location of the maximum power is small for Cases 1 and 2. For larger perturbations, e.g. Cases 3 and 4, the effect of the spatial shift on the sensitivity is appreciable and cannot be neglected.

VIII. SUMMARY AND CONCLUSIONS

This work has presented an efficient method to investigate one-dimensional, space-dependent variations $\delta R(x)$ in the power density $R(x)$. This method has been called the Taylor-GPT method in order to highlight its two main characteristics: (a) use of a Taylor series expansion of $\delta R(x)$ in the spatial variable x, and (b) use of first-order generalized perturbation theory (GPT)[1-4] to efficiently evaluate the derivative operators that appear as coefficients in this Taylor series.

Equations satisfied by the importance (i.e., adjoint) functions for the i-th spatial derivative of $\delta R(x)$ have been derived within the framework of GPT. Using finite differences, it has been shown that these equations can be solved in a straightforward manner with existing GPT codes to obtain the importance functions. The main characteristics of these importance functions have been highlighted analytically by deriving certain relationships that they satisfy. A deeper understanding of these characteristics has been facilitated by deriving the complete analytical expressions of the importance functions for an illustrative (one-region, one-group) reactor model.

It has been shown that the Taylor-GPT method is efficient not only for estimating space-dependent variations in the power density, but also for estimating spatial shifts that parameter perturbations induce in the peak power density. To illustrate its usefulness, this method has been applied to four test cases involving a simplified three-region one-dimensional model of a heterogeneous LMFBR. The results given by the Taylor-GPT method have been compared to those produced by the standard GPT method, and both have been verified by comparisons to exact results

(obtained by actual recalculations with altered parameter values).

These comparisons indicate that the results given by the Taylor-GPT method are practically as accurate as those given by the standard GPT method. The Taylor-GPT method includes all the advantages offered by adjoint methods, e.g., the same importance functions are used to assess the effects on the response of many parameter perturbations. In addition, the Taylor-GPT method could substantially reduce (even by comparison to standard GPT) the number of calculations for investigations of space-dependent variations in the power density. Note, though, that the Taylor-GPT method does not account for second- and higher-order effects of parameter variations. Nevertheless, the Taylor-GPT method provides detailed information regarding specific contributions (e.g., due to leakage, absorption) to the overall variation in the response. The availability of such detailed information is valuable for systematic and efficient reactor design studies.

References and Footnotes

1. A. Gandini, J. Nucl. Energy, 21, 755 (1967).

2. G.P. Cecchini and M. Salvatores, Nucl. Sci. Eng., 46, 304 (1971).

3. J.H. Marable, C.R. Weisbin, and G. De Saussure, Nucl. Sci. Eng., 75, 30 (1980).

4. C.R. Weisbin et al., Sensitivity and Uncertainty Analysis of Reactor Performance Parameters, Advances in Nuclear Science and Technology, J. Lewins and M. Becker, Eds., Vol. 14, Plenum Pess, New York (1982); see, in particular, chapter 5 by E. Greenspan.

5. J.M. Kallfelz, D. Biswas, C.L. Cowan, J.H. Marable, M.L. Williams, C.R. Weisbin, J.D. Drischler, T.B. Fowler, and J.R. White, "Design and Sensitivity Analysis of a CDS-Type LMFBR Heterogeneous Core," in 1980 Advances in Reactor Physics and Shielding, p. 467, American Nuclear Society (1980).

6. J.H. Marable, D. G. Cacuci, C.R. Weisbin, J.R. White, D. Biswas, J.M. Kallfelz, C.L. Cowan, and R. Protsik, "Sensitivities and Uncertainties of a Large LMFBR Using Adjusted Cross Section Library ORACLE-1", Proc. Topical Meeting on Advances in Reactor Physics and Core Thermal Hydraulics, Kiamesha Lake, New York, Sept. 22-24, 1982, NUREG/CP-0034, Vol. 2, pp. 1120-1134, U.S. Nucl. Reg. Com., Washington, D.C. (1982).

7. D.G. Cacuci, J. Math. Phys., 22, 2794 (1981).

8. D.G. Cacuci, J. Math. Phys., 22, 2803 (1981).

9. V.A. Perone, J.M. Kallfelz, and L.A. Belblidia, Nucl. Sci. Eng., 79, 326 (1981).

10. L.A. Belblidia, A. Gandini, J.M. Kallfelz, and V.A. Perone, Trans. Am. Nucl. Soc., 39, 957 (1981).

11. A.F. Henry, Nuclear-Reactor Analysis, MIT Press, Cambridge, Mass., (1975).

12. D.G. Cacuci, P.J. Maudlin, and C.V. Parks, "Adjoint Sensitivity Analysis of Extremum-Type Responses in Reactor Safety", Nucl. Sci Eng., 83, 112 (1983).

13. A Gandini, Nucl. Sci. Eng., 77, 316 (1981).

14. In ref. 15, Cacuci et al. considered the heat conduction equation, and gave examples of the importance function for the first derivative of the temperature.

15. D.G. Cacuci, C.F. Weber, E.M. Oblow, and J.H. Marable, Nucl. Sci. Eng., 75, 88 (1980).

16. I. Dal Bono, "TAIM-Multigroup Diffusion Code," Doc. CEC(66)12, Comitato Nazionale per L'Energia Nucleare (1966).

17. I. Dal. Bono, V. Leproni, and M. Salvatores, "The CIAP-1D Code," RT/FI(68)9, Comitato Nazionale per L'Energia Nucleare (1968).

18. I. Dal Bono, V. Leproni, and M. Salvatores, "The GLOBPERT-1D Code," RT/FI(68)10, Comitato Nazionale per L'Energia Nucleare (1968).

19. Such a model has also been used by Pomraning[20] to analyze, via a variational approach, the behavior of the peak-to-average power density. Note, though, that this quantity is not the same as our R_k.

20. G. C. Pomraning, J. Nucl. Energy, 21,285 (1967).

21. A.H. Zemanian, Distribution Theory and Transform Analysis, McGraw-Hill, New York (1965).

22. J.M. Kallfelz, G.B. Bruna, G. Palmiotti and M. Salvatores, Nucl. Sci. Eng., 62, 304 (1977).

23. T.B. Fowler and D.R. Vondy, "Nuclear Reactor Analysis Code: CITATION," ORNL-TM-2496, Rev. 2, Oak Ridge National Laboratory (1971).

24. E.M. Oblow, "Reactor Cross-Section Sensitivity Studies in Critical Reactors Using Transport Theory," ORNL-TM-4437, Oak Ridge National Laboratory (1974).

25. W.G. Davey and A.L. Hess, "Additional Fast Reactor Benchmarks for Phase II Data Testing of ENDF/B," CSEWG Newsletter 18, Cross Section Evaluation Working Group (March 1969).

APPENDIX A

APPLICATION OF THE ITALIAN GPT CODE PACKAGE TO CALCULATE SPATIAL DERIVATIVES OF $\delta R(x)$

A. 1. Calculation of $\Gamma^{*(i)}$

In general, the solution to the adjoint problem is computed by CIAP[17] for ratios of the form:

$$R_0 = \frac{\int_{V_1} \sum_j \Sigma_{1,j}(x)\ \phi_j(x)\ dx}{\int_{V_2} \sum_j \Sigma_{2,j}(x)\ \phi_j(x)\ dx} \quad . \tag{A-1}$$

Eq. (A-1) can be cast in a form amenable to calculate $\delta R^{(i)}/R^{(i)}$ by simply preparing, as indicated below, the input data for the adjoint source.

The energy-production cross sections in the numerator and denominator of Eq. (A-1) are written as

$$\Sigma_{1,j}(x) = \sum_k p^k\ N_1^k(x)\ \sigma_{f,j}^k \ , \tag{A-2}$$

and

$$\Sigma_{2,j}(x) = \sum_k p^k\ N_2^k(x)\ \sigma_{f,j}^k \ , \tag{A-3}$$

respectively, where N_i^k denotes densities for nuclide k. Subscripts 1 and 2 in N_1^k and N_2^k, respectively, allow for potentially distinct spatial behavior of the energy-production cross sections. With these specifications,

CIAP computes the desired $\underline{\Gamma}^{*(i)}$ if the densities are chosen in the following manner:

(a) $N_2^k(x) = N_m^k$ for all x in region m, m=1, M

(b) for $\underline{\Gamma}^{*(1)}$ calculations:

$$N_1(x) = \begin{cases} +N_{m0}, & \text{for } x=x_{k+1} \text{ and } x \in m0 \\ -N_{m0}, & \text{for } x=x_{k-1} \text{ and } x \in m0 \\ 0.0, & \text{elsewhere} \end{cases}$$

(c) for $\underline{\Gamma}^{*(2)}$ calculations:

$$N_1(x) = \begin{cases} +N_{m0}, & \text{for } x=x_{k+1},\ x_{k-1} \text{ and } x \in m0 \\ -2N_{m0}, & \text{for } x=x_k \text{ and } x \in m0 \\ 0.0, & \text{elsewhere} \end{cases}$$

Here, m and M refer, respectively, to the region number and the number of regions, m0 denotes the number of the region where the peak power occurs, and N_m^k and N_{m0}^k are the densities of nuclide k in regions m and m0, respectively.

Note that CIAP includes the volumes associated with the mesh points in the integrations over space. But, as long as the mesh spacing is uniform in the vicinity of x_k, this does not affect the values of the fractional variation of the derivatives. Note also that CIAP attaches a factor of 0.5 to the contribution of a point to the integral value if the contribution of the point preceding it or the point following it is zero. To guard against this, one must use a very small value for the input density (of the order of 10^{-14}) at x_{k-2} and x_{k+2}.

A.2. Direct-Effect Calculations

The code GLOBPERT-1D[18] can be used to calculate the direct-effect component of $\delta R^{(i)}/R^{(i)}$. For this purpose, the input data for the direct-effect calculations must be prepared as follows:

(a) for $\delta R^{(1)}/R^{(1)}$ calculations,

$$\delta N = \begin{cases} +\delta N_i, & x=x_{k+1} \\ -\delta N_i, & x=x_{k-1} \\ 0.0, & \text{elsewhere} \end{cases}$$

(b) for $\delta R^{(2)}/R^{(2)}$ calculations,

$$\delta N = \begin{cases} +\delta N_i, & x=x_{k+1}, \text{ or } x=x_{k-1} \\ -2\delta N_i, & x=x_k \\ 0.0, & \text{elsewhere} \end{cases}$$

Here, δN_i denotes the density change for nuclide i and effected in the quantity $Q_{l,k}$ [see Eq. (22)].

Also note that GLOBPERT-1D was modified to treat more accurately the interfaces between regions. In addition, an algorithm was implemented to calculate δD (i.e., the perturbation in the diffusion coefficient) exactly, rather than via a first-order expansion in $\delta\Sigma_{tr}$ as done in the original version of this code.

APPENDIX B

DETERMINATION OF $\Gamma_1^{*(2)}$

In view of Eqs. (45) and (51), the function $\Gamma_1^{*(2)}$ is the solution of

$$\left.\begin{aligned} &\frac{d^2\,\Gamma_1^{*(2)}}{dx^2} + B^2\,\Gamma_1^{*(2)} = \frac{1}{DQ_2} - \frac{1}{DQ_{1,2}}\,\delta''(x - x_k) \\ &\Gamma_1^{*(2)} = 0 \quad \text{at } x = L \\ &\frac{d\Gamma_1^{*(2)}}{dx} = 0 \text{ at } x = 0 \end{aligned}\right\} \tag{B.1}$$

Applying a Laplace-transform to Eq. (B.1), and defining

$$U(p) = \int_0^\infty e^{-px}\,\Gamma_1^{*(2)}\,dx, \tag{B.2}$$

gives

$$U(p) = K\,\frac{p}{p^2+B^2} - \frac{1}{DQ_{1,2}}\,\frac{p^2\exp(-px_k)}{p^2+B^2} + \frac{1}{DQ_2}\,\frac{1}{p(p^2+B^2)}, \tag{B.3}$$

where K is, at this stage, an unknown constant to be determined.

Taking the inverse Laplace-transform of Eq. (B.3) gives

$$\Gamma_1^{*(2)} = K\cos Bx + \frac{1}{B^2 DQ_2}\,(1-\cos Bx)$$

$$- \frac{1}{DQ_{1,2}}\left[\delta(x-x_k) - B\,H(x-x_k)\,\sin B(x-x_k)\right] . \qquad (B.4)$$

For a critical reactor, the boundary conditions given in Eq. (B.1) are automatically satisfied; thus, the constant K is determined by using the orthogonality condition given in Eq. (88). This leads to

$$K = \frac{1}{B^2 DQ_2}\left(1 - \frac{2}{BL}\right) + \frac{B}{DQ_{1,2}}\left(\frac{\cos Bx_k}{BL} + \frac{L - x_k}{L}\sin Bx_k\right) . \qquad (B.5)$$

Replacing Eq. (B.5) in Eq. (B.4) yields

$$\Gamma_I^{*(2)} = \frac{1}{B^2 DQ_2} + \left[\frac{\cos Bx_k + B(L-x_k)\sin Bx_k}{LDQ_{1,2}} - \frac{2}{DB^3 LQ_2}\right]\cos Bx$$

$$+ \frac{B}{DQ_{1,2}}\,H(x-x_k)\sin B(x-x_k) - \frac{\delta(x-x_k)}{DQ_{1,2}} . \qquad (B.6)$$

TABLE I

Nuclide Concentrations for Test Model

Nuclide	Concentration [10^{24} atom/cm^3]	
	Driver	Blankets (IB,EB)
U-238	0.006	0.012
Pu-239	0.001	0.0
Na	0.010	0.007

TABLE II

Selected Perturbations and Corresponding Test Cases

Case	Zonal Perturbation[a]		
	Int. Blkt. (IB)	Driver (D)	Ext. Blkt. (EB)
1		$\frac{\delta N^{49}}{N^{49}} = -3\%$	$\delta N^{49} = +0.045\ N_D^{49}$
2	$\frac{\delta N^{28}}{N^{28}} = +5\%$	$\frac{\delta N^{49}}{N^{49}} = -5\%$	$\frac{\delta N^{28}}{N^{28}} = +5\%$
3	Replaced with driver.	Inner boundary extended to core center (x=0).	
4	Outer three cm replaced with driver	Inner boundary extended to x=7.5 cm.	

a. N_x^{yz} is the number density in zone x of the nuclide with the last digits in its atomic number and weight of y and z, respectively. If no x appears, N is for the zone designated by the column heading. N values are given in Table I.

TABLE III

GPT and Exact $\delta R^{(i)}(x_k)$ Results for Case 1[a-e]

Derivative Order, i	GPT Results for $\delta R^{(i)}/R^{(i)}$			$\delta R_p^{(i)}$ (GPT)	$\Delta R_e^{(i)}$ (Exact)[g]	$\frac{\text{GPT-Exact}}{\text{Exact}}$ [%]
	Direct[f]	Indirect[f]	Total			
0	-9.16-3	-2.25-3	-1.14-2	-3.56-4	-3.69-4	-3.7
1	+2.26+1	+2.97-1	+5.23-1	+2.71-6	+2.88-6	-5.8
2	-3.59-3	-1.16-2	-1.52-2	+2.86-7	+3.04-7	-5.8

a. All values are for x_k = 22.5 cm.

b. Because of the characteristics of CIAP, R has a ΔVol factor of 1.5 cm^3 in the numerator which is not contained in Eq. (9).

c. Read ±x-y as ±x . 10^{-y}.

d. See Table II for description of perturbation cases.

e. Values presented in the last three columns are calculated with more significant figures than shown.

f. See discussion of Eq. (7).

g. Exact value determined from two direct calculations; see Eq. (67).

TABLE IV

GPT and Exact $\delta R^{(i)}$ Results for Case 2.[a]

Derivative Order, i	GPT Results for $\delta R^{(i)}/R^{(i)}$ Direct	Indirect	Total	$\delta R_p^{(i)}$ (GPT)	$\Delta R_e^{(i)}$ (Exact)	$\frac{\text{GPT-Exact}}{\text{Exact}}$ [%]
0	5.41-4	2.59-3	3.13-3	9.77-5	9.09-5	7.4
1	3.93-1	-2.17+0	-1.78+0	-9.21-6	-9.05-6	7.7
2	9.82-3	-7.26-3	2.55-3	-4.80-8	-3.4-8	39.

a. See footnotes for Table III

Table V

GPT and Exact $\delta R^{(i)}$ Results Case 3.[a]

Derivative Order, i	GPT Results for $\delta R^{(i)}/R^{(i)}$ Direct	Indirect	Total	$\delta R_p^{(i)}$ (GPT)	$\Delta R_e^{(i)}$ (Exact)	$\frac{\text{GPT-Exact}}{\text{Exact}}$ [%]
0	-1.59-1	3.78-2	-1.21-1	-3.79-3	-3.79-3	-0.14
1	-1.59-1	-5.44+1	-5.46+1	-2.83-4	-2.14-4	32.
2	-1.59-1	-4.52-1	-6.11-1	1.15-5	1.00-5	14.

a. See footnotes for Table III.

Table VI

GPT and Exact $\delta R^{(i)}$ Results for Case 4.[a]

Derivative Order, i	GPT Results for $\delta R^{(i)}/R^{(i)}$ Direct	Indirect	Total	$\delta R_p^{(i)}$ (GPT)	$\Delta R_e^{(i)}$ (Exact)	$\frac{\text{GPT-Exact}}{\text{Exact}}$ [%]
0	-4.54-2	1.14-2	-3.39-2	-1.06-3	-1.05-3	0.75
1	-4.54-2	-1.58+1	-1.58+1	-8.19-5	-7.64-5	7.2
2	-4.54-2	-1.31-1	-1.76-1	3.32-6	3.22-6	3.1

a. See footnotes for Table III.

TABLE VII

Taylor-GPT and Exact $\delta R(x)$ Results[a] for Case 1;[b] x_k = 22.5 cm

x [cm]	$x-x_k$ [cm]	Exact[c] ΔR_e	Taylor-GPT[d] δR_{tp}	$\frac{\delta R_{tp} - \Delta R_e}{\Delta R_e}$ [%][d]	
				3-term[e]	2-term[f]
13.5	-9	-3.84-4	-3.69-4	-4.0	-1.0
16.5	-6	-3.82-4	-3.67-4	-3.9	-2.5
25.5	+3	-3.60-4	-3.46-4	-3.7	-3.3
28.5	+6	-3.47-4	-3.34-4	-3.6	-2.1
34.5	+12	-3.13-4	-3.02-4	-3.3	+3.2
40.5	+18	-2.68-4	-2.61-4	-2.9	+14.
52.5	+30	-1.53-4	-1.46-4	-4.9	+79.

a. Read $\pm x-y$ as $\pm x \cdot 10^{-y}$.

b. See Table II for description of test cases.

c. Exact value determined from two direct calculations; see Eq. (67).

d. Values presented in the last three columns are calculated with more significant figures than shown.

e. Values for δR_{tp} obtained by using all three terms in Eq. (69).

f. Values for δR_{tp} obtained by using only the first two terms in Eq. (69).

TABLE VIII

Taylor-GPT and Exact Results[a] for Case 2; x_k = 22.5 cm

x [cm]	$x-x_k$ [cm]	Exact ΔR_e	Taylor-GPT δR_{tp}	$\frac{\delta R_{tp} - \Delta R_e}{\Delta R_e}$ [%]	
				3-term	2-term
10.5	-12	+1.93-4	+2.05-4	+6.0	+8.
13.5	-9	+1.69-4	+1.79-4	+5.4	+7.
16.5	-6	+1.44-4	+1.52-4	+5.5	+6.
19.5	-3	-	+1.25-4	-	-
25.5	+3	-	+6.98-5	-	-
28.5	+6	+3.64-5	+4.16-5	+14.	+17.
34.5	+12	-1.71-5	-1.63-5	-4.9	-25.
40.5	+18	-6.79-5	-7.59-5	+12.	+0.3
52.5	+30	-1.57-4	-2.00-4	+27.	+13.

a. See footnotes for Table VII.

TABLE IX

Taylor-GPT and Exact Results[a] for Case 4; x_k = 22.5 cm

x [cm]	$x-x_k$ [cm]	Exact ΔR_e	Taylor-GPT δR_{tp}	$\frac{\delta R_{tp} - \Delta R_e}{\Delta R_e}$ [%]	
				3-term	2-term
10.5	-12	+8.32-5	+1.63-4	+96.	+190.
13.5	-9	-2.38-4	-1.87-4	-21.	+35.
16.5	-6	-5.36-4	-5.07-4	-5.	+6.
19.5	-3	-	-7.98-4	-	-
25.5	+3	-	-1.29-3	-	-
28.5	+6	-1.45-3	-1.49-3	+3.	+7.
34.5	+12	-1.73-3	-1.80-3	+4.	+18.
40.5	+18	-1.88-3	-2.00-3	+6.	+34.
52.5	+30	-1.81-3	-2.02-3	+12.	+94.

a. See footnotes for Table VII.

TABLE X

Comparisons of $\Delta R_e(x)$, $\delta R_p(x)$, and $\delta R_{tp}(x)$ for Large Perturbations and Large $|x - x_k|$

Perturbation Case	x [cm]	TAP[a] [%]	TAE[b] [%]
4	13.5	-3.7	-22.
4	40.5	+1.9	+6.3
3	13.5	-3.3	-47.
3	40.5	+2.0	+17.

a. See Eq. (70).

b. See Eq. (71).

TABLE XI

Spatial Shifts [cm] in Location of Peak Power

Shifts[a]	Case 1	Case 2	Case 3	Case 4
$S_{e,T}$	+0.160	-0.482	-22.8	-4.85
$S_{tp,T}$[b]	+0.151	-0.490	-38.2	-5.23
$S_{tp,I}$	+0.086	-0.601	-27.1	-4.96
$S_{tp,D}$	+0.064	+0.105	0.0	0.0
$S_{tp,I}+S_{tp,D}$	+0.150	-0.496	-27.1	-4.96
$\frac{S_{tp,T}-S_{e,T}}{S_{e,T}}$	-5.6%	+1.7%	+67.8%	+8.0%

a. Shifts are defined in Sec. VII.D.

b. $S_{tp,T}$ differs slightly from $(S_{tp,I} + S_{tp,D})$ because the sum neglects the second-order terms mentioned immediately after Eq. (80).

TABLE XII

Influence of the Spatial Shift on the Peak-Power Density

Case	SE[a] [%]
1	0.009
2	-0.029
3	-63.5
4	-17.0

a. See Eq. (86).

LIST OF FIGURES

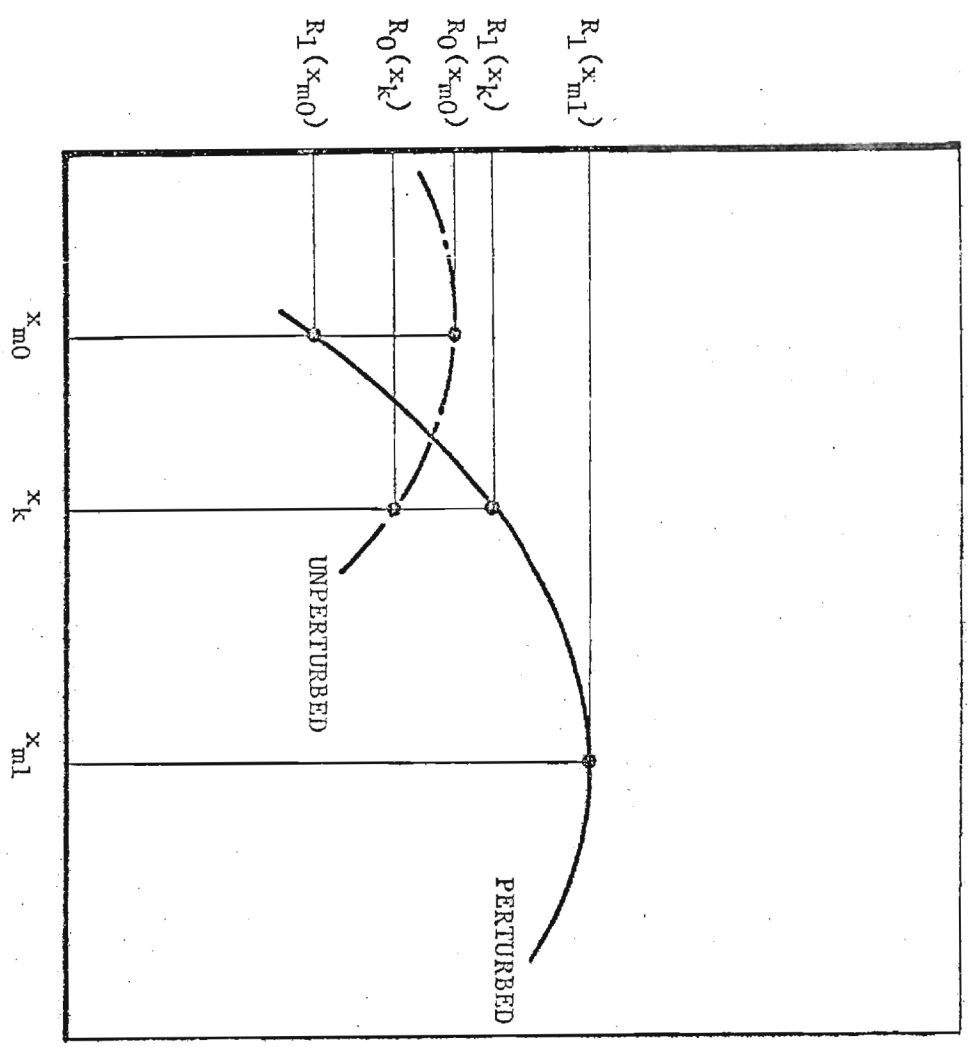

Belblidia et al., "Generalized Perturbation Theory with Derivative Operators for Power Density Investigations," Figure 1.

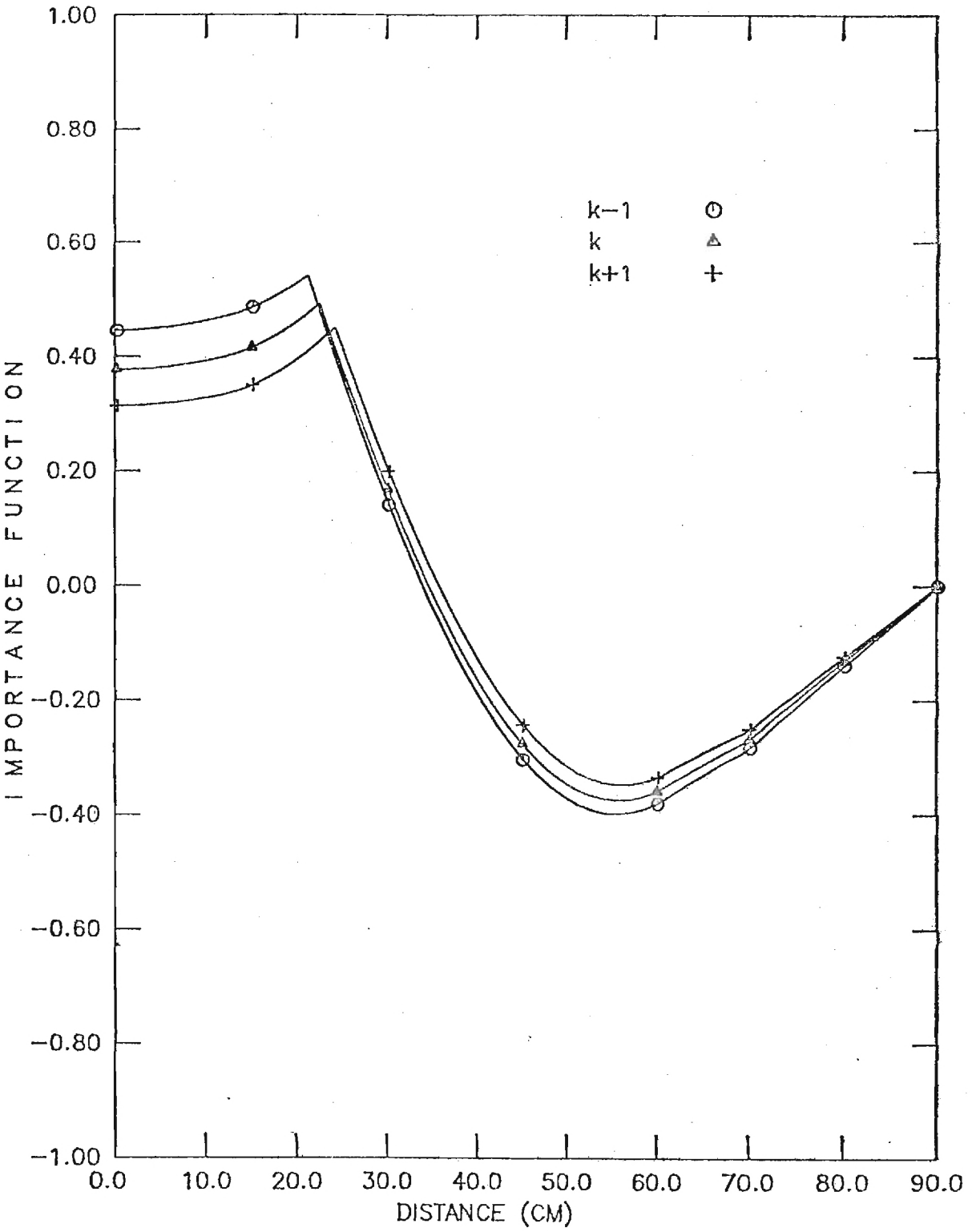

Belblidia et al., "Generalized Perturbation Theory with Derivative Operators for Power Density Investigations,"

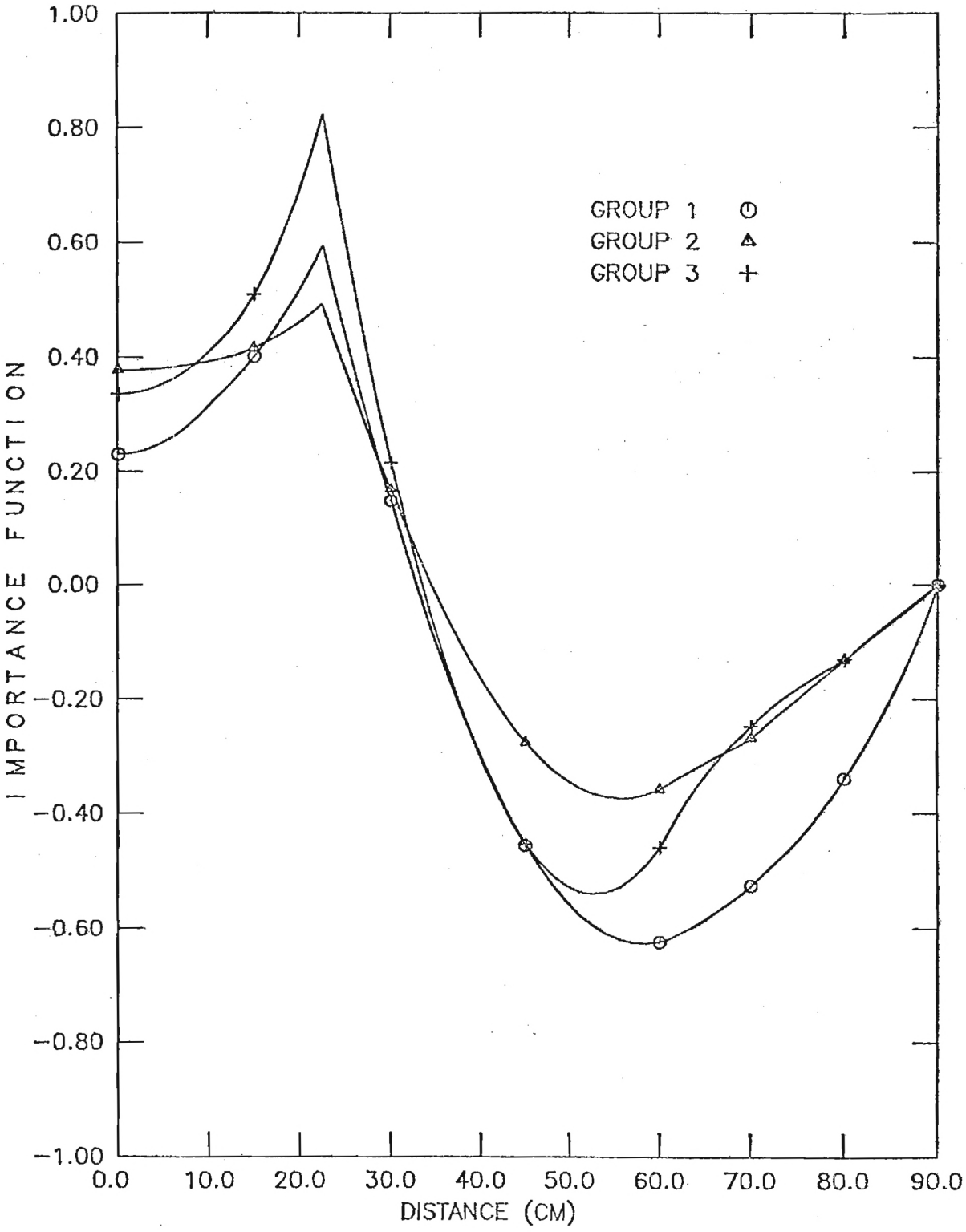

Belblidia et al., "Generalized Perturbation Theory with Derivative Operators for Power Density Investigations,"
Figure 3.

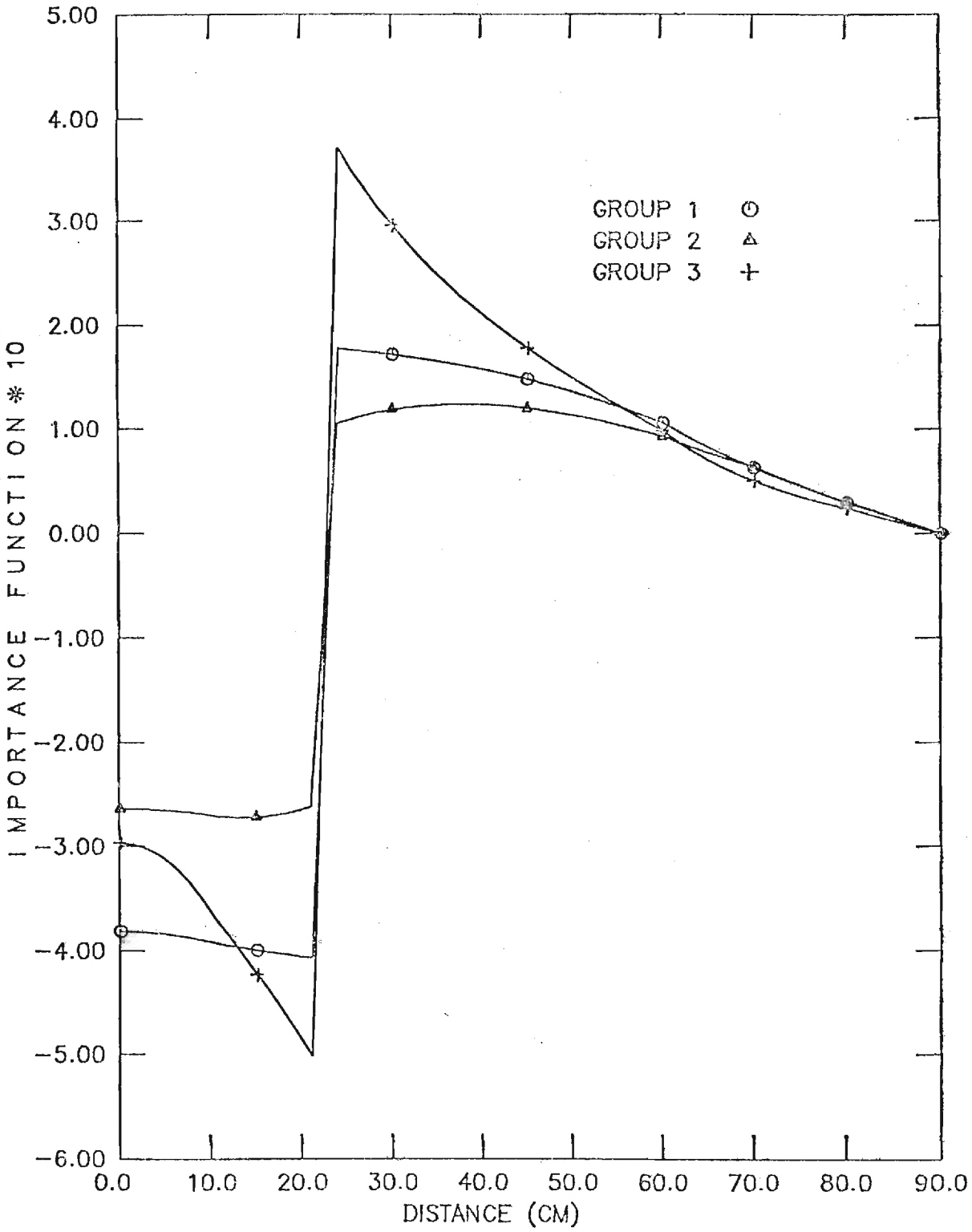

Belblidia et al., "Generalized Perturbation Theory with Derivative Operators for Power Density Investigations,"

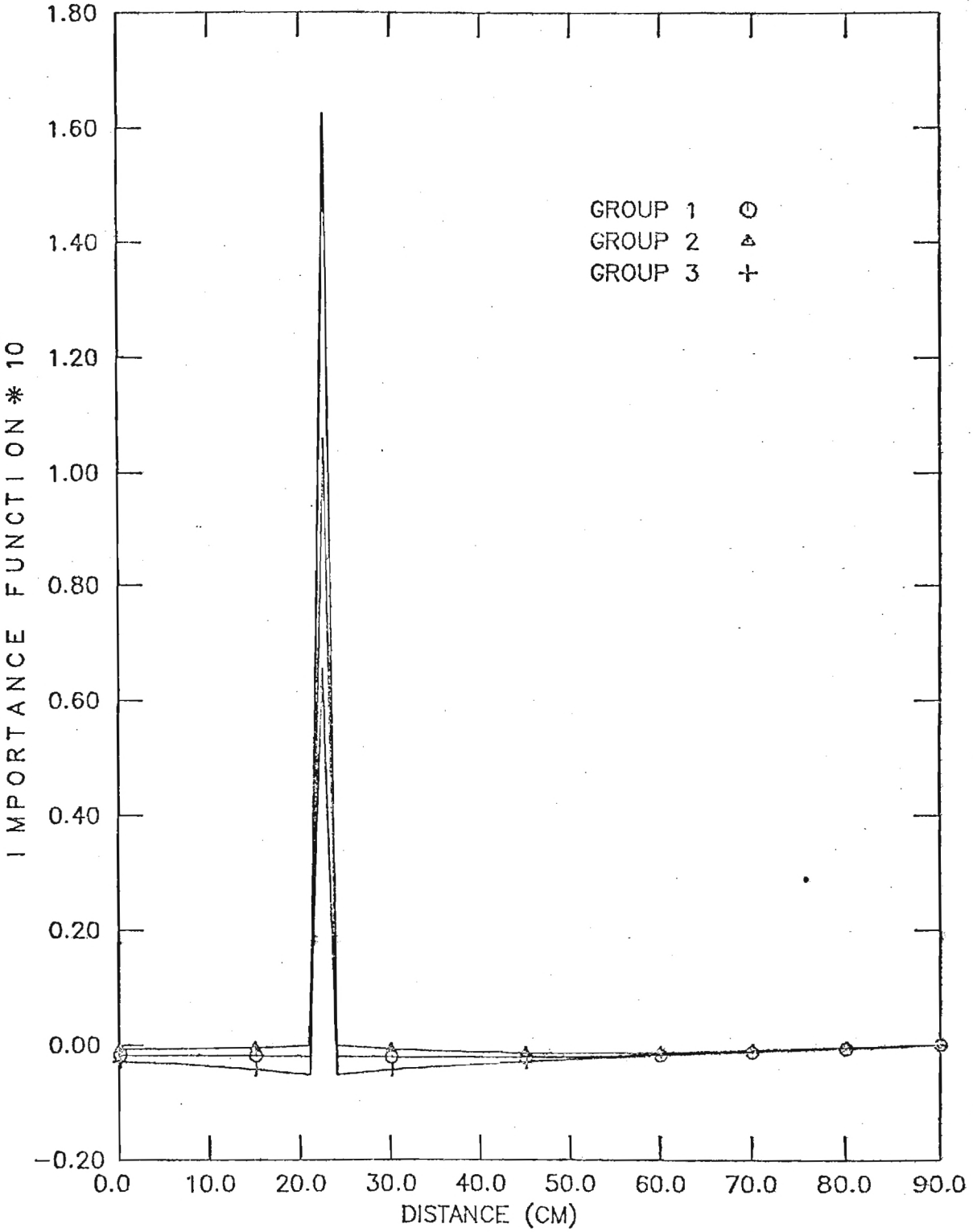

Belblidia et al., "Generalized Perturbation Theory with Derivative Operators for Power Density Investigations," Figure 5.

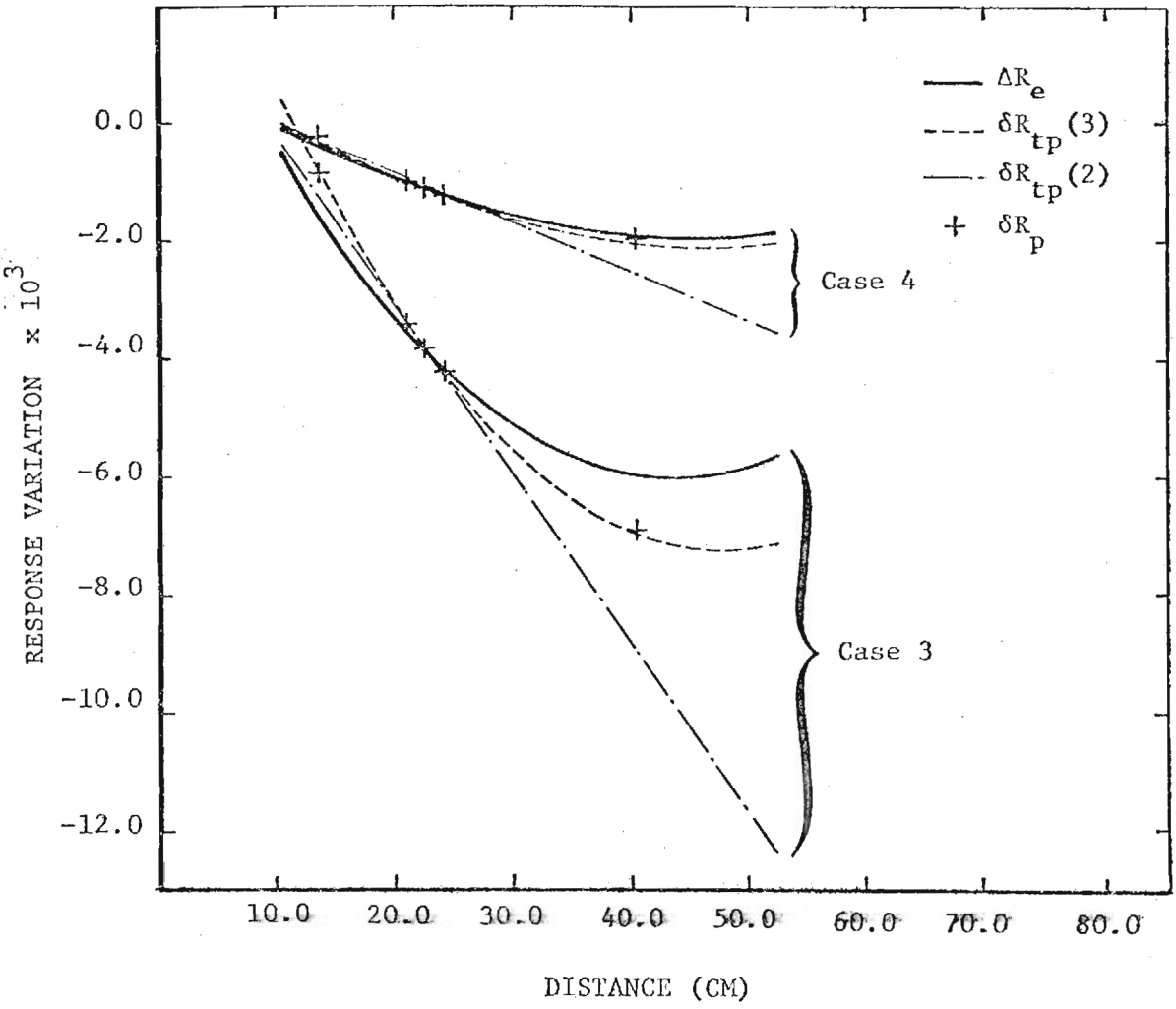

Bellidia et al., "Generalized Perturbation Theory with Derivat[illegible] Operators for Power Density Investigations,"

E26-B03

Georgia Institute of Technology
A UNIT OF THE UNIVERSITY SYSTEM OF GEORGIA
SCHOOL OF NUCLEAR ENGINEERING AND HEALTH PHYSICS
ATLANTA, GEORGIA 30332
(404) 894-3720

August 9, 1983

MEMORANDUM

TO: C. R. Weisbin and D. G. Cacuci (ORNL)

FROM: J. M. Kallfelz and L. A. Belblidia

SUBJECT: Progress Report for ORNL Subcontract 7802
Months of April, May and June 1983

No activity on the project occured for the above report period because of staffing problems.

JMK/vw

E26-B03

Georgia Institute of Technology
A UNIT OF THE UNIVERSITY SYSTEM OF GEORGIA
SCHOOL OF NUCLEAR ENGINEERING AND HEALTH PHYSICS
ATLANTA, GEORGIA 30332
(404) 894-3720

August 9, 1983

MEMORANDUM

TO: D. G. Cacuci, C. R. Weisbin and B. A. Worley (ORNL)

FROM: J. M. Kallfelz

SUBJECT: Progress Report for ORNL Subcontract 7802
Period July 1 - August 1, 1983

Accomplishments During Report Period

- A survey was performed of literature pertinent to the development of an on-line power distribution and reactivity monitor (PDRM) (1-24). Based on this survey and discussions with various individuals, a brief memo containing comments on this topic was prepared (25).

- I visited ORNL on August 1 for a project meeting with John Lewellen to discuss plans and priorities for next year's work, and in particular PDRM development.

Plans for Work for Next Month

- The literature survey and discussions with various individuals concerning PDRM development will be continued. As requested by Dan Cacuci, I will prepare a brief statement describing the potential of PDRMs for improving the economics and safety of large LMFBRs. This statement is for inclusion in information to be transmitted to John Lewellen.

JMK/vw

REFERENCES

1. B. Frogner, A. Ipaktchi and A. B. Long, "Model Calibration Methods for the BWR Hybrid Power Shape Monitoring System," Paper presented at ANS/ENS Int. Topical Mtg. on Adv. in Math. Meth. for Nucl. Engr. Probs., Munich, Apr. 27-29, 1981.

2. H. A. Larson and B. R. Peterson, "The EBR-II Reactivity Meter: Conceptual Design," ANL-79-52, Argonne Nat. Lab.

3. "Status Report on the On-Line Core Physics Simulator Cygnus," HWR-26, OECD Halden Reactor Project, Institutt for Energiteknikk, Halden, Norway.

4. "Core Surveillance Systems: Development at the Halden Project and Within Signatory Organizations," HWR 32, (as ref. 3).

5. "The Core Surveillance System Scorpio," HWR-56, (as ref. 3).

6. "A Description of the Two-Point Model Used as Strategy Generator in the Core Surveillance System Scorpio," HWR-79 (as ref. 3).

7. C. Bertin et al., "Superphenix Core Surveillance and Protection System," Proc. Internat. Topical Mtg. on LMFBR Safety and Related Design and Operational Aspects, Lyon, France, July 19-23, 1982.

8. B. Berthet et al., "Operation Experience of A Reactivity Balance Meter at Rapsodie," (same as Ref. 7).

9. "Cooperative Nuclear Data and Methods Development, Fiscal Year 1982," GEFR-14073-8 (see section 3.3) Sept. 1982.

10. J. H. Marable, "Tel. Conversation with Charlie Cowan," memo to M. L. Williams et al. dated Mar 1981.

11. J. H. Marable, "On-Line Power Distribution and Reactivity Monitoring," Memo to D. G. Cacuci dated Jan. 18, 1983.

12. C. L. Cowan, telecom with J. Kallfelz dated April 18, 1983.

13. C. L. Cowan, telecom with J. Kallfelz dated July 28, 1983.

14. D. Meneghetti, telecom with with J. Kallfelz dated July 28, 1983.

15. D. Meneghetti, "Reactivity Feebacks of EBR-II," Trans. ANS 44, 515 (June 1983)

16. All papers in Spec Session: "Reactivity Feedbacks of LMFBRs at Power: Prediction & Monitoring Techniques," organized by J. Daughtry (FFTF) Trans. ANS 44 513-519.

17. H. Yamamoto et al., "Reactor Physics Characteristics from Operations Testing of the JOYO Experimental Reactor," in 1980 Advances in Reactor Physics and Shielding ANS, p. 199 (1980).

18. B. Guillemard et al., "Start-up and Initial Operating Experience of Phenix," in J. Kallfelz and R. Karam, eds., Advanced Reactors: Physics, Design and Economics, Pergamon, 1975. (p. 747).

19. All papers in section 2, "Physics of Operating Fast Reactors," in Fast Reactor Physics 1979, Vol. 1, IAEA, 1980 (p. 395-496).

20. J. J. Wagschal et al., "LWR-PV Damage Estimate Methodology," 1980 Advances in Reactor Physics and Shielding, ANS, 1980 (p. 612-624).

21. G. F. Flanagan et al., "Analysis of Stored Fuel, Control Rod and Inherent Source Effects on the CRBR Ex-Vessel Source Range Monitoring System," in same book as Ref 18., p. 699.

22. Special Session: "New Computer Technology's Impact on Mathematics and Computation," organized by N. Hmeck. Trans. ANS 44, p. 267 (1983).

23. D. Cacuci et al., "Developments in Sensitivity Theory," in same preceedings as Ref. 20.

24. D. Saphier et al., "Analysis of the Asymmetric Power Tilt Phenomenon in Operating PWR's," Trans. ANS 38, 436 (1981)

25. J. Kallfelz, "On-Line Power Distribution and Reactivity Monitoring," Memo to D Cacuci and B. Worley dated July 27, 1983.

E-26-803

Georgia Institute of Technology
A UNIT OF THE UNIVERSITY SYSTEM OF GEORGIA
SCHOOL OF NUCLEAR ENGINEERING AND HEALTH PHYSICS
ATLANTA, GEORGIA 30332
(404) 894-3720

September 7, 1983

MEMORANDUM

TO: D. G. Cacuci, C. R. Weisbin and B. A. Worley (ORNL)

FROM: J. M. Kallfelz

SUBJECT: Progress Report for ORNL Subcontract 7802
Period August 2 - September 1, 1983

Accomplishments During Report Period

- A survey of literature pertinent to the development of an on-line power distribution and reactivity monitor (PDRM) was continued. Section 1 (p. 1-3) of this report contains comments on PDRM development.
- A statement discussing the contribution of a PDRM to the safety and economics of an LMFBR was prepared. This statement, requested by John Lewellen, is contained in Section 2 (p. 3-5) of this report.
- An investigation of ex-core detector reading sensitivities to the core power density distribution was initiated, using generalized perturbation theory (GPT). The methods and results of the initial calculations are discussed in Section 3 (p. 5-7) of this report.

Plans for Work for Next Month

- GPT investigations of ex-core detector reading sensitivities will be continued, for detectors at greater distances from the core.
- A report will be prepared, which states the conclusions of the investigations performed in this project period (July - September 1983) related to PDRM development, and presents recommendations for further work.

JMK/vw

cc: C. L. Cowan (GE-Sunnyvale)

J. M. Kallfelz
ORNL Progress Report
September 7, 1983

1. General Comments on PDRM Development

The goal for development of an on-line power distribution and reactivity monitor (PDRM) is to provide a system which is "capable of providing a rapid assessment of the status of core parameters which are important for economical and safe reactor operation."[1] It is important to recognize the significant difference in the applicable experience for the two components of the monitor name, i.e. "power distribution" and "reactivity." There is considerable experience in the development and application of "reactivity balance meters" [2] in LMFBRs. However, development of power distribution monitoring capability in fast reactors is in a relatively early stage, partially because related experience in thermal reactors is not directly applicable. As discussed below, this is because of the difference in the location of neutron detectors in fast and thermal reactors.

1.1 Reactivity Balance Meters

Basically, a reactivity balance meter (RBM) compares on-line the "real" or "measured" reactivity with the "expected" or "theoretical" reactivity.[2-4] The measured reactivity is determined with a "reactivity meter" (RM), utilizing neutron detector readings and the inverse kinetics equations.[4] The theoretical reactivity is calculated, using reactivity feedback coefficients and various measured parameters, e.g. power, control rod positions, coolant T_{inlet}, coolant ΔT in core, etc.[2] Such a device is also called an anomalous-reactivity (ANOR) meter[4], and the associated

monitoring procedure has been referred to as "reactivity surveillance procedure-anomaly detection" (RSP-AD).[5]

Reactivity balance meters have been used in Rapsodie[2] and FFTF[5], and use of the CAROL RBM is planned for Super-Phenix.[3] An RBM was planned for the Fermi-1 "malfunction detection analyzer"[6], and a conceptual RBM design was performed for EBR-II.[4]

1.2 Power Distribution Monitor

For thermal reactors, several systems which include power shape monitoring have been developed.[7,8] Of particular interest is the BWR Hybrid Power Shape Monitoring System (PSMS) developed under EPRI sponsorship.[7] This system monitors the state of the core in real time, and allows for adjustment of a few parameters to mimimize the difference between measured and theoretical values for in-core detector readings.[7] A nodal[10] physics code coupled to a thermal hydraulics code is used for monitoring and predictive analysis.

The presence of in-core detectors is obviously a great advantage in power distribution monitoring. The readings from these monitors are used to check and adjust the calculated power distribution. The following performance parameter is minimized:[7]

$$J = \sum_{l,k} w(l,k) R^2(l,k) \qquad (1)$$

where l and k designated location, the residual R is the normalized difference between the measured and calculated detector readings, and w is a weighting factor.

Unfortunately, it is difficult to use in-core detectors in fast reactors, because of the core environmental conditions,[9] and most designs

call for ex-vessel detectors. For instance, the neutron detectors for Super-Phenix are located outside the safety vessel, which encloses the main containment vessel.[3] It is obvious that the information content of such detectors concerning the core power shape is relatively small, compared to that of in-core detectors.

This raises the obvious question:

> Are there any measurable parameters for an LMFBR which are appropriate for adjustment of data used for calculated power shapes?

Gamma scan data for fuel elements can be used, but only at end-of-cycle. For a BWR it has been shown that adjustment during the cycle is necessary to avoid a serious deterioration in the accuracy of calculated cycles.[7]

Possibly the best standard of comparison for on-line LMFBR calculational models is a detailed off-line 3D calculation, to be performed periodically. Sandra and Azekura[9] used detailed 3D calculations to validate results from an influence function method they propose for on-line LMFBR calculations.

2. Impact of PDRM on LMFBR Safety and Economics

In our August 1 meeting with John Lewellen, he requested a brief statement discussing the contribution of a PDRM to the safety and economics of an LMFBR. Following is a draft of this statement.

It is generally recognized that on-line core surveillance systems using special computers can have a significant impact on the safe and economic operation of both thermal and fast reactors.[1,3,7-9] The introduction of powerful mini-computers coupled to the surveillance process facilitates a significant improvement in on-line performance evaluation of a fast reactor core. The reactor state functions, e.g. reactivity and power distribution, can be estimated with increased accuracy using such systems.

The improvement in safety achieved by an on-line Power Distribution and Reactivity Monitor (PDRM) is accomplished in a variety of ways, including the following:

- o By the detection of incipient incidents as soon as possible. For instance, analysis has indicated that with a device to detect "anomalous reactivity" (the difference between predicted and measured reactivity) the Fermi-1 flow blockage incident would have been detected at a much smaller excess reactivity than for the actual case.[4]
- o By diagnosing any incipient incident promptly. Such diagnosis may be utilized to protect the core either by input to an automatic safety system, or by helping the operator to determine the proper action to control the incident.[3]
- o By insuring that various safety-related limits (e.g. peak clad temperature, peak fuel temperature) are not exceeded.

Many features of a PDRM contribute to improved economics of an LMFBR, e.g.

- o Prompt control of incipient incidents which have a potential for core damage obviously influences the reactor economics.
- o Early diagnosis of an incident may allow control thereof without scram. This avoids mechanical stresses which impact on the core life, and may allow continued operation at a reduced power, improving the plant load factor compared to that for a scram occurence.[3]
- o Increased knowledge of the reactor state aids in insuring that the design fuel life is reached.

- o Increased reliability of reactor state prediction also allows operation nearer the design limits, increasing the reactor power output.
- o Used to predict the influence of operator actions, the PDRM can assist in short-term operational strategy planning, considering economic criteria.

In summary, a PDRM can be a valuable tool to improve knowledge of the core state, to reduce the impact of incipient incidents, and to help the reactor staff to optimize reactor operation with regard to safety and economic criteria.

3. GPT Investigation of Ex-Core Detector Reading Sensitivity to Core Power Distribution

Generalized perturbation theory[11,12] (GPT) can be used to investigate the sensitivity of ex-core detector readings to the core power distribution. "Ex-core" is a very general expression, and apparently "ex-vessel" is a more appropriate term for most LMFBR designs. As mentioned in section 1.2, the neutron detectors for Super-Phenix are far from the core, under the safety vessel. For a realistic analysis of such a system, transport theory methods[13] are necessary.

For initial calculations related to this problem, I have used diffusion theory GPT codes[12], the simple 1D slab model of an LMFBR described in Ref. 11, and an assumed detector location in the outer blanket, 10 cm from the core. This simple case is an appropriate starting point, and will yield some physical insight into the problem we are considering; definitive results will require gradual extension to a model approximating the realisitc ex-vessel case, described above.

For these initial calculations, the response function is similar to that considered in our studies[11] of the core power density. Assuming the detector response is proportional to σ_f (U-235), the normalized response ratio is:

$$R(x_D) = \frac{Q_1(x_D)}{Q_2} \qquad (2)$$

where x_D is the detector location,

$$Q_1(x_D) = \int \sum_j \sigma_{f_j} \phi_j(x') \delta(x'-x_D)\, dx' \qquad (3)$$

and Q_2, given by eqns. (11) and (12) of Ref. 11, is the total reactor power. Normalization with Q_2 represents the constraint of constant power for power density shape changes. It should be noted that R in eqn. (2) is of the same form as the response considered in our power density studies[11].

The generalized adjoint function, $\vec{\Gamma}^*(x)$, calculated for $R(x_D)$, gives the importance of neutrons at x in various energy groups to the ratio R.[11] The sensitivity of the core power density (PD) to the neutron flux distribution is given by the fixed source in the $\vec{\Gamma}^*$ eqn. for PD, as indicated by eqn. (5) of Ref. 11. Conversion from neutron flux sensitivity to that for the neutron density is trivial; thus the functions mentioned in this paragraph can be used to study the sensitivity of detector response to PD shape.

Figure 1 gives results for $\vec{\Gamma}^*$ for $R(x_D)$ of eqn. (2). The group cross section set is the same as that used in Ref. 11. Following are some aspects of interest, and their implications:

a. For obvious reasons, the importance curves are smooth in the core. Thus it seems unlikely that detection of <u>localized</u> flux perturba-

tions with ex-core detectors will be possible, even with a large number of detectors.

b. The importance curves have an appreciable space dependence over the core. Neutrons near the core edge have a larger probability of contributing to the detector reading, and thus have a positive importance, while those near the reactor center are more likely to contribute to the normalization denominator of $R(x_D)$, and have a negative importance. Thus for the case considered the ex-core detector could be useful in the determination of "core-wide" flux shape changes, e.g. "flux tilt". (Other information, e.g. total power and coolant ΔTs, would also be necessary.) This aspect should be investigated for detectors farther from the core.

c. If we are interested in sensitivity to relative changes in the flux shape, the curves in Fig. 1 should be multiplied by $\phi_g(x)$ to determine regions of significance. (The product $\phi\Gamma^*$ includes information on the location of neutrons which may contribute to R.) Since ϕ drops rapidly with distance from the core, this multiplication increases the significance of the core regions to $R(x_D)$.

At this point we are primarily interested in the sensitivity to changes in flux shape, rather than the cause of such changes. However, a perturbation calculation was performed for "Case 3" of Ref. 1, which replaces the inner blanket with driver. The impact on $R(x_D)$ was determined by GPT and "exactly" (by solving for ϕ for the base and perturbed cases.) The "exact" $\delta R/R$ is - 24.5%, while the GPT code result was -18.3% with by far the largest contribution from the "direct-effect" term[11]. As mentioned in Ref. 11, for this quite large perturbation second-and higher-order terms involving $\delta\Sigma$ and $\delta\phi$ are significant.

REFERENCES

1. "Cooperative Nuclear Data and Methods Development, Fiscal Year 1982," GEFR-14073-8, General Electric Co., September 1982.

2. B. Berthet et al., "Operation Experience of a Reactivity Balance Meter at Rapsodie" in Proc. Internat. Topical Meting on LMFBR Safety and Related Design and Operational Aspects, Lyon, July 19-23, 1982.

3. C. Berlin et al., "Super-Phenix Core Surveillance and Protection System," in same procedings as ref. 2.

4. H. A. Larson and B. R. Peterson, "The EBR-II Reactivity Meter: Conceptual Design," ANL-79-52, Argonne Nat. Lab.

5. R. A. Harris et al., "Reactivity Feedbacks in the FFTF: Predictions and Monitoring Techniques" in Trans. ANS 44, 513 (1983).

6. E. R. Volk et al., "Direct Connectin of the Femi-1 Malfunction Detection Analyzer with the Plant Safety System," in Proc. Internat. Conf. on Engineering of Fast Reactors for Safe and Reliable Operation, Karlsruhe, Oct. 9-13, 1972, Gesellschaft fur Kernforschung, Karlsruhe, 1973.

7. B. Frogner, A. Ipaktchi and A. B. Long, "Hydraulic Calibration Methods for the BWR Hybrid Power Shape Monitoring System," in Proc. ANS/ENS Internat. Topical Meeting on Advances in Mathematical Methods for Nuclear Engineering Problems, Munich, April 27-29, 1981.

8. OECD Halden Reactor Project, "Core Surveillance Systems: Development at the Halden Project and Within Signatory Organizations," HWR-32, Institutt for Energiteknikk, Halden, Norway.

9. T. Sandra and K. Azekura, "Calculational Model Based on Influence Function Method for Power Distribution and Control Rod Worth in Fast Reactors," Nucl. Sci. Engr. 85, 70 (1983).

10. H. W. Graves, Jr., "Power-Reactor Performance Evaluation Using Nodal/Modal Analysis, Ann. Nucl. Energy 10, 395 (1983).

11. L. A. Belblidia, J. M. Kallfelz, and D. G. Cacuci, "Generalized Perturbation Theory with Derivative Operators for Power Density Investigations in Nuclear Reactors" Nucl. Sci. Engr. 84, 206 (1983).

12. Refs. 16-18 of Ref. 11.

13. G. F. Flanagan et al., "Analysis of Stored Fuel, Control Rod and Inherent Source Effects on the CRBR Ex-Vessel Source Range Monitoring System" in J. M. Kallfelz and R. A. Karam, Eds., Advanced Reactors: Physics, Design and Economics, Pergamon Press, New York, 1975.

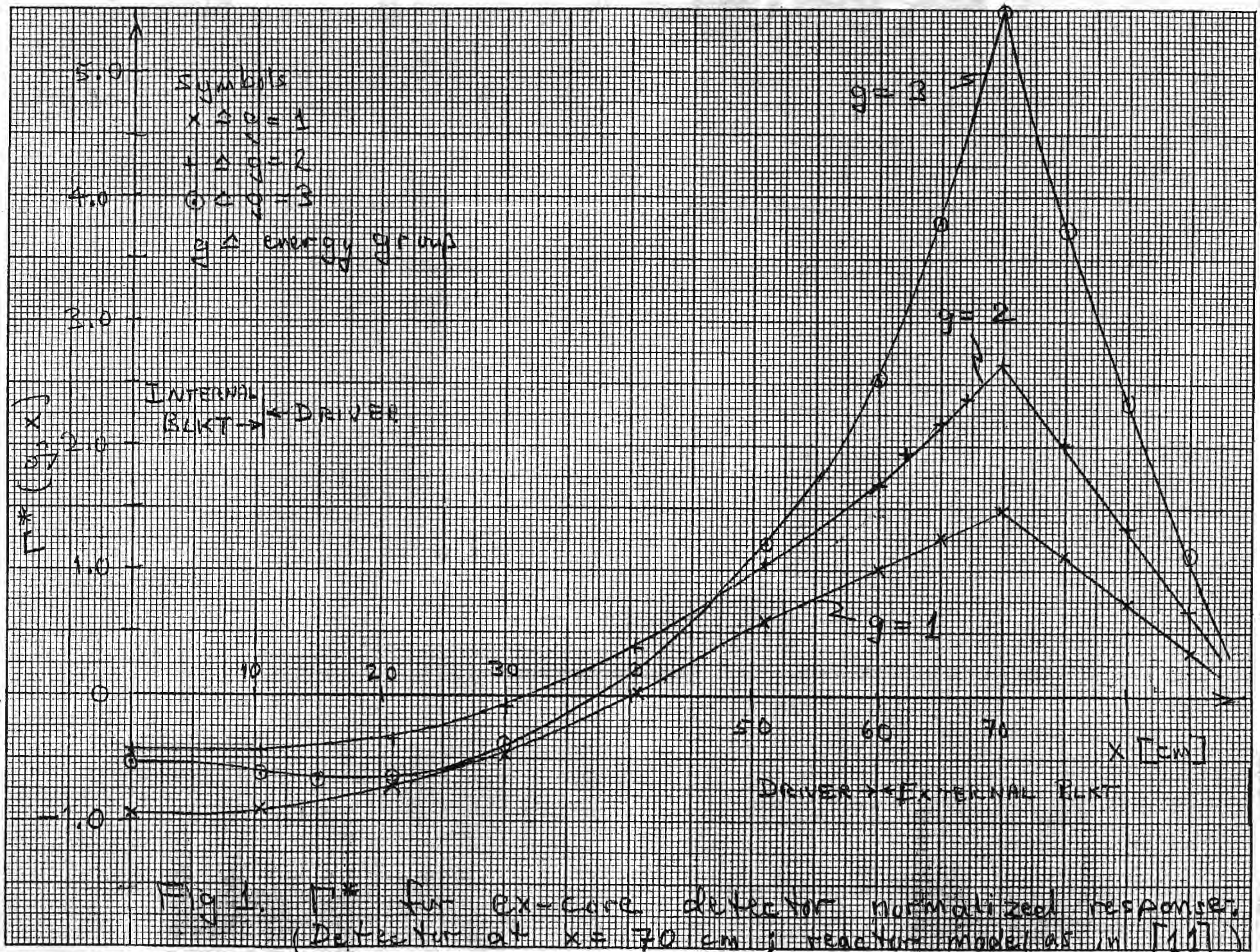

Fig 1. Γ^* for Ex-core driver normalized response. (Detector at x = 70 cm; reactor model as in [11])

GITNE-82/1

GENERALIZED PERTURBATION THEORY WITH DERIVATIVE OPERATORS FOR POWER DENSITY INVESTIGATIONS

by

J. M. Kallfelz and L. A. Belblidia

Annual Progress Report for ORNL Subcontract 7802

December 1982

SUMMARY

This annual progress report covers the activity of the Georgia Institute of Technology during the period October 1, 1981 - September 30, 1982 under Oak Ridge National Laboratory subcontract 7802-X01. This work has been described in detail in our monthly progress reports [1-7], and several articles [8,9]. The primary effort of this activity involved the development of generalized perturbation theory with derivative operators for power investigations, as described in detail in the attached manuscript. This work was performed jointly with Dan Cacuci of ORNL.

The intent of the research was to develop an efficient method to analyze variations that nuclear data perturbations induce in power density distributions. This method was called the Taylor-GPT method since it was based on: (a) the use of a Taylor-series expansion of the response variation, and (b) the use of generalized perturbation theory (GPT) to evaluate the derivative operators that appeared as coefficients in this Taylor series. Equations satisfied by the importance functions for the derivatives of the response variations were derived for a one-dimensional model and solved with existing GPT codes. The characteristics of these functions were highlighted analytically.

Particular attention was focused on the numerical value and location of the maximum power density. This was because perturbations in system parameters affect not only the value at the maximum, but also affect the location of this maximum. The Taylor-GPT method can

efficiently assess these effects.

The practical usefulness of the Taylor-GPT method was illustrated by considering test cases involving a simplified heterogeneous LMFBR model. The results indicated that this method was as accurate as the GPT method, yet required fewer calculations when investigating space-dependent power density variations.

REFERENCES*

1. J. M. Kallfelz and L. A. Belblidia, "Progress Report for ORNL Subcontract 7802, Months of October, November, and December, 1981," Memorandum to C. R. Weisbin, J. H. Marable, and D. G. Cacuci (ORNL), School of Nuclear Engineering, Georgia Institute of Technology, January 19, 1982.

2. J. M. Kallfelz and L. A. Belblidia, "Progress Report for ORNL Subcontract 7802, Months of January, February, and March, 1982," Memorandum to C. R. Weisbin, J. H. Marable, and D. G. Cacuci (ORNL), School of Nuclear Engineering, Georgia Institute of Technology, April 23, 1982.

3. J. M. Kallfelz and L. A. Belblidia, "Progress Report for ORNL Subcontract 7802, Month of April 1982," Memorandum to D. G. Cacuci, J. H. Marable, and C. R. Weisbin (ORNL), School of Nuclear Engineering, Georgia Institute of Technology, May 12, 1982.

4. J. M. Kallfelz and L. A. Belblidia, "Progress Report for ORNL Subcontract 7802, Month of May 1982," Memorandum to D. G. Cacuci, J. H. Marable, and C. R. Weisbin (ORNL), School of Nuclear Engineering, Georgia Institute of Technology, June 11, 1982.

5. L. A. Belblidia and J. M. Kallfelz, "Progress Report for ORNL Subcontract 7802, Month of June 1982," Memorandum to D. G. Cacuci, J. H. Marable, and C. R. Weisbin (ORNL), School of Nuclear Engineering, Georgia Institute of Technology, July 12, 1982.

6. L. A. Belblidia and J. M. Kallfelz, "Progress Report for ORNL Subcontract 7802, Month of July 1982," Memorandum to D. G. Cacuci, J. H. Marable, and C. R. Weisbin (ORNL), School of Nuclear Engineering, Georgia Institute of Technology, August 4, 1982.

7. J. M. Kallfelz and L. A. Belblidia, "Progress Report for ORNL Subcontract 7802, Months of August and September, 1982," Memorandum to C. R. Weisbin and D. G. Cacuci (ORNL), School of Nuclear Engineering, Georgia Institute of Technology, December 17, 1982.

---

* Note that the appendix has a separate reference list.

8. J. H. Marable, C. R. Weisbin, J. R. White, D. Biswas, J. M. Kallfelz, C. L. Cowan, and R. Protsik, "Sensitivities and Uncertainties of a Large LMFBR Using the Adjusted Cross-Section Library ORACLE-1," Trans. Am. Nucl. Soc., 41, 578 (1982).

9. J. H. Marable, D. G. Cacuci, C. R. Weisbin, J. R. White, D. Biswas, J. M. Kallfelz, C. L. Cowan, and R. Protsik, "Sensitivities and Uncertainties of a Large LMFBR Using Adjusted Cross-Section Library ORACLE-1," Proc. ANS Topical Meeting, Kiamesha Lake, New York, September 1982.

GENERALIZED PERTURBATION THEORY WITH DERIVATIVE OPERATORS FOR POWER DENSITY INVESTIGATIONS

L.A. Belblidia and J.M. Kallfelz*
School of Nuclear Engineering and Health Physics
Georgia Institute of Technology
Atlanta, Georgia 30332

and

D.G. Cacuci
Engineering Physics Division
Oak Ridge National Laboratory
P.O. Box X
Oak Ridge, TN 37830

Send proofs to:
Dan G. Cacuci
Engineering Physics Division
Oak Ridge National Laboratory
P.O. Box X
Oak Ridge, TN 37830

54 pages

6 figures

12 tables

*Present address: Kernforschungszentrum Karlsruhe,
D-7500 Karlsruhe 1, Germany

Abstract

This work presents an efficient method to analyze variations that nuclear data perturbations induce in power density distributions. This method is called the Taylor-GPT method since it is based on: (a) use of a Taylor-series expansion of the response variation, and (b) use of generalized perturbation theory (GPT) to evaluate the derivative operators that appear as coefficients in this Taylor series. Equations satisfied by the importance functions for the derivatives of the response variations are derived for a one-dimensional model and solved with existing GPT codes. The characteristics of these functions are highlighted analytically.

Particular attention is focused on the numerical value and location of the maximum power density. This is because perturbations in system parameters affect not only the value at the maximum, but also affect the location of this maximum. The Taylor-GPT method can efficiently assess such effects.

The practical usefulness of the Taylor-GPT method is illustrated by considering test cases involving a simplified heterogeneous LMFBR model. The results indicate that this method is as accurate as the GPT method, yet requires fewer calculations when investigating space-dependent power density variations.

Acknowledgments

Stimulating discussions with A. Gandini and V. Perone are gratefully acknowledged. We thank Jim Marable for his critical review of the manuscript which led to some modifications in the presentation. Special thanks are due to Lynn Messenger and Sharon Reeves for their expert typing of this manuscript.

This research was performed under Subcontract No. 7802(X01) with Georgia Institute of Technology under Union Carbide Corporation contract W-7405-eng-26 with the U.S. Department of Energy.

I. INTRODUCTION

Generalized perturbation theory (GPT)[1-4] has been used for many years to investigate[2-6] the influence of cross section perturbations and design changes on integral performance parameters (customarily called responses) in reactors. The successful application of GPT to analysis of the power density response[5,6] provided a strong motivation to study in detail the effects of parameter perturbations on such space-dependent responses. Thus, this paper presents an application of first-order GPT to efficiently evaluate the space derivatives of the response that appear as coefficients in a Taylor-series expansion technique. This technique will henceforth be referred to as the "Taylor-GPT" method, and will be used to investigate the space-dependent characteristics of variations in the power density response. The shift in the location of the maximum of this response is of particular interest.[5, 7-10]

I. A. Generalized Perturbation Theory

In reactor design studies, "sensitivities" $\delta P/\delta\alpha$ of a response P to input data α (typically nuclide densities or cross sections) are of interest.[2-6] In particular, P can denote a ratio of linear functionals of the real flux $\underline{\Phi}(\underline{r})$. For such a P, the use of GPT to calculate sensitivities requires that the following adjoint inhomogeneous Boltzmann equation be solved for $\underline{\Gamma}^*$:

$$(\mathbf{A}^* - \lambda\mathbf{B}^*)\,\underline{\Gamma}^* = \underline{S}^*. \qquad (1)$$

In Eq. (1), $\mathbf{A}^*$ is the adjoint loss and scattering operator, $\mathbf{B}^*$ is the adjoint fission operator, and λ is the system eigenvalue.

In multigroup formalism, $\underline{\Gamma}^*(\underline{r})$ is the generalized adjoint function, whose component $\Gamma_j^*(\underline{r})$ gives the importance of neutrons at $\underline{r}$ in energy group j to the ratio P. Thus, Γ_j^* satisfies the following equation that, except for the S_j^* term,[2] is formally identical to the "normal" adjoint equation[11] for ϕ_j^*:

$$-D_j \nabla^2 \Gamma_j^*(\underline{r}) + \Sigma_{rem,j} \Gamma_j^*(\underline{r}) =$$

$$\sum_h \Sigma_{j \to h} \Gamma_h^*(\underline{r}) + \lambda \nu \Sigma_{f,j} \sum_h \chi_h \Gamma_h^*(\underline{r}) + S_j^*(\underline{r}). \qquad (2)$$

In Eq. (2), all cross sections are functions of $\underline{r}$. The boundary conditions associated with Eq. (2) are formally identical to those for the ϕ_j^* equation, e.g., $\Gamma_j^* = 0$ at the outer reactor boundary (or extrapolated boundary).

Consider a ratio P of functionals of the real flux defined as

$$P = \frac{a_1}{a_2} = \frac{\int_{V_1} \sum_j \sigma_{1,j}(\underline{r}) \phi_j(\underline{r}) \, d\underline{r}}{\int_{V_2} \sum_j \sigma_{2,j}(\underline{r}) \phi_j(\underline{r}) \, d\underline{r}}, \qquad (3)$$

where V_1 and V_2 specify the volumes associated with the space integration over $\underline{r}$. (In the sequel, lack of such specification implies integration over the entire reactor volume.) For P defined by Eq. (3), there corresponds the following fixed source for Eq. (2):

$$S_j^*(\underline{r}) = \frac{\sigma_{1,j}}{a_1} - \frac{\sigma_{1,j}}{a_2}. \qquad (4)$$

Typically, $\sigma_{i,j}$ is some microscopic or macroscopic cross section.

In previous works[3,4] that used the concepts of GPT, the expression for the fixed source $\underline{S}^*$ was generally written as

$$\underline{S}^* = \frac{1}{P} \frac{\partial P}{\partial \underline{\Phi}} . \tag{5}$$

The expression $\partial P/\partial \underline{\Phi}$, though, was used in a formal sense and did not have a precise mathematical meaning. Based on the rigorous and comprehensive sensitivity theory[7,8] for nonlinear systems that has recently been developed, it can be shown that $\partial P/\partial \underline{\Phi}$ is in fact the partial Gateaux-derivative of P with respect to $\underline{\Phi}$, i.e., $\partial P/\partial \underline{\Phi}$ is the operator defined via the relationship

$$\frac{d}{d\varepsilon} \left[P(\underline{\Phi} + \varepsilon \underline{h}) \right]_{\varepsilon=0} = \frac{\partial P}{\partial \underline{\Phi}} \underline{h}, \tag{6}$$

where ε is a real scalar and $\underline{h}$ is an arbitrary vector of "increments" around $\underline{\Phi}$. Having thus specified its precise mathematical meaning, the notation $\partial P/\partial \underline{\Phi}$ will be retained, for convenience, in the sequel.

In the GPT method, the relative response variation is given by[4]

$$\frac{\delta P}{P} = \int \underline{\Phi} \, \underline{\delta G} \, d\underline{r} + \int \underline{\Gamma}^* \, \delta L \, \underline{\Phi} \, d\underline{r}, \tag{7}$$

where $\underline{\Phi}$ and $\underline{\Gamma}^*$ are, respectively, the real flux and generalized adjoint function, δL represents the perturbation in the Boltzmann operator, and the component of $\underline{\delta G}$ for energy group j is defined as

$$\delta G_j(\underline{r}) = \frac{\delta\sigma_{1,j}(\underline{r})}{a_1} - \frac{\delta\sigma_{2,j}(\underline{r})}{a_2} . \qquad (8)$$

The first term on the right side of Eq. (7) arises from changes in the cross sections that appear explicitly in Eq. (3), and is customarily referred to as the "direct-effect" term. The second term on the right side of Eq. (7) is customarily referred to as the "indirect-effect" term, and arises from the change in the flux corresponding to the perturbation $\delta\mathbf{L}$ of the Boltzmann operator.

I. B. Power Density Ratios and Related Spatial Shifts

In studies of uncertainties in calculated responses, P, for the heterogeneous core of a large LMFBR,[5,6] GPT has been employed to determine the sensitivities $\delta P/\delta\sigma$ to variations in the cross sections. The responses studied included, for each driver zone, the ratio $R_M(\underline{r}_m)$ of the zonal maximum power density to the total reactor power, defined as

$$R_M(\underline{r}_m) = \frac{Q_1(\underline{r}_m)}{Q_2} , \qquad (9)$$

where $\underline{r}_m$ is the location at which the zonal maximum power density occurs in the unperturbed case (i.e., the "base case"). The terms in the above equation are defined by the following expressions:

$$Q_1(\underline{r}_m) = \int \sum_j \Sigma_{1,j}(\underline{r}') \, \phi_j(\underline{r}') \, \delta(\underline{r}'-\underline{r}_m) \, d\underline{r}', \qquad (10)$$

and

$$Q_2 = \int \sum_j \Sigma_{2,j}(\underline{r}) \, \phi_j(\underline{r}) \, d\underline{r}. \qquad (11)$$

The quantities $\Sigma_{i,j}$ have identical forms for i = 1 and i = 2; considering only fission energy and assuming localized energy deposit, their explicit expression is

$$\Sigma_{i,j}(\underline{r}) = \sum_k p^k \Sigma^k_{f,j}(\underline{r}), \tag{12}$$

where p^k is the total energy release per fission in the k-th isotope.

The power density ratio $R(\underline{r})$ is defined as in Eq. (9), except that $\underline{r}$ is not necessarily the location where a maximum occurs. In this paper, a one-dimensional (x) model is considered, and the power density ratio is defined as

$$R(x) = \frac{Q_1(x)}{Q_2} . \tag{13}$$

Reference 5 discussed "far-range" shifts in the location of the reactor peak power density (e.g., shifts between driver zones) and "near-range" shifts around the location of the initial maximum R in a particular driver zone. There, the influence of near-range shifts in the location of the zonal peak power on the sensitivities $\delta R_M/R_M$ was estimated to be small. Note, though, that the nature of these spatial shifts was not rigorously analyzed.

The theory of Cacuci[7,8], which uses Gateaux-differentials, can be applied to problems involving such maxima. This theory has successfully been applied[12] to obtain sensitivities for the numerical values of the maximum power response and the maximum fuel temperature response, and for the sensitivities of the phase-space locations for these maxima, for a

reactor safety problem describing a protected transient with scram on high power level in the Fast Flux Test Facility.

Recently, Gandini suggested the application of GPT to functionals involving derivative operators (see footnote 26 of Ref. 13). References 9 and 10 reported preliminary investigations that used GPT in conjunction with a Taylor-series expansion for a simple response function. These investigations indicated that this method appears promising for explicitly investigating near-range spatial shifts.

The purpose of this work is to present new developments and results regarding this topic, including the first examples in reactor physics of importance functions associated with derivative operators,[14] and a detailed discussion of the characteristics of these functions. To analyze both direct and indirect effects caused by cross-section perturbations, this work considers a more general response than previously considered in Refs. 9 and 10. The basics of the Taylor-GPT method are described in Sec. II, and the application of GPT to space derivatives of the response R(x) is discussed in Sec. III. A theoretical analysis that highlights the main characteristics of the importance functions for these derivatives is presented in Sec. IV. Section V describes the use of the Taylor-GPT method for predicting effects of cross-section variations on the point-power density and on the spatial shifts in the maximum power density. In addition, this section discusses several indicators that can be used to assess the accuracy of the Taylor-GPT method. Comparison of results given by exact calculations, GPT, and Taylor-GPT have been performed for several test cases involving a simplified model of a heterogeneous LMFBR core. These test cases are described in Sec. VI, and the numerical results and specific comparisons are presented in Sec. VII. Finally, the summary and

conclusions presented in Sec. VIII highlight the usefulness of the Taylor-GPT method for assessing effects of variations in nuclide densities and/or nuclear data on the localized power density peak and on its spatial location.

II. TAYLOR-SERIES EXPANSION WITH GENERALIZED PERTURBATION THEORY (TAYLOR-GPT)

II. A. Taylor-Series Expansion for Response Variation

The variation $\delta R(x)$ in the power-density ratio $R(x)$, caused by perturbations in cross sections, can be determined by using a Taylor-series expansion about an arbitrary spatial point x_k. Retaining the first three terms only, this Taylor series is

$$\delta R(x) = \delta R(x_k) + (x - x_k)\, \delta R^{(1)}(x_k) + \frac{1}{2}(x - x_k)^2\, \delta R^{(2)}(x_k), \quad (14)$$

where $\delta R^{(i)}(x_k)$ denotes the i-th spatial derivative of the response variation $\delta R(x)$, evaluated at x_k.

Two alternative approaches can be used to calculate the derivatives $\delta R^{(i)}$. One approach is to use the finite-difference approximations of the derivatives $\delta R^{(i)}$ at x_k, while an alternative approach is to use the adjoint solution that corresponds to $\delta R^{(i)}/R^{(i)}$ at x_k. As subsequent developments will show, either of these approaches can be implemented by using existing GPT codes,[16-18] thereby avoiding any additional programming. This inherent implemental expendiency enhances the practical usefulness of the Taylor-GPT method.

II. B. Finite-Difference Implementation of the Taylor-GPT Method

The values of the derivatives $\delta R^{(1)}(x)$ and $\delta R^{(2)}(x)$ can be approximated at $x = x_k$ by using the finite-difference expressions

$$\delta R_k^{(1)} = \frac{\delta R_{k+1} - \delta R_{k-1}}{2\Delta} , \tag{15}$$

and

$$\delta R_k^{(2)} = \frac{\delta R_{k+1} - 2\,\delta R_k + \delta R_{k-1}}{\Delta^2} . \tag{16}$$

In Eq. (15) and (16), Δ denotes the mesh spacing, and subscripts k-1, k, k+1 refer to values at x_{k-1}, x_k, x_{k+1}, respectively; for example, $\delta R_k = \delta R(x_k)$.

In view of Eqs. (15) and (16), three GPT calculations are needed to determine the derivatives $\delta R^{(i)}$ and to enable the subsequent use of Eq. (14).

III. GENERALIZED PERTURBATION THEORY FOR RESPONSES INVOLVING DERIVATIVE OPERATORS

Equation (1) represents a "fixed-source" problem, and, due to linearity, such problems are known to possess the so-called "additivity" property. That is, if $\underline{\Gamma}_1^*$ is a solution of Eq. (1) with source $\underline{S}_1^*$, and $\underline{\Gamma}_2^*$ is a solution with $\underline{S}_2^*$, then $(\underline{\Gamma}_1^*+\underline{\Gamma}_2^*)$ is a solution corresponding to $(\underline{S}_1^* + \underline{S}_2^*)$. In the finite-difference approximation, the derivatives $\delta R^{(i)}$ are linear combinations of δR evaluated at x_k and at its neighboring mesh points. Therefore, it is possible, in principle, to find a source $\underline{S}^{*(i)}$ so that the corresponding adjoint equation and boundary conditions would yield the $\underline{\Gamma}^{*(i)}$ necessary to calculate $\delta R^{(i)}$. The actual procedure is detailed below.

III. A. Adjoint Functions for Calculating Spatial Derivatives of Response Variations

The ratio $\delta R^{(i)}/R^{(i)}$ at $x = x_k$ can be computed most efficiently by using adjoint functions. These adjoint functions, denoted by $\underline{\Gamma}_k^{*(i)}$, are solutions of

$$(\mathbf{A}^* - \lambda \mathbf{B}^*)\, \underline{\Gamma}_k^{*(i)} = \underline{S}_k^{*(i)}, \tag{17}$$

where, by analogy with Eq. (5), the adjoint source is

$$\underline{S}_k^{*(i)} = \frac{1}{R_k^{(i)}} \frac{\partial R_k^{(i)}}{\partial \underline{\Phi}}. \tag{18}$$

In the above equations, the operator $\partial R_k^{(i)}/\partial \underline{\Phi}$ is defined in the same way as $\partial R_k/\partial \underline{\Phi}$ [see Eq. (6)], $\underline{\Gamma}_k^{*(i)}$ is subject to the same boundary conditions as $\underline{\Gamma}_k^*$, and $R_k^{(i)}$ denotes the i-th derivative at x_k, of R(x) with respect to x.

Changing the order of differentiation, Eq. (18) becomes

$$\underline{S}_k^{*(i)} = \frac{1}{R_k^{(i)}} \left[\frac{\partial R}{\partial \underline{\Phi}} \right]_{x=x_k}^{(i)} . \tag{19}$$

Recalling Eq. (5), Eq. (19) is finite-differenced for i=1 and i=2 to obtain

$$\underline{S}_k^{*(1)} = \frac{1}{R_k^{(1)}} \frac{R_{k+1}\underline{S}_{k+1}^* - R_{k-1}\underline{S}_{k-1}^*}{2\Delta} , \tag{20}$$

and

$$\underline{S}_k^{*(2)} = \frac{1}{R_k^{(2)}} \frac{R_{k+1}\underline{S}_{k+1}^* - 2R_k\underline{S}_k^* + R_{k-1}\underline{S}_{k-1}^*}{\Delta^2} , \tag{21}$$

respectively.

For calculational purposes, Eqs. (20) and (21) can be further simplified by using the expression

$$R_k = \frac{Q_{1,k}}{Q_2} = \frac{Q_1(x_k)}{Q_2} , \tag{22}$$

and using similar expressions for R_{k-1} and R_{k+1}. Replacing these expressions in Eqs. (20) and (21), and using Eq. (5) yields, for energy group j,

$$S^{*(1)}_{k,j} = \frac{\Sigma_{1,j}(x)\,\delta(x - x_{k+1}) - \Sigma_{1,j}(x)\,\delta(x - x_{k-1})}{Q_{1,k+1} - Q_{1,k-1}} - \frac{\Sigma_{2,j}(x)}{Q_2}, \quad (23)$$

and

$$S^{*(2)}_{k,j} = \frac{\Sigma_{1,j}(x)\,\delta(x - x_{k+1}) - 2\,\Sigma_{1,j}(x)\,\delta(x - x_k) + \Sigma_{1,j}(x)\,\delta(x - x_{k-1})}{Q_{1,k+1} - 2Q_{1,k} + Q_{1,k-1}} - \frac{\Sigma_{2,j}(x)}{Q_2}. \quad (24)$$

respectively. Equations (23) and (24) can be used with existing GPT codes to calculate the corresponding $\underline{\Gamma}^{*(i)}_k$, thereby avoiding any additional programming. The procedure is described in Appendix A for the Italian GPT package.[16-18]

For the finite-difference approximations given by Eqs. (20) and (21), the functions $\underline{\Gamma}^{*(i)}_k$ can be related to the generalized adjoint fluxes (i.e., importances) for the response sensitivities at x_{k-1}, x_k, and x_{k+1} by making use of the previously mentioned additivity property of fixed-source problems. For the sources given by Eqs. (20) and (21), the use of this property gives, for i=1 and i=2,

$$\underline{\Gamma}^{*(1)}_k = \frac{1}{R^{(1)}_k} \frac{R_{k+1}\,\underline{\Gamma}^{*}_{k+1} - R_{k-1}\,\underline{\Gamma}^{*}_{k-1}}{2\,\Delta}, \quad (25)$$

and

$$\underline{\Gamma}_k^{*(2)} = \frac{1}{R_k^{(2)}} \frac{R_{k+1}\,\underline{\Gamma}_{k+1}^{*} - 2R_k\,\underline{\Gamma}_k^{*} + R_{k-1}\,\underline{\Gamma}_{k-1}^{*}}{\Delta^2}, \tag{26}$$

respectively. The adjoint functions $\underline{\Gamma}_k^{*(1)}$ and $\underline{\Gamma}_k^{*(2)}$ are used to determine the values of $\delta R^{(1)}/R^{(1)}$ and $\delta R^{(2)}/R^{(2)}$ at x_k, respectively.

III. B. Calculation of Direct Effects

From the definition of the power density at x_k, the expression giving the direct-effect component of the response sensitivity is obtained as

$$\frac{\delta R_{k,D}}{R_k} = \frac{\sum_j \delta\Sigma_{1,j}(x_k)\,\phi_j(x_k)}{Q_{1,k}} - \frac{\int \sum_j \delta\Sigma_{2,j}(x)\,\phi_j(x)\,dx}{Q_2}. \tag{27}$$

Multiplying Eq. (27) by R_k gives

$$\delta R_{k,D} = \frac{1}{Q_2}\left[\sum_j \delta\Sigma_{1,j}(x_k)\,\phi_j(x_k) - R_k Q_3\right], \tag{28}$$

where

$$Q_3 = \int \sum_j \delta\Sigma_{2,j}(x)\;\phi_j(x)\,dx. \tag{29}$$

Using a uniform mesh spacing about x_k, the first spatial derivative at x_k of the direct-effect component can be approximated as

$$\delta R^{(1)}_{k,D} = \frac{1}{2\Delta}\frac{1}{Q_2}\left[\sum_j \delta\Sigma_{1,j}(x_{k+1})\,\phi_j(x_{k+1}) - R_{k+1}Q_3 - \sum_j \delta\Sigma_{1,j}(x_{k-1})\,\phi_j(x_{k-1}) + R_{k-1}Q_3\right] . \tag{30}$$

Dividing Eq. (30) by $R^{(1)}_k$, and simplifying the resulting expression gives

$$\frac{\delta R^{(1)}_{k,D}}{R^{(1)}_k} = \frac{1}{Q_2}\frac{1}{R_{k+1} - R_{k-1}}\sum_j\left[\delta\Sigma_{1,j}(x_{k+1})\;\phi_j(x_{k+1}) - \delta\Sigma_{1,j}(x_{k-1})\;\phi_j(x_{k-1})\right] - \frac{Q_3}{Q_2} . \tag{31}$$

Using the fact that

$$Q_2(R_{k+1} - R_{k-1}) = \sum_j\left[\Sigma_{i,j}(x_{k+1})\;\phi_j(x_{k+1}) - \Sigma_{i,j}(x_{k-1})\;\phi_j(x_{k-1})\right] ,$$

and replacing Q_2 and Q_3 by their respective expressions, Eq. (31) becomes

$$\frac{\delta R^{(1)}_{k,D}}{R^{(1)}_k} = \frac{\sum_j\left[\delta\Sigma_{1,j}(x_{k+1})\,\phi_j(x_{k+1}) - \delta\Sigma_{1,j}(x_{k-1})\,\phi_j(x_{k-1})\right]}{\sum_j\left[\Sigma_{1,j}(x_{k+1})\;\phi_j(x_{k+1}) - \Sigma_{1,j}(x_{k-1})\;\phi_j(x_{k-1})\right]} - \frac{\int\sum_j \delta\Sigma_{2,j}(x)\,\phi_j(x)\,dx}{\int\sum_j \Sigma_{2,j}(x)\,\phi_j(x)\,dx} . \tag{32}$$

The procedure that has led to Eq. (32) is repeated to derive the expression for the second spatial derivative at x_k of the direct-effect component. The final result is

$$\frac{\delta R^{(2)}_{k,D}}{R^{(2)}_{k}} = \frac{\sum_j \left[\delta\Sigma_{1,j}(x_{k+1})\phi_j(x_{k+1}) - 2\delta\Sigma_{1,j}(x_k)\phi_j(x_k) + \delta\Sigma_{1,j}(x_{k-1})\phi_j(x_{k-1})\right]}{\sum_j \left[\Sigma_{1,j}(x_{k+1})\phi_j(x_{k+1}) - 2\Sigma_{1,j}(x_k)\phi_j(x_k) + \Sigma_{1,j}(x_{k-1})\phi_j(x_{k-1})\right]}$$

$$- \frac{\int \sum_j \delta\Sigma_{2,j}(x)\phi_j(x)\,dx}{\int \sum_j \Sigma_{2,j}(x)\phi_j(x)\,dx} \quad . \tag{33}$$

The expressions given by Eqs. (32) and (33) can be calculated with existing GPT codes[18] as described in Appendix A.

IV. THE FUNCTIONS $\underline{\Gamma}^*$ and $\underline{\Gamma}^{*(i)}$: A THEORETICAL ANALYSIS OF THEIR PROPERTIES

Noting that R_k and $R_k^{(i)}$ do not depend on x, the equations and boundary conditions satisfied by the adjoint functions $\underline{\Gamma}_k^*$ and $\underline{\Gamma}_k^{*(i)}$ are recast in the form

$$\left.\begin{aligned} &\mathbf{A}^*(R_k\,\underline{\Gamma}_k^*) - \lambda \mathbf{B}^*(R_k\,\underline{\Gamma}_k^*) = R_k\,\underline{S}_k^*\,, \\ &(R_k\,\underline{\Gamma}_k^*) = 0 \quad \text{at } x = L\,, \\ &d(R_k\,\underline{\Gamma}_k^*)/dx = 0 \quad \text{at } x = 0\,, \end{aligned}\right\} \tag{34}$$

and

$$\left.\begin{aligned} &\mathbf{A}^*\left[R_k^{(i)}\,\underline{\Gamma}_k^{*(i)}\right] - \lambda \mathbf{B}^*\left[R_k^{(i)}\,\underline{\Gamma}_k^{*(i)}\right] = R_k^{(i)}\,\underline{S}_k^{*(i)}\,, \\ &\left[R_k^{(i)}\,\underline{\Gamma}_k^{*(i)}\right] = 0 \quad \text{at } x = L\,, \\ &d\left[R_k^{(i)}\,\underline{\Gamma}_k^{*(i)}\right]/dx = 0 \quad \text{at } x = 0\,, \end{aligned}\right\} \tag{35}$$

where L denotes the outer (or the extrapolated) boundary of the reactor system, and all other quantities have the same meanings as before.

Eqs. (34) and (35) are the basis for establishing and analyzing relationships among the adjoint functions $\underline{\Gamma}_k^{*(i)}$, i = 1,2, ..., and $\underline{\Gamma}_k^*$. Of course, the functions $\underline{\Gamma}_k^{*(0)}$ and $\underline{\Gamma}_k^*$ are identical, since Eq. (35) reduces to Eq. (34) when i = 0.

Differentiating Eq. (35) with respect to x_k gives

$$\left.\begin{aligned} &\mathbf{A}^*\left[d(R_k^{(i)}\ \underline{\Gamma}_k^{*(i)})/dx_k\right] - \lambda\mathbf{B}^*\left[d(R_k^{(i)}\ \underline{\ }_k^{*(i)})/dx_k\right] = \\ &\qquad d\left[R^{(i)}\ \underline{S}^{*(i)}\right]/dx_k\ , \\ &d\left[R_k^{(i)}\ \underline{\Gamma}_k^{*(i)}\right]/dx_k \quad = 0 \quad \text{at } x = L, \\ &d\left\{d\left[R_k^{(i)}\ \underline{\Gamma}_k^{*(i)}\right]/dx_k\right\}/dx = 0 \quad \text{at } x = 0\ . \end{aligned}\right\} \tag{36}$$

Using the definition of $\underline{S}_k^{*(i)}$ [i.e., Eq. (20)], the quantity $R_k^{(i)}\ \underline{S}_k^{*(i)}$ can be expressed as

$$R_k^{(i)}\ \underline{S}_k^{*(i)} = \int \left\{d^i\left[dR/d\underline{\phi}\right]/dx^i\right\}\ \delta(x-x_k)dx. \tag{37}$$

Differentiating Eq. (37) with respect to x_k, and using the definition[19] of the δ'-functional, i.e.

$$\int f(x)\ \delta'(x-a)\ dx \ = \ -\int f'(x)\ \delta(x-a)\ dx, \tag{38}$$

leads to

$$d\left[R_k^{(i)}\ \underline{S}_k^{*(i)}\right]/dx_k = -\int\left\{d^i\left[dR/d\underline{\phi}\right]/dx^i\right\}\delta'(x-x_k)dx$$

$$=\int\left\{d^{i+1}\left[dR/d\underline{\phi}\right]/dx^{i+1}\right\}\delta(x-x_k)dx\ . \qquad (39)$$

Writing Eq. (37) for i+1, and comparing the result with Eq. (39) shows that

$$d\left[R_k^{(i)}\ \underline{S}_k^{*(i)}\right]/dx_k = R_k^{(i+1)}\ \underline{S}_k^{*(i+1)}. \qquad (40)$$

Using Eq. (40) to replace the corresponding source term in Eq. (36), and comparing the resulting system of equations to the system obtained by writing Eq. (35) for i+1 leads to the conclusion that

$$d\left[R_k^{(i)}\ \underline{\Gamma}_k^{*(i)}\right]/dx_k = R_k^{(i+1)}\ \underline{\Gamma}_k^{*(i+1)},\ i = 0,\ 1,\ 2,... \qquad (41)$$

A simple inductive reasoning can now be used in conjunction with Eq. (41) to conclude that

$$R_k^{(i)}\ \underline{\Gamma}_k^{*(i)} = d^i\left[R_k\ \underline{\Gamma}_k^*\right]/dx_k^i. \qquad (42)$$

The qualitative behavior of $\underline{\Gamma}_k^*$, $\underline{\Gamma}_k^{*(1)}$, and $\underline{\Gamma}_k^{*(2)}$ as functions of x can be studied analytically by considering a one-group, one-region representation of the adjoint diffusion equations given by Eqs. (34) and (35). For clarity, the functions satisfying the corresponding simplified adjoint diffusion equations are denoted by Γ_1^*, $\Gamma_1^{*(1)}$, and $\Gamma_1^{*(2)}$, where the subscript 1 now refers to the one-

group model rather than to the location of x_k. The respective equations can be written explicitly as follows:

$$\left.\begin{aligned} &d^2\Gamma_1^*/dx^2 + B^2\Gamma_1^* = -S^*/D \,, \\ &\Gamma_1^* = 0 \quad \text{at } x = L \,, \\ &d\Gamma_1^*/dx = 0 \quad \text{at } x = 0 \,, \end{aligned}\right\} \tag{43}$$

$$\left.\begin{aligned} &d^2\Gamma_1^{*(1)}/dx^2 + B^2\,\Gamma_1^{*(1)} = -\,S^{*(1)}/D \,, \\ &\Gamma_1^{*(1)} = 0 \quad \text{at } x = L \,, \\ &d\Gamma_1^{*(1)}/dx = 0 \quad \text{at } x = 0 \,, \end{aligned}\right\} \tag{44}$$

and

$$\left.\begin{aligned} &d^2\Gamma_1^{*(2)}/dx^2 + B^2\Gamma_1^{*(2)} = -\,S^{*(2)}/D \,, \\ &\Gamma_1^{*(2)} = 0 \quad \text{at } x = L \,, \\ &d\Gamma_1^{*(2)}/dx = 0 \quad \text{at } x = 0 \,. \end{aligned}\right\} \tag{45}$$

In Eqs. (43) through (45), B^2 and D represent the customary one-group, one-region buckling and diffusion coefficient, respectively. The analytical expressions for S^*, $S^{*(1)}$, and $S^{*(2)}$ are obtained by using Eqs. (9) through (11) in conjunction with Eq. (19) and with the definitions[19] of the δ'- and

δ''-functionals. Also, for simplicity, the constants $\Sigma_{i,j}$ [see Eq. (12)] are arbitrarily set to unity. Under these conditions, the following analytical expressions are obtained:

$$R_k = Q_{1,0}/Q_2 \ , \tag{46}$$

$$R_k^{(1)} = Q_{1,1}/Q_2 \ , \tag{47}$$

$$R_k^{(2)} = Q_{1,2}/Q_2 \ , \tag{48}$$

$$S^* = \frac{\delta(x-x_k)}{Q_{1,0}} - \frac{1}{Q_2} \ , \tag{49}$$

$$S^{*(1)} = - \frac{\delta'(x-x_k)}{Q_{1,1}} - \frac{1}{Q_2} \ , \tag{50}$$

$$S^{*(2)} = \frac{\delta''(x-x_k)}{Q_{1,2}} - \frac{1}{Q_2} \ , \tag{51}$$

where

$$Q_{1,0} = \phi(x_k), \tag{52}$$

$$Q_{1,1} = \left\{ d\phi/dx \right\}_{x=x_k}, \tag{53}$$

$$Q_{1,2} = \left\{ d^2\phi/dx^2 \right\}_{x=x_k}, \tag{54}$$

and

$$Q_2 = \int \phi(x)\, dx. \tag{55}$$

The adjoint diffusion equations given by Eqs. (43) through (45), with the source terms given by Eqs. (49) through (51), respectively, can be solved analytically to determine Γ_1^*, $\Gamma_1^{*(1)}$, and $\Gamma_1^{*(2)}$. For this purpose, it is convenient to use the Laplace-transform method, as illustrated in Appendix B where Eq. (45) is solved in detail. The following analytical expressions for the solutions of Eqs. (43) through (45) are thus obtained:

$$\Gamma_1^* = \frac{1}{B^2 DQ_2} + \left[\frac{1}{BDQ_{1,0}} \left(\frac{\cos Bx_k}{BL} - \frac{L - x_k}{L} \sin Bx_k \right) - \frac{2}{LB^3 DQ_2} \right] \cos Bx$$

$$- \frac{1}{BDQ_{1,0}} H(x-x_k) \sin B(x-x_k), \tag{56}$$

$$\Gamma_1^{*(1)} = \frac{1}{B^2 DQ_2} - \left(\frac{L - x_k}{DLQ_{1,1}} \cos Bx_k + \frac{2}{LB^3 DQ_2} \right) \cos Bx$$

$$+ \frac{1}{DQ_{1,1}} H(x-x_k) \cos B(x-x_k), \tag{57}$$

$$\Gamma_1^{*(2)} = \frac{1}{B^2 DQ_2} + \left[\frac{\cos Bx_k + B(L-x_k) \sin Bx_k}{LDQ_{1,2}} - \frac{2}{DB^3 LQ_2} \right] \cos Bx$$

$$+ \frac{B}{DQ_{1,2}} H(x-x_k) \sin B(x-x_k) - \frac{\delta(x-x_k)}{DQ_{1,2}}, \qquad (58)$$

where $H(x)$ represents the customary [19] Heaviside (unit-step) functional.

In view of Eqs. (56) through (58), the behavior of the functions Γ_1^*, $\Gamma_1^{*(1)}$, and $\Gamma_1^{*(2)}$ as x approaches x_k becomes of particular interest. Thus, Γ_1^* is continuous at x_k, where

$$\Gamma_1^*(x_k) = \frac{1}{B^2 DQ_2} + \left[\frac{1}{BDQ_{1,0}} \left(\frac{\cos Bx_k}{BL} - \frac{L - x_k}{L} \sin Bx_k \right) \right.$$

$$\left. - \frac{2}{LB^3 DQ_2} \right] \cos Bx_k, \qquad (59)$$

but the first- and second-derivatives of Γ_1^* with respect to x have a Heaviside - and a Dirac delta-type discontinuity, respectively, at $x = x_k$, since

$$\left\{ d\Gamma_1^*/dx \right\}_{x=x_k} = \left[\frac{2}{LB^2 DQ_2} - \frac{1}{DQ_{1,0}} \left(\frac{\cos Bx_k}{BL} - \frac{L - x_k}{L} \sin Bx_k \right) \right] \sin Bx_k$$

$$- \frac{1}{DQ_{1,0}} H(x-x_k), \qquad (60)$$

and

$$\left\{d^2\Gamma_1^*/dx^2\right\}_{x=x_k} = \left[\frac{2}{LBDQ_2} - \frac{B}{DQ_{1,0}}\left(\frac{\cos Bx_k}{BL} - \frac{L - x_k}{L}\sin Bx_k\right)\right]\cos Bx_k - \frac{\delta(x-x_k)}{DQ_{1,0}} . \tag{61}$$

At $x = x_k$, the function $\Gamma_1^{*(1)}$ has a Heaviside-type discontinuity, since

$$\left\{\Gamma_1^{*(1)}\right\}_{x=x_k} = \frac{1}{B^2DQ_2} - \left(\frac{L - x_k}{DLQ_{1,1}}\cos Bx_k + \frac{2}{LB^3DQ_2}\right)\cos Bx_k + \frac{1}{DQ_{1,1}} H(x-x_k), \tag{62}$$

while the first derivative of $\Gamma_1^{*(1)}$ with respect to x has a Dirac delta-discontinuity, since

$$\left\{d\Gamma_1^{*(1)}/dx\right\}_{x=x_k} = \left[\frac{B(L-x_k)}{DLQ_{1,1}}\cos Bx_k + \frac{2}{LB^2DQ_2}\right]\sin Bx_k + \frac{\delta(x-x_k)}{DQ_{1,1}} . \tag{63}$$

Finally, $\Gamma_1^{*(2)}$ has a Dirac delta-type discontinuity at $x = x_k$, since

$$\left\{\Gamma_1^{*(2)}\right\}_{x=x_k} = \frac{1}{B^2 DQ_2} + \left[\frac{\cos Bx_k + B(L-x_k)\sin Bx_k}{LDQ_{1,2}} - \frac{2}{DB^3 LQ_2}\right]\cos Bx_k - \frac{\delta(x-x_k)}{DQ_{1,2}} . \tag{64}$$

When x_k is close to the exact location x_M of the maximum, but such that $x_k < x_m$, $Q_{1,0}$ and $Q_{1,1}$ are positive, while $Q_{1,2}$ is negative. In this case, Eqs. (59) through (64) indicate that:

1. The functions $\Gamma_1^{*(1)}$ and $d\Gamma_1^*/dx$ both undergo step-jumps at $x = x_k$, but the former function undergoes a positive step-jump, while the latter undergoes a negative step-jump, and
2. The functions $\Gamma_1^{*(2)}$, $d\Gamma_1^{*(1)}/dx$, and $d^2\Gamma_1^*/dx^2$ all display "spikes", i.e. Dirac delta-type discontinuities at $x = x_k$. These delta-functionals cause positive spikes in $\Gamma_1^{*(2)}$ and $d\Gamma_1^{*(1)}/dx$, but cause a negative spike in $d^2\Gamma_1^*/dx^2$.

Since Eqs. (43) through (45) are particular forms of Eqs. (34) through (36), respectively, the functions Γ_1^*, $\Gamma_1^{*(1)}$, and $\Gamma_1^{*(2)}$ should also satisfy the relationships given by Eqs. (41) and (42). This fact can readily be verified by using Eqs. (56) through (58) and Eqs. (46) through (48) to show that

$$d(R_k \Gamma_1^*)/dx_k = R_k^{(1)} \Gamma_1^{*(1)}, \tag{65}$$

and

$$d^2(R_k \Gamma_1^*)/dx_k^2 = d\left[R_k^{(1)} \Gamma_1^{*(1)}\right]/dx_k = R_k^{(2)} \Gamma_1^{*(2)}. \tag{66}$$

V. RESPONSE VARIATIONS AND SPATIAL SHIFTS: CALCULATIONAL PROCEDURES AND ACCURACY OF PREDICTIONS

V. A. Response Variations and Accuracy of Predictions

The effects on the point-power density of variations in the macroscopic cross sections can be evaluated by three methods:

(1) direct calculations;

(2) use of generalized perturbation theory (GPT);

(3) use of Taylor-series expansion method with GPT (Taylor-GPT).

The first method consists of calculating the response (in this case, the point-power density) for the unperturbed case (denoted by the subscript 0), the response for the perturbed case (denoted by the subscript 1), and subtracting the two to determine the change. The result of this process gives

$$\Delta R_e(x) = R_1(x) - R_0(x). \tag{67}$$

This method will henceforth be called "exact".

For the GPT method, the response variation, denoted by $\delta R_p(x)$, is given by

$$\delta R_p(x) = R(x) \left.\frac{\delta R}{R}\right|_x , \tag{68}$$

where $\delta R/R$ has the same expression as $\delta P/P$ in Eq. (7), except that P is replaced by the particular response R(x) defined by Eq. (13).

For the Taylor-GPT method, the response variation at x, denoted by $\delta R_{tp}(x)$, is considered to be given by the following three-term Taylor-series expansion about x:

$$\delta R_{tp}(x) = \delta R_p(x_k) + (x-x_k)\ \delta R_p^{(1)}(x_k) + \frac{1}{2}(x-x_k)^2\ \delta R_p^{(2)}(x_k). \qquad (69)$$

In Eq. (69), the variation in the power density at x_k and its first two derivatives at x_k are determined from GPT calculations.

The accuracy of the Taylor-GPT method can be assessed by comparing the left side of Eq. (69) to the result of a GPT sensitivity calculation at x, i.e., Eq. (68). A relative error, denoted by TAP and defined as

$$TAP = \frac{\delta R_{tp}(x) - \delta R_p(x)}{\delta R_p(x)} . \qquad (70)$$

can be used to assess this accuracy.

On the other hand, the relative error that results from:

a. the inaccuracy of GPT, and

b. the differences between Eq. (68) and the Taylor-series expansion of $\delta R(x)$ about x_k

is found by taking the direct calculations as the basis for comparison. This relative error is henceforth denoted by TAE, and is defined as

$$TAE = \frac{\delta R_{tp}(x) - \Delta R_e(x)}{\Delta R_e(x)} . \qquad (71)$$

V. B. Spatial Shifts in the Maximum Power Density

Numerically, a discrete set $\left\{R_i = R_0(x_i),\ i=1,2,\ \ldots,\ N\right\}$ is obtained when the unperturbed power density response $R_0(x)$ is calculated as a function of x. Consider now that x_k represents the discrete point at which the largest discrete value R_k is obtained. In general, x_k does not coincide with the spatial location, denoted by x_{m0}, at which $R_0(x)$ attains its actual maximum. To second order in x, the location x_{m0} can be determined as follows: (a) approximate $R_0(x)$ by a quadratic polynomial in x that passes through the points (x_{k-1}, R_{k-1}), (x_k, R_k), and (x_{k+1}, R_{k+1}) in the $\left\{x, R_0(x)\right\}$ -plane, and (b) set the first spatial derivative of this polynomial to zero. This gives

$$x_{m0} - x_k = - \frac{R_0^{(1)}(x_k)}{R_0^{(2)}(x_k)} . \tag{72}$$

When the system parameters are perturbed, the perturbed response, denoted by $R_1(x)$, attains its actual maximum at a location x_{m1} which, in general, will not coincide with x_{m0}. To second order, the perturbed response at x_{m1} can be expressed as

$$R_1(x_{m1}) = R_1(x_k) + (x_{m1} - x_k)\, R_1^{(1)}(x_k) + \frac{1}{2}\,(x_{m1} - x_k)^2\, R_1^{(2)}(x_k) . \tag{73}$$

Note that since $R_1(x_{m1})$ is the perturbed peak (i.e., maximum) power, the first spatial derivative of $R_1(x)$ vanishes at x_{m1}. Therefore, Eq. (73) can be used to obtain

$$x_{m1} - x_k = - \frac{R_1^{(1)}(x_k)}{R_1^{(2)}(x_k)} . \tag{74}$$

The spatial shift $(x_{m1} - x_{m0})$ in the peak power can now be estimated by subtracting Eq. (72) from Eq. (74). This gives

$$x_{m1} - x_{m0} = - \frac{R_0^{(1)} + \delta R^{(1)}}{R_0^{(2)} + \delta R^{(2)}} + \frac{R_0^{(1)}}{R_0^{(2)}} , \tag{75}$$

where all $R^{(i)}$ and $\delta R^{(i)}$, i=1,2, are understood as being evaluated at $x = x_k$. When $\delta R^{(2)}/R^{(2)}$ is much less than unity, Eq. (75) reduces to

$$x_{m1} - x_{m0} \simeq - \frac{\delta R^{(1)}}{R_0^{(2)}} . \tag{76}$$

Within the framework of first-order GPT, the perturbed response can be written as the sum of the unperturbed response and the response variation δR_p, where the latter term consists of a direct-effect component, δR_d, and an indirect-effect component, δR_i, i.e.,

$$\begin{aligned} R_1 &= R_0 + \delta R_p \\ &= R_0 + \delta R_d + \delta R_i . \end{aligned} \tag{77}$$

Similar expressions can be written for the spatial derivatives of the perturbed response:

$$\left.\begin{aligned} R_1^{(1)} &= R_0^{(1)} + \delta R_d^{(1)} + \delta R_i^{(1)} , \\ R_1^{(2)} &= R_0^{(2)} + \delta R_d^{(2)} + \delta R_i^{(2)} . \end{aligned}\right\} \tag{78}$$

If, on the one hand, the direct-effect components vanish, then Eqs. (74) and (78) give

$$(x_{m1} - x_k)_i = - \frac{R_0^{(1)} + \delta R_i^{(1)}}{R_0^{(2)} + \delta R_i^{(2)}} . \tag{79}$$

If, on the other hand, the indirect-effect components vanish, then Eqs. (74) and (78) give

$$(x_{m1} - x_k)_d = - \frac{R_0^{(1)} + \delta R_d^{(1)}}{R_0^{(2)} + \delta R_d^{(2)}} . \tag{80}$$

Adding Eqs. (79) and (80), and neglecting second-order terms of the form $\delta R_d^{(i)} \delta R_i^{(j)}$, gives

$$(x_{m1} - x_k)_d + (x_{m1} - x_k)_i = - \frac{R_0^{(1)} + \delta R_d^{(1)} + \delta R_i^{(1)}}{R_0^{(2)} + \delta R_i^{(2)} + \delta R_i^{(2)}} - \frac{R_0^{(1)}}{R_0^{(2)}} . \tag{81}$$

In view of Eqs. (74) and (78), the first term on the right side of Eq. (81) is the expression for $(x_{m1} - x_k)$ when both direct and indirect effects are present. The second term on the right side of Eq. (81) corresponds to the unperturbed case, i.e., to $(x_{m0} - x_k)$ as given by Eq. (72). Therefore, Eq. (81) becomes

$$(x_{m1} - x_k)_d + (x_{m1} - x_k)_i = (x_{m1} - x_k) + (x_{m0} - x_k). \tag{82}$$

Noting that x_k is a fixed point, and subtracting twice the quantity $(x_{m0} - x_k)$ from Eq. (82) gives

$$(x_{m1} - x_{m0})_d + (x_{m1} - x_{m0})_i = x_{m1} - x_{m0}. \tag{83}$$

Equation (83) shows that the spatial shift in the peak-power location can be expressed as the sum of a spatial shift due solely to direct effects and a spatial shift due solely to indirect effects.

V. C. Influence of the Spatial Shift on the Sensitivity of the Peak-Power Density

When a macroscopic cross section is perturbed, the resulting variation in peak-power density is given by

$$\Delta R_{es} = R_1(x_{m1}) - R_0(x_{m0}). \tag{84}$$

Note that Eq. (84) is exact, i.e., it contains no approximations.

If the shift in the location of the maximum power is neglected, the variation in the response is given by Eq. (67) evaluated at x_{m0}, that is,

$$\Delta R_{e0} = R_1(x_{m0}) - R_0(x_{m0}). \tag{85}$$

In view of Eqs. (84) and (85), the effect of the spatial shift on the sensitivity of the peak-power density can be assessed by using the expression

$$SE = \frac{\Delta R_{es} - \Delta R_{e0}}{\Delta R_{e0}} . \tag{86}$$

Since Cacuci[8] has shown that

$$\left| R_1(x_{m1}) - R_1(x_{m0}) \right| = O[(\delta\sigma)^2] , \tag{87}$$

where $\delta\sigma$ represents variations in the system parameters, it follows that the numerator of Eq. (86) is also of second order in these variations.

Numerically, the locations x_{m0} and x_{m1} are determined by using Eqs. (72) and (74). Therefore, the numerical results for SE are also subject to the second-order approximations associated with Eqs. (72) through (74). Figure 1 illustrates the spatial shift caused by near-range effect and its influence on the sensitivity of the extremum.

VI. DESCRIPTION OF TEST CASES

VI. A. Model and Cross Sections

A simplified three-region model, which has some of the significant characteristics[10] of a heterogeneous LMFBR, has been chosen to test the theoretical developments outlined in the previous sections. This model consists of an infinite slab, finite in the x-direction, with internal blanket (IB), driver (D), and external blanket (EB). The concentrations of Na, U-238, and Pu-239 are given in Table I, and are the same as for the beginning-of-life LMFBR model considered in Ref. 20. The three-group cross sections used are from the CITATION test case.[21]

The outer boundaries of regions IB, D, and EB are located at 10.5 cm, 60 cm, and 90.0 cm from the reactor center (x = 0), respectively. A driver zone mesh spacing of 1.5 cm is used for all reported results; however, this spacing was varied in some of the test calculations discussed in Sec. VII.B.

VI. B. Selection of Perturbations

Perturbations of nuclide densities or microscopic cross sections cause changes in the Boltzmann operator, $\mathbf{L}$, and in the macroscopic cross sections, Σ. To choose perturbations appropriate for testing the proposed method, several desirable, and sometimes conflicting, conditions should be considered:

(i) To test the Taylor series method, $\delta\Sigma$ should cause a response variation $\delta R(x)$ that appreciably depends on x. This implies that the change in at least one of the derivatives $\delta R^{(i)}(x_k)$ should be appreciable.

(ii) To check the GPT method [see Eq. (7)], the indirect-effect component of the total perturbation $\delta R(x)$ should be appreciable.

(iii) To allow useful comparisons with "exact" (i.e., direct calculation) results, the perturbation $\delta\Sigma$ should not be so large that second- and higher-order terms in $\delta\Sigma$, which are ignored in the first-order GPT applied herein, become overwhelmingly large.

In view of the conditions described above, four test cases, as described in Table II, have been devised. These cases meet the above conditions adequately, but the following exceptions should be noted:

(a) Case 1 does not satisfy condition (i) well, but is a good test for predicting a small spatial shift in the peak power.

(b) Case 3 does not satisfy condition (iii) well, but is an interesting example of a very large perturbation that effectively transforms the heterogeneous core into a homogeneous one.

VII. RESULTS FOR TEST CASES

VII. A. $\underline{\Gamma}_k^{*(i)}$ Results

Various characteristics of the functions $\underline{\Gamma}_k^{*(i)}$ are illustrated by the results presented in Figs. 2 through 5. All numerical results discussed in this and the following sections are for x_k=22.5 cm, the mesh point at which the maximum value of R_k occurred in the unperturbed (i.e., "base-case" calculation of the power density response R(x). The spatial shape of $\underline{\Gamma}_k^*$ is illustrated in Figs. 2 and 3. The neutron importance to $R(x_k)$ is greatest near x_k; there, a neutron most probably contributes to the numerator of Eq. (13). As a function of x, $\underline{\Gamma}_k^*(x)$ is negative over a wide range due to the neutron contributions to the denominator of Eq. (13).

The shape of the curves for $\underline{\Gamma}_k^{*(1)}$ and $\underline{\Gamma}_k^{*(2)}$ can be discussed in terms of the expressions derived in Sec. IV. For this purpose, recall that $\underline{\Gamma}_k^*$ depends both on x_k and x, and that the associated response $R_k \equiv R(x_k)$ depends on x_k but not on x. In the following, the dependence of $\underline{\Gamma}^{*(i)}(x,x_k) \equiv \underline{\Gamma}_k^{*(i)}(x)$ on each of the two independent variables x and x_k will be addressed separately.

As functions of x_k, the relationships between the $\Gamma_{k,j}^{*(i)}$ for the j-th energy group have been generally given, in vector form, by Eq. (42), i.e.,

$$R_k^{(i)} \underline{\Gamma}_k^{*(i)} = d^i \left[R_k \underline{\Gamma}_k^* \right] / dx_k^i . \qquad [(42)]$$

Qualitatively, this behavior is illustrated in Fig. 4, which presents $\underline{\Gamma}_k^{*(1)}(x)$ as a function of x. For group 2, for example, given the fact that $R_k^{(1)}$ is positive, the shape shown in Fig. 4 can be obtained by considering

various fixed, but successively larger, values of x on the set of curves for $\underline{\Gamma}^*(x,x_k)$ shown in Fig. 2.

As functions of x, the qualitative behavior of $\Gamma^{*(i)}_{k,j}$, shown in Figs. 2 through 5, can be supported by considering the analytic results for Γ^*_1, $\Gamma^{*(1)}_1$ and $\Gamma^{*(2)}_1$ obtained in Sec. IV for a simple one-group, one-region case. Although the results shown in Figs. 2 through 5 are for a multi-region, multigroup case, the predominant features of these results near x_k are expected to be similar to those of the simpler one-group, one-region model. This is because:

(i) the fixed point x_k is well within the interior of the driver region, and hence is neutronically "far" (several mean free paths) from other regions;

(ii) the x-dependence of $\Gamma^{*(i)}_{k,j}(x)$ is strongly influenced by the spatial form of the fixed sources, $\underline{S}^{*(i)}_k(x)$; for our test cases, these sources are space-energy separable in the driver region;

(iii) coupling between groups for the multigroup case does not change the predominant features of the x-dependence of $\Gamma^{*(i)}_{k,j}(x)$, since this dependence is similar for all groups. This similarity, illustrated in Fig. 3, is principally due to (ii), above.

The discussion that followed Eqs. (59) through (64), and that focused on the predominant features of the x-dependence of the functions $\Gamma^{*(1)}_1$ and $\Gamma^{*(2)}_1$, also provides a good description of the predominant features of the x-dependence of the derivative importance functions shown in Figs. 4 and 5.

The values of $\Gamma^{*(2)}_k$ for $x \neq x_k$ are significantly smaller than the value at x_k, and are sensitive to the "fundamental harmonic correction"[2,22] that must be used to eliminate fundamental harmonic

contamination when calculating $\underline{\Gamma}^{*(i)}$. Although the CIAP-INO version of CIAP-1D[17] that was employed to calculate the adjoint functions performs this correction, the correction was numerically inadequate to determine $\underline{\Gamma}_k^{*(2)}$. This situation was resolved by noting that the functions $\underline{\Gamma}_k^{*(i)}$ satisfy the orthogonality property

$$\langle \underline{\Gamma}_k^{*(i)}, \mathbf{B}\, \underline{\Phi} \rangle = 0, \tag{88}$$

where **B** is the fission operator. As a result of applying this orthogonality property to eliminate fundamental harmonic contamination, the values for $\underline{\Gamma}_k^{*(2)}$ obtained by using the fixed source $\underline{S}_k^{*(2)}$ [see Eq. (24)] agreed well with the corresponding values obtained by using Eq. (26).

The numerical accuracy of calculating $\Gamma_k^{*(1)}$ was verified in a similar manner: on the one hand, $\underline{\Gamma}_k^{*(1)}$ was calculated by using the fixed source $S_k^{*(1)}$ [see Eq. (23)] and, on the other hand, $\underline{\Gamma}_k^{*(1)}$ was calculated by using Eq. (25). These calculations gave essentially identical results.

A mesh spacing of 1.5 cm, which is a typical value specified for benchmark calculations of critical assemblies with LMFBR characteristics (e.g., ZPR-3-48),[23] was initially chosen for both forward and adjoint calculations. The results for the functions $\underline{\Gamma}_k^{*(i)}$ were obtained by using this mesh spacing. The sharp variations displayed by these functions provided a strong motivation to investigate whether this mesh spacing, which is adequate for calculating the comparatively smooth forward fluxes, is indeed adequate for accurately calculating the adjoint functions. This adequacy was investigated by performing several calculations with a finer mesh, obtained by reducing the 1.5 cm mesh spacing to 0.5 cm in a region around x_k. Although the shapes of $\underline{\Gamma}_k^{*(i)}$ changed slightly due to the additional mesh points (an expected outcome considering the sharp

variations involved), the use of the two meshes yielded essentially identical results for $\delta R_k^{(i)}$. This gives confidence that the 1.5 cm mesh spacing is indeed adequate. All numerical results reported in this work were obtained by using the 1.5 cm mesh-spacing.

VII. B. Comparison of Results for $\delta R^{(i)}(x_k)$ Obtained from GPT and Direct Calculations

The accuracy of values for $\delta R_k^{(i)}$ obtained from GPT calculations was verified by performing two direct TAIM[16] calculations. As discussed in Sec. V.A, the results of these direct calculations are termed "exact". The convergence criteria for these direct calculations were adequately stringent to insure that the exact results retained sufficient significant figures for comparisons with perturbation-theory results. As indicated in Tables III through VI, the exact and GPT results for $\delta R_k^{(i)}$ generally agreed within about 5%. Note that for all four cases, the indirect component of $\delta R_k^{(i)}$ is greater than the direct component for at least two of the three i values. Thus, condition (ii) of Sec. VI.B is largely satisfied.

The results shown in the last columns of Tables IV and V indicate that GPT and exact results do not agree well for $\delta R_k^{(2)}$ of Case 2, and for Case 3, respectively. For Case 3, the disagreement between GPT and exact results indicates that the nonlinear terms disregarded by first-order GPT are not small. This is not surprising, since Case 3 represents a very large perturbation. The disagreement between GPT and exact results for $\delta R_k^{(2)}$ of Case 2 can be analyzed by comparing the results for $\delta R_k^{(2)}/R_k^{(2)}$ presented in the fourth columns of Tables III through VI. This comparison shows that $\delta R_k^{(2)}/R_k^{(2)}$ is smallest for Case 2, being about an order of magnitude smaller than for Case 1 and about two orders of magnitude smaller than for

Cases 3 and 4. Note now that the effects of the nonlinear terms disregarded by first-order GPT are measured by $\varepsilon(x)$ defined as

$$\varepsilon(x) = \delta R_p(x) - \Delta R_e(x), \tag{89}$$

where ΔR_e and δR_p are given by Eqs. (67) and (68), respectively. Recalling that $\delta R_k^{(2)}$ for Case 2 is a very small quantity that is calculated by using Eq. (16), it is expected that even a weak dependence of $\varepsilon(x)$ on x would cause appreciable differences between exact and GPT results. Calculations of $\varepsilon(x)$ have indicated that this is indeed true for Case 2. Note, though, that if $\delta R_k^{(2)}$ is small compared to δR_k and/or $\delta R_k^{(1)}$, then inaccuracies in $\delta R_k^{(2)}$ will influence results for $\delta R(x)$ appreciably only if $(x - x_k)$ is large. This follows from the use of Eq. (14).

VII. C. Comparison of Taylor-GPT, GPT, and Exact Results for $\delta R(x)$

The use of the Taylor-GPT method raises questions concerning the accuracy of both the GPT and Taylor-series features. To investigate these questions, two series of comparisons were performed:

(a) First, results obtained for $\delta R_{tp}(x)$ were compared to exact values $\Delta R_e(x)$ [see Eqs. (69) and (67), respectively]. As discussed in Sec. V.A, this comparison assesses the composite accuracy of both features (i.e., second-order Taylor expansion around x_k, and use of GPT) of the Taylor-GPT method.

(b) Second, results for $\delta R_{tp}(x)$ were compared to results for $\delta R_p(x)$ [see Eqs. (69) and (68), respectively]. As discussed in Sec. V.A, this comparison assesses the accuracy of solely the Taylor series expansion feature of the Taylor-GPT method. (The

inaccuracies due to the use of GPT are eliminated in this comparison.)

Tables VII through IX present the comparisons mentioned in item (a) above. These comparisons show that for values of $x - x_k$ varying from -10 cm to 20 cm, $\delta R_{tp}(x)$ and $\Delta R_e(x)$ agree within about 5%. This generally good agreement worsens only when $x - x_k$ becomes large (in absolute value), or when $\delta R(x)$ is about to change sign while going smoothly through a zero (e.g., Case 4, x = 10.5 cm, in Table IX).

Although Case 1 does not generally satisfy condition (i) of Sec. VI.B, the values of $\delta R_{tp}(x)$ obtained by using all three terms in Eq. (69) agree well, within 5%, with the exact values $\Delta R_e(x)$. Notably, this good agreement persists even at distances $x - x_k$ as large as 30 cm. As will be discussed in Sec. VII.E, the perturbation considered in Case 1 causes only a small spatial shift in the location of the maximum power density. Thus, the good overall agreement between $\delta R_{tp}(x)$ and $\Delta R_e(x)$ obtained in this case represents an additional positive verification of the adequacy of the numerical methods used in this work.

The results presented in the last two columns of Tables VII through IX also indicate that the use of only the first two terms in the Taylor expansion given by Eq. (69) is adequate when x is not very far from x_k. The generally good agreement between $\Delta R_e(x)$ and the values of $\delta R_{tp}(x)$ obtained by using this two-term expansion indicates that, in certain cases, the number of adjoint calculations may be reduced; for example, calculation of $\underline{\Gamma}_k^{*(2)}$ may not be necessary if only small to moderately large distances $x - x_k$ are of interest. Of course, the adequacy of using a two-term expansion for calculating $\delta R_{tp}(x)$ also depends on the size of the perturbation. Cases 1 and 2 involve small perturbations, but Cases 3 and 4 involve larger

ones. For the latter cases, the importance of the term containing $\delta R_k^{(2)}$ in Eq. (69) is illustrated in Fig. 6.

Results for the second set of comparisons, i.e., those mentioned in item (b) at the beginning of this section, are presented in Table X. For completeness, this table presents not only comparisons of $\delta R_{tp}(x)$ vs. $\delta R_p(x)$, but also includes comparisons with the exact values $\Delta R_e(x)$. Note the selection of particular combinations of perturbation cases (i.e., Cases 3 and 4 of Table II) and values of x: each combination simultaneously involves a large perturbation and a large absolute value of $x - x_k$. The reason for selecting such combinations is to deliberately accentuate the space-dependent inaccuracies, expressed by $\varepsilon(x)$ defined by Eq. (89), of using first-order GPT.

The outcome of comparing $\delta R_{tp}(x)$, $\delta R_p(x)$, and $\Delta R_e(x)$ is concisely expressed in Table X by presenting the values for TAP and TAE obtained from Eqs. (70) and (71), respectively. As expected, the nonlinear effects ignored by the Taylor-GPT method are important in these cases; this importance is clearly indicated by the large values obtained for the quantity TAE. The main contribution to these nonlinear effects, though, arises from the GPT component of the Taylor-GPT method. This fact is indicated by the small values obtained for the quantity TAP, which show that the Taylor-GPT results agree closely with the GPT results. These characteristics are further highlighted in Fig. 6, which shows that, even though the GPT results differ from the exact ones by as much as 50%, the Taylor-GPT and GPT results agree within 4% for a large range of distances x. This indicates that whenever the GPT method is sufficiently accurate, the use of the Taylor-GPT method could substantially reduce the number of calculations for investigations of space-dependent response variations.

VII. D. Spatial Shifts, and Their Influence on Peak Power Density Sensitivities

Perturbations in nuclear data alter not only the maximum value taken on by the power density, but also cause spatial shifts in the location of this maximum. To calculate these shifts by using the Taylor-GPT method, it is convenient to rewrite Eq. (75) as

$$x_{m1} - x_{m0} = - \frac{R_0^{(1)}}{R_0^{(2)}} \cdot \frac{\delta R^{(1)}/R^{(1)} - \delta R^{(2)}/R^{(2)}}{1 + \delta R^{(2)}/R^{(2)}} . \qquad (90)$$

Table XI presents numerical values for the spatial shifts (i.e., $x_{m1} - x_{m0}$) caused by the perturbations described in Cases 1 through 4. "Direct," "indirect," and "total" contributions were calculated by using the Taylor-GPT method. The respective contributions are denoted in Table XI by $S_{tp,D}$, $S_{tp,I}$, and $S_{tp,T}$, and were obtained by replacing the quantity $\delta R^{(i)}$ in Eq. (90) with $\delta R_D^{(i)}$, $\delta R_I^{(i)}$, and $(\delta R_D^{(i)} + \delta R_I^{(i)})$, respectively. For comparison, Table XI also presents exact results, denoted by $S_{e,T}$, for the total shift. These values were obtained by using actual recalculations, with perturbed data, in conjunction with Eqs. (72) and (74).

The indirect contributions (i.e., $S_{tp,I}$) are generally preponderant; the direct contributions $S_{tp,D}$ are zero for Cases 3 and 4, and are still much smaller than $S_{tp,I}$ for Case 2. Only for Case 1, which involves a very small shift, are the values of $S_{tp,I}$ and $S_{tp,D}$ comparable.

The results presented in the last row of Table XI show that shifts predicted by the Taylor-GPT method agree well with the exact ones for distances between approximately 0.15 cm and 5 cm. For Case 3, which represents a perturbation so large that it effectively transforms the

heterogeneous core into a homogeneous one, the shift predicted by the Taylor-GPT method substantially overestimates the actual shift. This highlights the importance of the nonlinear terms that are neglected by first-order GPT.

The influence of spatial shifts on the sensitivity of peak-power density has been discussed in Sec. V.C. This influence is characterized by the quantity SE defined by Eq. (86). Table XII shows that the error caused by the shift in the location of the maximum power is small for Cases 1 and 2. For larger perturbations, e.g. Cases 3 and 4, the effect of the spatial shift on the sensitivity is appreciable and cannot be neglected.

VIII. SUMMARY AND CONCLUSIONS

This work has presented an efficient method to investigate one-dimensional, space-dependent variations $\delta R(x)$ in the power-density distribution $R(x)$. This method has been called the Taylor-GPT method in order to highlight its two main characteristics: (a) use of a Taylor series expansion of $\delta R(x)$ in the spatial variable x, and (b) use of generalized perturbation theory (GPT)[1-4] to efficiently evaluate the derivative operators that appear as coefficients in this Taylor series.

Equations satisfied by the importance (i.e., adjoint) functions for the i-th spatial derivative of $\delta R(x)$ have been derived within the framework of GPT. Using finite-differences, it has been shown that these equations can be solved in a straightforward manner with existing GPT codes to obtain the importance functions. The main characteristics of these importance functions have been highlighted analytically by deriving certain relationships that they satisfy. A deeper understanding of these characteristics has been facilitated by deriving the complete analytical expressions of the importance functions for an illustrative (one-region, one-group) reactor model.

It has been shown that the Taylor-GPT method is efficient not only for estimating space-dependent variations in the power density, but also for estimating spatial shifts that parameter perturbations induce in the localized peak-power density. To illustrate its usefulness, this method has been applied to four test cases involving a simplified three-region one-dimensional model of a heterogeneous LMFBR. The results given by the Taylor-GPT method have been compared to those produced by the standard GPT

method, and both have been verified by comparisons to exact results (obtained by actual recalculations with altered parameter values).

These comparisons indicate that the results given by the Taylor-GPT method are practically as accurate as those given by the standard GPT method. The Taylor-GPT method includes all the advantages offered by adjoint methods, e.g., the same importance functions are used to assess the effects on the response of many parameter perturbations. In addition, the Taylor-GPT method could substantially reduce (even by comparison to standard GPT) the number of calculations for investigations of space-dependent variations in the power density. Note, though, that the Taylor-GPT method does not account for second- and higher-order effects of parameter variations. Nevertheless, the Taylor-GPT method provides detailed information regarding specific contributions (e.g., due to leakage, absorption) to the overall variation in the response. The availability of such detailed information is valuable for systematic and efficient reactor design studies.

References and Footnotes

1. A. Gandini, J. Nucl. Energy, 21, 755 (1967).

2. G.P. Cecchini and M. Salvatores, Nucl. Sci. Eng., 46, 304 (1971).

3. J.H. Marable, C.R. Weisbin, and G. De Saussure, Nucl. Sci. Eng., 75, 30 (1980).

4. C.R. Weisbin et al., Sensitivity and Uncertainty Analysis of Reactor Performance Parameters, Advances in Nuclear Science and Technology, Plenum Press, Vol. 14 (1980).

5. J.M. Kallfelz, D. Biswas, C.L. Cowan, J.H. Marable, M.L. Williams, C.R. Weisbin, J.D. Drischler, T.B. Fowler, and J.R. White, "Design and Sensitivity Analysis of a CDS-Type LMFBR Heterogeneous Core," in 1980 Advances in Reactor Physics and Shielding, p. 467, American Nuclear Society (1980).

6. J.H. Marable, C.R. Weisbin, J.R. White, D. Biswas, J.M. Kallfelz, C.L. Cowan And R. Protsik, "Sensitivities and Uncertainties of a Large LMFBR Using Adjusted Cross Section Library ORACLE-1," Trans. Am. Nucl. Soc., 41, 578 (1982).

7. D.G. Cacuci, J. Math. Phys., 22, 2794 (1981).

8. D.G. Cacuci, J. Math. Phys., 22, 2803 (1981).

9. V.A. Perone, J.M. Kallfelz, and L.A. Belblidia, Nucl. Sci. Eng., 79, 326 (1981).

10. L.A. Belblidia, A. Gandini, J.M. Kallfelz, and V.A. Perone, Trans. Am. Nucl. Soc., 39, 957 (1981).

11. A.F. Henry, Nuclear-Reactor Analysis, MIT Press, Cambridge, Mass., (1975).

12. D.G. Cacuci, P.J. Maudlin, and C.V. Parks, "Adjoint Sensitivity Analysis of Extremum-Type Responses in Reactor Safety," ORNL/TM-7717, Oak Ridge National Laboratory (1982).

13. A Gandini, Nucl. Sci. Eng., 77, 316 (1981).

14. In ref. 15, Cacuci et al. considered the heat conduction equation, and gave examples of the importance function for the first derivative of the temperature.

15. D.G. Cacuci, C.F. Weber, E.M. Oblow, and J.H. Marable, Nucl. Sci. Eng., 75, 88 (1980).

16. I. Dal Bono, "TAIM-Multigroup Diffusion Code," Doc. CEC(66)12, Comitato Nazionale per L'Energia Nucleare (1966).

17. I. Dal. Bono, V. Leproni, and M. Salvatores, "The CIAP-1D Code," RT/FI(68)9, Comitato Nazionale per L'Energia Nucleare (1968).

18. I. Dal Bono, V. Leproni, and M. Salvatores, "The GLOBPERT-1D Code," RT/FI(68)10, Comitato Nazionale per L'Energia Nucleare (1968).

19. A.H. Zemanian, Distribution Theory and Transform Analysis, McGraw-Hill, New York (1965).

20. J.M. Kallfelz, G.B. Bruna, G. Palmiotti and M. Salvatores, Nucl. Sci. Eng., 62, 304 (1977).

21. T.B. Fowler and D.R. Vondy, "Nuclear Reactor Analysis Code: CITATION," ORNL-TM-2496, Rev. 2, Oak Ridge National Laboratory (1971).

22. E.M. Oblow, "Reactor Cross-Section Sensitivity Studies in Critical Reactors Using Transport Theory," ORNL-TM-4437, Oak Ridge National Laboratory, 1974.

23. W.G. Davey and A.L. Hess, "Additional Fast Reactor Benchmarks for Phase II Data Testing of ENDF/B," CSEWG Newsletter 18, Cross Section Evaluation Working Group (March 1969).

APPENDIX A

APPLICATION OF THE ITALIAN GPT CODE PACKAGE TO CALCULATE SPATIAL DERIVATIVES OF $\delta R(x)$

A. 1. Calculation of $\Gamma^{*(i)}$

In general, the solution to the adjoint problem is computed by CIAP[17] for ratios of the form:

$$R_0 = \frac{\int_{V_1} \sum_j \Sigma_{1,j}(x)\ \phi_j(x)\ dx}{\int_{V_2} \sum_j \Sigma_{2,j}(x)\ \phi_j(x)\ dx} \quad . \tag{A-1}$$

Eq. (A-1) can be cast in a form amenable to calculate $\delta R^{(i)}/R^{(i)}$ by simply preparing, as indicated below, the input data for the adjoint source.

The energy-production cross sections in the numerator and denominator of Eq. (A-1) are written as

$$\Sigma_{1,j}(x) = \sum_k p^k\ N_1^k(x)\ \sigma_{f,j}^k \quad , \tag{A-2}$$

and

$$\Sigma_{2,j}(x) = \sum_k p^k\ N_2^k(x)\ \sigma_{f,j}^k \quad , \tag{A-3}$$

respectively, where N_i^k denotes densities for nuclide k. Subscripts 1 and 2 in N_1^k and N_2^k, respectively, allow for potentially distinct spatial behavior of the energy-production cross sections. With these specifications,

CIAP computes the desired $\underline{\Gamma}^{*(i)}$ if the densities are chosen in the following manner:

(a) $N_2^k(x) = N_m^k$ for all x in region m, m=1, M

(b) for $\underline{\Gamma}^{*(1)}$ calculations:

$$N_1(x) = \begin{cases} +N_{m0}, & \text{for } x=x_{k+1} \text{ and } x \in m0 \\ -N_{m0}, & \text{for } x=x_{k-1} \text{ and } x \in m0 \\ 0.0, & \text{elsewhere} \end{cases}$$

(c) for $\underline{\Gamma}^{*(2)}$ calculations:

$$N_1(x) = \begin{cases} +N_{m0}, & \text{for } x=x_{k+1},\ x_{k-1} \text{ and } x \in m0 \\ -2N_{m0}, & \text{for } x=x_k \text{ and } x \in m0 \\ 0.0, & \text{elsewhere} \end{cases}$$

Here, m and M refer, respectively, to the region number and the number of regions, m0 denotes the number of the region where the peak power occurs, and N_m^k and N_{m0}^k are the densities of nuclide k in regions m and m0, respectively.

Note that CIAP includes the volumes associated with the mesh points in the integrations over space. But, as long as the mesh spacing is uniform in the vicinity of x_k, this does not affect the values of the fractional variation of the derivatives. Note also that CIAP attaches a factor of 0.5 to the contribution of a point to the integral value if the contribution of the point preceding it or the point following it is zero. To guard against this, one must use a very small value for the input density (of the order of 10^{-14}) at x_{k-2} and x_{k+2}.

A.2. Direct-Effect Calculations

The code GLOBPERT-1D[18] can be used to calculate the direct-effect component of $\delta R^{(i)}/R^{(i)}$. For this purpose, the input data for the direct-effect calculations must be prepared as follows:

(a) for $\delta R^{(1)}/R^{(1)}$ calculations,

$$\delta N = \begin{cases} +\delta N_i, & x=x_{k+1} \\ -\delta N_i, & x=x_{k-1} \\ 0.0, & \text{elsewhere} \end{cases}$$

(b) for $\delta R^{(2)}/R^{(2)}$ calculations,

$$\delta N = \begin{cases} +\delta N_i, & x=x_{k+1}, \text{ or } x=x_{k-1} \\ -2\delta N_i, & x=x_k \\ 0.0, & \text{elsewhere} \end{cases}$$

Here, δN_i denotes the density change for nuclide i and effected in the quantity $Q_{l,k}$ [see Eq. (22)].

Also note that GLOBPERT-1D was modified to treat more accurately the interfaces between regions. In addition, an algorithm was implemented to calculate δD (i.e., the perturbation in the diffusion coefficient) exactly, rather than via a first-order expansion in $\delta\Sigma_{tr}$ as done in the original version of this code.

APPENDIX B

DETERMINATION OF $\Gamma_1^{*(2)}$

In view of Eqs. (45) and (51), the function $\Gamma_1^{*(2)}$ is the solution of

$$\left.\begin{aligned} &\frac{d^2\,\Gamma_1^{*(2)}}{dx^2} + B^2\,\Gamma_1^{*(2)} = \frac{1}{DQ_2} - \frac{1}{DQ_{1,2}}\,\delta''(x - x_k) \\ &\Gamma_1^{*(2)} = 0 \quad \text{at } x = L \\ &\frac{d\Gamma_1^{*(2)}}{dx} = 0 \text{ at } x = 0 \end{aligned}\right\} \qquad \text{(B.1)}$$

Applying a Laplace-transform to Eq. (B.1), and defining

$$U(p) = \int_0^\infty e^{-px}\,\Gamma_1^{*(2)}\,dx, \qquad \text{(B.2)}$$

gives

$$U(p) = K\,\frac{p}{p^2+B^2} - \frac{1}{DQ_{1,2}}\,\frac{p^2\exp(-px_k)}{p^2+B^2} + \frac{1}{DQ_2}\,\frac{1}{p(p^2+B^2)}, \qquad \text{(B.3)}$$

where K is, at this stage, an unknown constant to be determined.

Taking the inverse Laplace-transform of Eq. (B.3) gives

$$\Gamma_1^{*(2)} = K\cos Bx + \frac{1}{B^2 DQ_2}\,(1-\cos Bx)$$

$$- \frac{1}{DQ_{1,2}} \left[\delta(x-x_k) - B\, H(x-x_k)\, \sin B(x-x_k)\right] . \qquad \text{(B.4)}$$

For a critical reactor, the boundary conditions given in Eq. (B.1) are automatically satisfied; thus, the constant K is determined by using the orthogonality condition given in Eq. (88). This leads to

$$K = \frac{1}{B^2 DQ_2}\left(1 - \frac{2}{BL}\right) + \frac{B}{DQ_{1,2}}\left(\frac{\cos Bx_k}{BL} + \frac{L - x_k}{L}\sin Bx_k\right) . \qquad \text{(B.5)}$$

Replacing Eq. (B.5) in Eq. (B.4) yields

$$\Gamma_1^{*(2)} = \frac{1}{B^2 DQ_2} + \left[\frac{\cos Bx_k + B(L-x_k)\sin Bx_k}{LDQ_{1,2}} - \frac{2}{DB^3 LQ_2}\right]\cos Bx$$

$$+ \frac{B}{DQ_{1,2}}\, H(x-x_k)\sin B(x-x_k) - \frac{\delta(x-x_k)}{DQ_{1,2}} . \qquad \text{(B.6)}$$

TABLE I

Nuclide Concentrations for Test Model

Nuclide	Concentration [10^{24} atom/cm^3]	
	Driver	Blankets (IB,EB)
U-238	0.006	0.012
Pu-239	0.001	0.0
Na	0.010	0.007

TABLE II

Selected Perturbations and Corresponding Test Cases

Case	Zonal Perturbation[a]		
	Int. Blkt. (IB)	Driver (D)	Ext. Blkt. (EB)
1		$\frac{\delta N^{49}}{N^{49}} = -3\%$	$\delta N^{49} = +0.045\ N_D^{49}$
2	$\frac{\delta N^{28}}{N^{28}} = +5\%$	$\frac{\delta N^{49}}{N^{49}} = -5\%$	$\frac{\delta N^{28}}{N^{28}} = +5\%$
3	Replaced with driver.	Inner boundary extended to core center (x=0).	
4	Outer three cm replaced with driver	Inner boundary extended to x=7.5 cm.	

a. N_x^{yz} is the number density in zone x of the nuclide with the last digits in its atomic number and weight of y and z, respectively. If no x appears, N is for the zone designated by the column heading. N values are given in Table I.

TABLE III

GPT and Exact $\delta R^{(i)}(x_k)$ Results for Case 1[a-e]

Derivative Order, i	GPT Results for $\delta R^{(i)}/R^{(i)}$			$\delta R_p^{(i)}$ (GPT)	$\Delta R_e^{(i)}$ (Exact)[g]	$\frac{\text{GPT-Exact}}{\text{Exact}}$ [%]
	Direct[f]	Indirect[f]	Total			
0	-9.16-3	-2.25-3	-1.14-2	-3.56-4	-3.69-4	-3.7
1	+2.26-1	+2.97-1	+5.23-1	+2.71-6	+2.88-6	-5.8
2	-3.59-3	-1.16-2	-1.52-2	+2.86-7	+3.04-7	-5.8

a. All values are for x_k = 22.5 cm.

b. Because of the characteristics of CIAP, R has a ΔVol factor of 1.5 cm^3 in the numerator which is not contained in Eq. (9).

c. Read ±x-y as $\pm x \cdot 10^{-y}$.

d. See Table II for description of perturbation cases.

e. Values presented in the last three columns are calculated with more significant figures than shown.

f. See discussion of Eq. (7).

g. Exact value determined from two direct calculations; see Eq. (67).

TABLE IV

GPT and Exact $\delta R^{(i)}$ Results for Case 2.[a]

Derivative Order, i	GPT Results for $\delta R^{(i)}/R^{(i)}$ Direct	Indirect	Total	$\delta R_p^{(i)}$ (GPT)	$\Delta R_e^{(i)}$ (Exact)	$\frac{\text{GPT-Exact}}{\text{Exact}}$ [%]
0	5.41-4	2.59-3	3.13-3	9.77-5	9.09-5	7.4
1	3.93-1	-2.17+0	-1.78+0	-9.21-6	-9.05-6	7.7
2	9.82-3	-7.26-3	2.55-3	-4.80-8	-3.4-8	39.

a. See footnotes for Table III

Table V

GPT and Exact $\delta R^{(i)}$ Results Case 3.[a]

Derivative Order, i	GPT Results for $\delta R^{(i)}/R^{(i)}$ Direct	Indirect	Total	$\delta R_p^{(i)}$ (GPT)	$\Delta R_e^{(i)}$ (Exact)	$\frac{\text{GPT-Exact}}{\text{Exact}}$ [%]
0	-1.59-1	3.78-2	-1.21-1	-3.79-3	-3.79-3	-0.14
1	-1.59-1	-5.44+1	-5.46+1	-2.83-4	-2.14-4	32.
2	-1.59-1	-4.52-1	-6.11-1	1.15-5	1.00-5	14.

a. See footnotes for Table III.

Table VI

GPT and Exact $\delta R^{(i)}$ Results for Case 4.[a]

Derivative Order, i	GPT Results for $\delta R^{(i)}/R^{(i)}$ Direct	Indirect	Total	$\delta R_p^{(i)}$ (GPT)	$\Delta R_e^{(i)}$ (Exact)	$\frac{\text{GPT-Exact}}{\text{Exact}}$ [%]
0	-4.54-2	1.14-2	-3.39-2	-1.06-3	-1.05-3	0.75
1	-4.54-2	-1.58+1	-1.58+1	-8.19-5	-7.64-5	7.2
2	-4.54-2	-1.31-1	-1.76-1	3.32-6	3.22-6	3.1

a. See footnotes for Table III.

TABLE VII

Taylor-GPT and Exact $\delta R(x)$ Results[a] for Case 1;[b] x_k = 22.5 cm

x [cm]	$x-x_k$ [cm]	Exact[c] ΔR_e	Taylor-GPT[d] δR_{tp}	$\frac{\delta R_{tp} - \Delta R_e}{\Delta R_e}$ [%][d]	
				3-term[e]	2-term[f]
13.5	-9	-3.84-4	-3.69-4	-4.0	-1.0
16.5	-6	-3.82-4	-3.67-4	-3.9	-2.5
25.5	+3	-3.60-4	-3.46-4	-3.7	-3.3
28.5	+6	-3.47-4	-3.34-4	-3.6	-2.1
34.5	+12	-3.13-4	-3.02-4	-3.3	+3.2
40.5	+18	-2.68-4	-2.61-4	-2.9	+14.
52.5	+30	-1.53-4	-1.46-4	-4.9	+79.

a. Read $\pm x-y$ as $\pm x \cdot 10^{-y}$.

b. See Table II for description of test cases.

c. Exact value determined from two direct calculations; see Eq. (67).

d. Values presented in the last three columns are calculated with more significant figures than shown.

e. Values for δR_{tp} obtained by using all three terms in Eq. (69).

f. Values for δR_{tp} obtained by using only the first two terms in Eq. (69).

TABLE VIII

Taylor-GPT and Exact Results[a] for Case 2; x_k = 22.5 cm

x [cm]	$x-x_k$ [cm]	Exact ΔR_e	Taylor-GPT δR_{tp}	$\frac{\delta R_{tp} - \Delta R_e}{\Delta R_e}$ [%]	
				3-term	2-term
10.5	-12	+1.93-4	+2.05-4	+6.0	+8.
13.5	-9	+1.69-4	+1.79-4	+5.4	+7.
16.5	-6	+1.44-4	+1.52-4	+5.5	+6.
19.5	-3	-	+1.25-4	-	-
25.5	+3	-	+6.98-5	-	-
28.5	+6	+3.64-5	+4.16-5	+14.	+17.
34.5	+12	-1.71-5	-1.63-5	-4.9	-25.
40.5	+18	-6.79-5	-7.59-5	+12.	+0.3
52.5	+30	-1.57-4	-2.00-4	+27.	+13.

a. See footnotes for Table VII.

TABLE IX

Taylor-GPT and Exact Results[a] for Case 4; x_k = 22.5 cm

x [cm]	$x-x_k$ [cm]	Exact ΔR_e	Taylor-GPT δR_{tp}	$\frac{\delta R_{tp} - \Delta R_e}{\Delta R_e}$ [%]	
				3-term	2-term
10.5	-12	+8.32-5	+1.63-4	+96.	+190.
13.5	-9	-2.38-4	-1.87-4	-21.	+35.
16.5	-6	-5.36-4	-5.07-4	-5.	+6.
19.5	-3	-	-7.98-4	-	-
25.5	+3	-	-1.29-3	-	-
28.5	+6	-1.45-3	-1.49-3	+3.	+7.
34.5	+12	-1.73-3	-1.80-3	+4.	+18.
40.5	+18	-1.88-3	-2.00-3	+6.	+34.
52.5	+30	-1.81-3	-2.02-3	+12.	+94.

a. See footnotes for Table VII.

TABLE X

Comparisons of $\Delta R_e(x)$, $\delta R_p(x)$, and $\delta R_{tp}(x)$ for Large Perturbations and Large $|x - x_k|$

Perturbation Case	x [cm]	TAP[a] [%]	TAE[b] [%]
4	13.5	-3.7	-22.
4	40.5	+1.9	+6.3
3	13.5	-3.3	-47.
3	40.5	+2.0	+17.

a. See Eq. (70).

b. See Eq. (71).

TABLE XI

Spatial Shifts [cm] in Location of Peak Power

Shifts[a]	Case 1	Case 2	Case 3	Case 4
$S_{e,T}$	+0.160	-0.482	-22.8	-4.85
$S_{tp,T}$[b]	+0.151	-0.490	-38.2	-5.23
$S_{tp,I}$	+0.086	-0.601	-27.1	-4.96
$S_{tp,D}$	+0.064	+0.105	0.0	0.0
$S_{tp,I}+S_{tp,D}$	+0.150	-0.496	-27.1	-4.96
$\frac{S_{tp,T}-S_{e,T}}{S_{e,T}}$	-5.6%	+1.7%	+67.8%	+8.0%

a. Shifts are defined in Sec. VII.E.

b. $S_{tp,T}$ differs slightly from $(S_{tp,I} + S_{tp,D})$ because the sum neglects the second-order terms mentioned immediately after Eq. (80).

TABLE XII

Influence of the Spatial Shift on the Peak-Power Density

Case	SE[a] [%]
1	0.009
2	-0.029
3	-63.5
4	-17.0

a. See Eq. (86).

LIST OF FIGURES

Figure

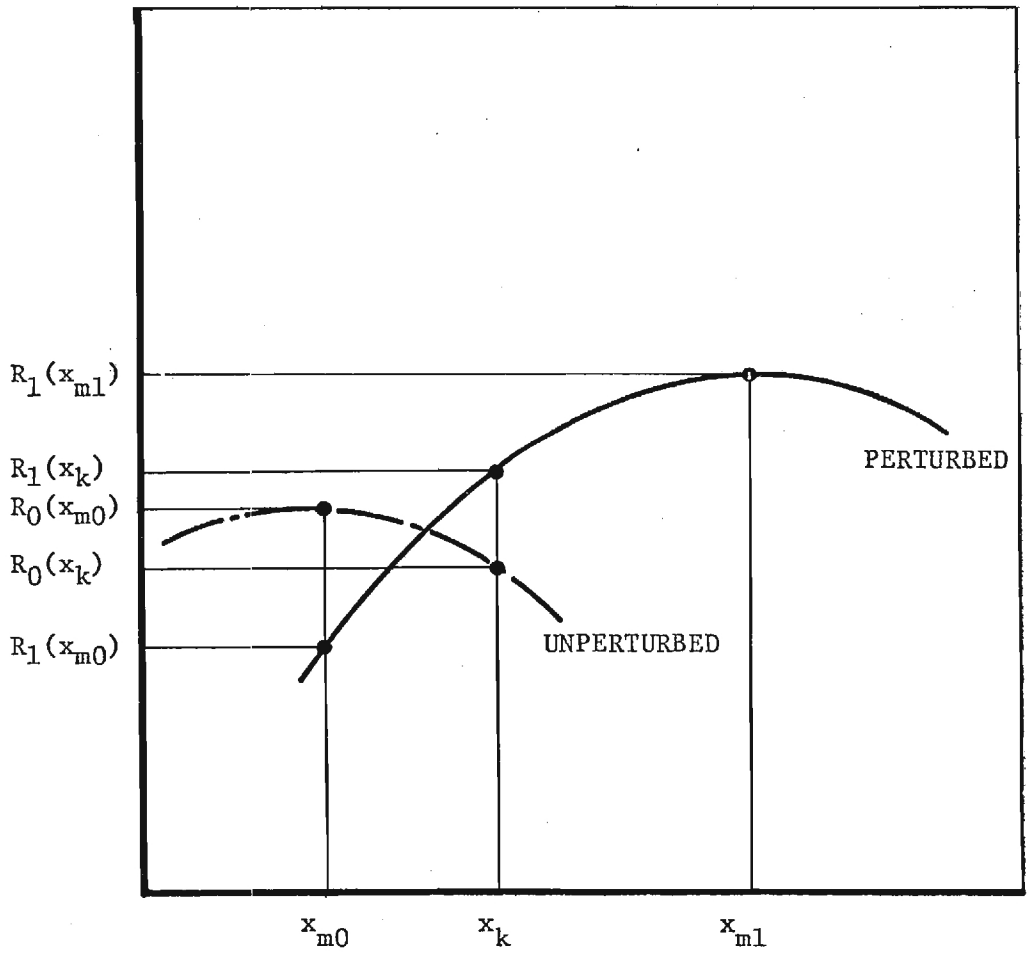
$R_1(x_{m1})$
$R_1(x_k)$
$R_0(x_{m0})$
$R_0(x_k)$
$R_1(x_{m0})$
PERTURBED
UNPERTURBED
x_{m0}
x_k
x_{m1}

Figure 1

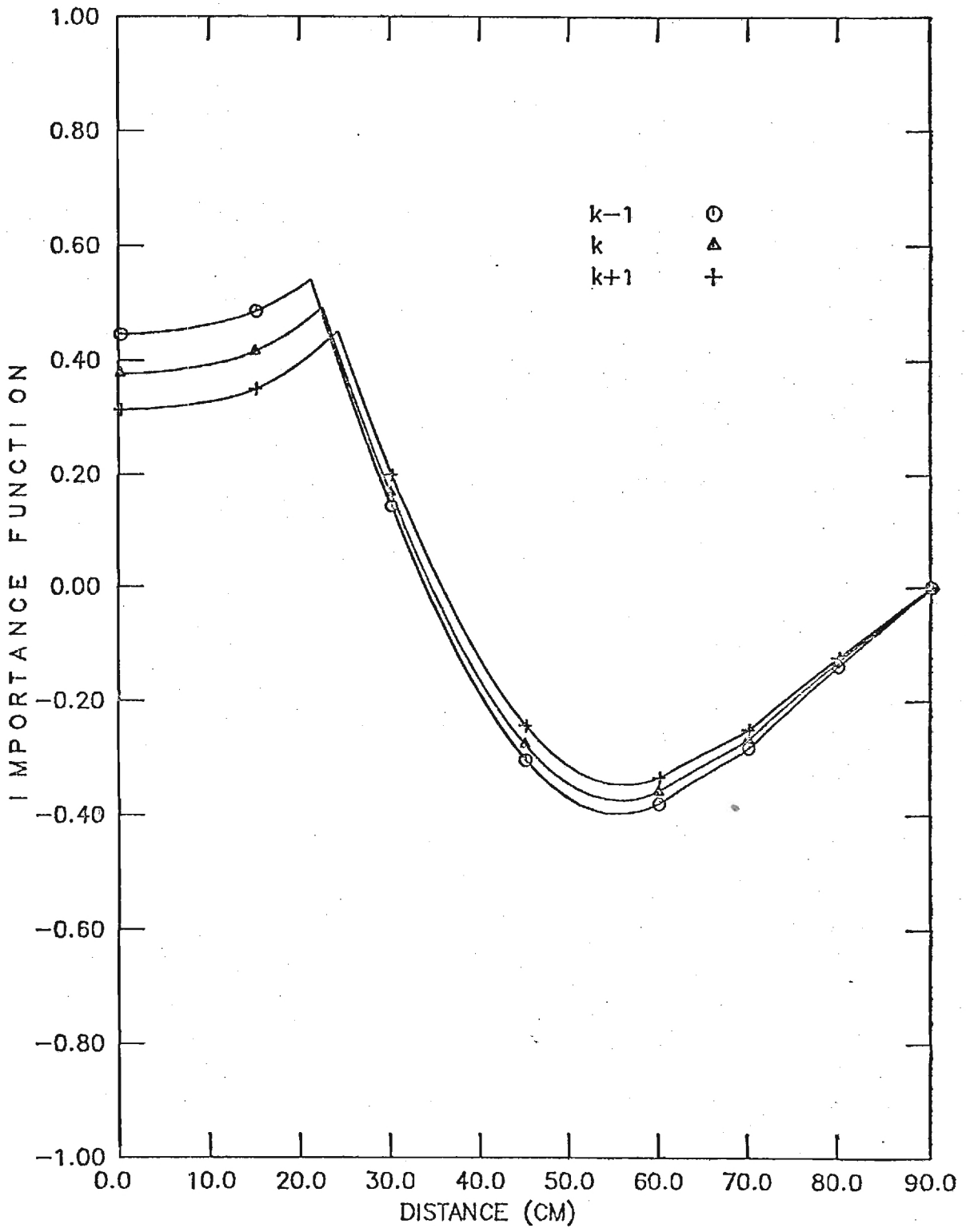
1.00
0.80
0.60
0.40
0.20
0.00
−0.20
−0.40
−0.60
−0.80
−1.00
IMPORTANCE FUNCTION
k−1
k
k+1
0.0
10.0
20.0
30.0
40.0
50.0
60.0
70.0
80.0
90.0
DISTANCE (CM)

Figure 2

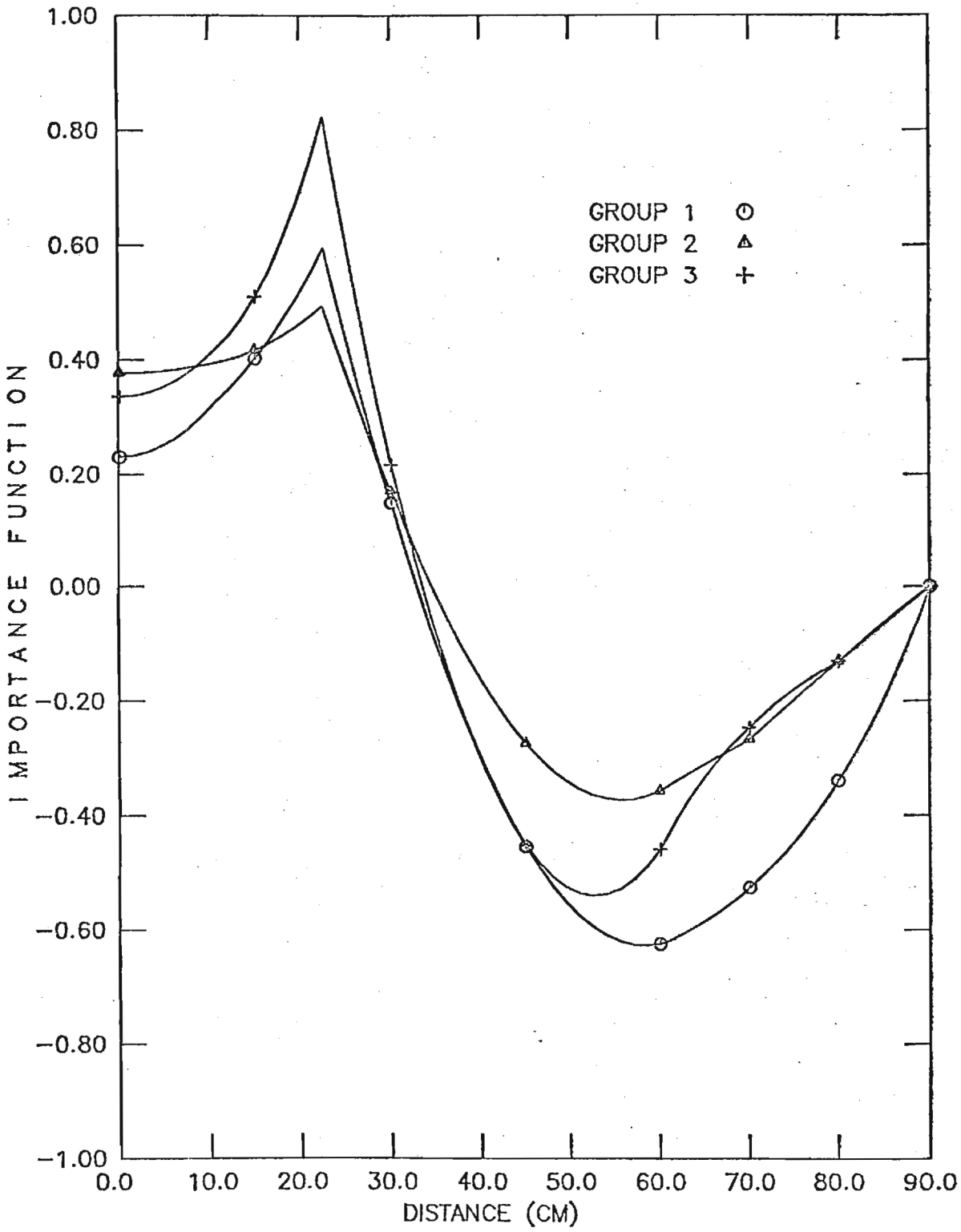
1.00
0.80
0.60
0.40
0.20
0.00
−0.20
−0.40
−0.60
−0.80
−1.00
IMPORTANCE FUNCTION
GROUP 1
GROUP 2
GROUP 3
0.0
10.0
20.0
30.0
40.0
50.0
60.0
70.0
80.0
90.0
DISTANCE (CM)

Figure 3

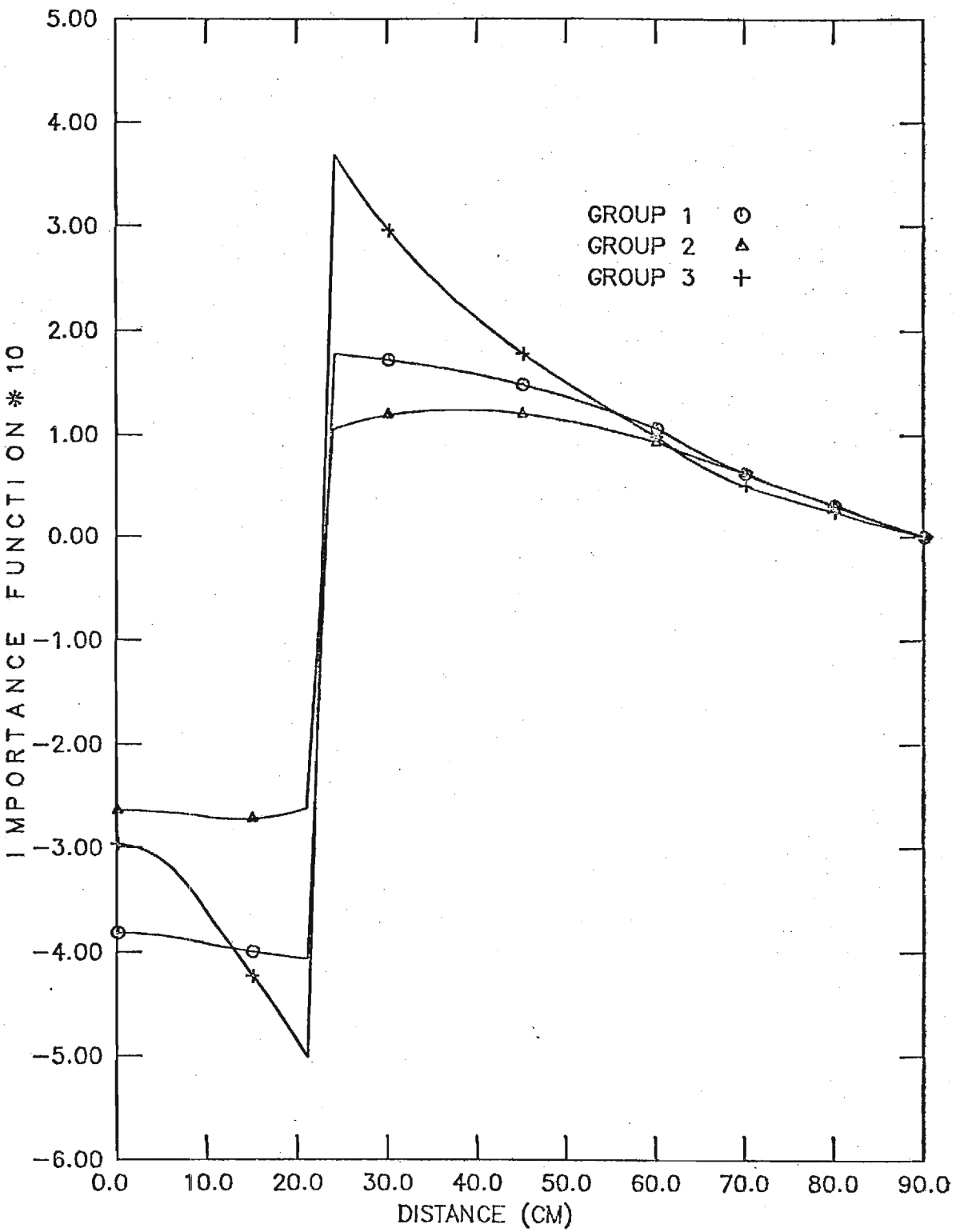
5.00
4.00
3.00
2.00
1.00
0.00
−1.00
−2.00
−3.00
−4.00
−5.00
−6.00
IMPORTANCE FUNCTION * 10 2
0.0
10.0
20.0
30.0
40.0
50.0
60.0
70.0
80.0
90.0
DISTANCE (CM)
GROUP 1
GROUP 2
GROUP 3

Figure 4

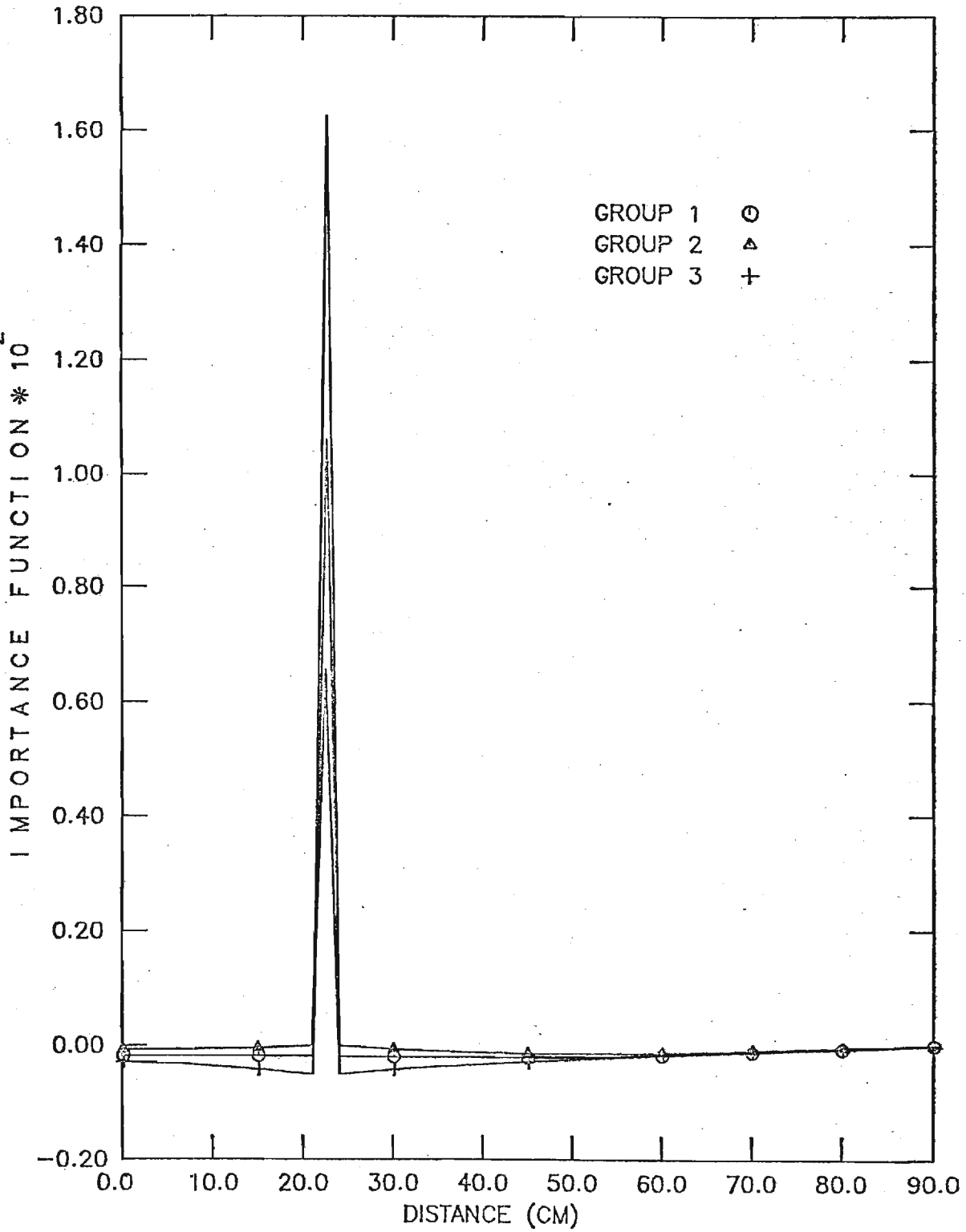
1.80
1.60
1.40
1.20
1.00
0.80
0.60
0.40
0.20
0.00
−0.20
IMPORTANCE FUNCTION * 10^2
GROUP 1
GROUP 2
GROUP 3
0.0
10.0
20.0
30.0
40.0
50.0
60.0
70.0
80.0
90.0
DISTANCE (CM)

Figure 5

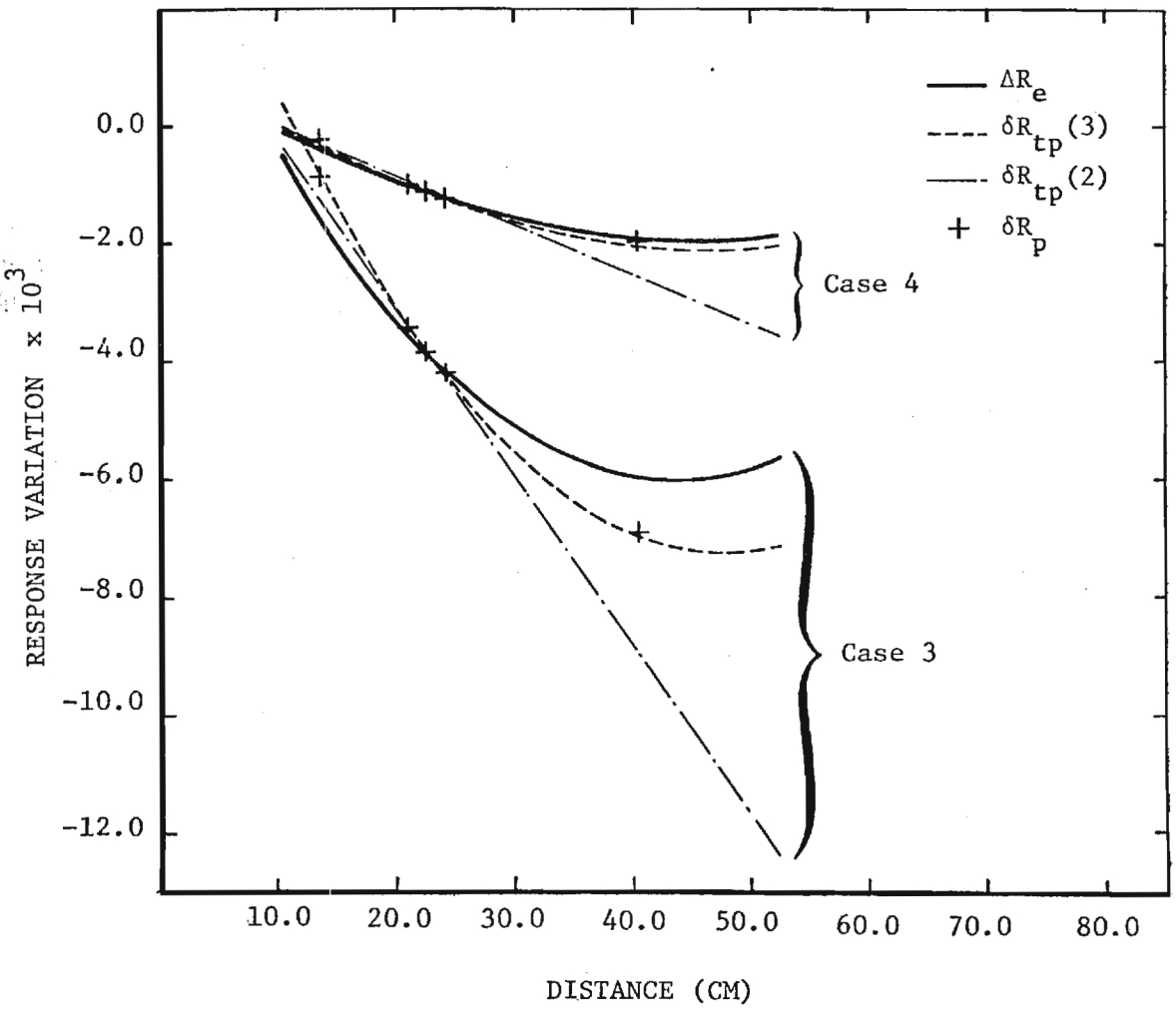
ΔR_e
$\delta R_{tp}(3)$
$\delta R_{tp}(2)$
δR_p
Case 4
Case 3
0.0
-2.0
-4.0
-6.0
-8.0
-10.0
-12.0
RESPONSE VARIATION x 10^3
10.0
20.0
30.0
40.0
50.0
60.0
70.0
80.0
DISTANCE (CM)

Figure 6

GITNEHP-83/1

STUDIES FOR A POWER DISTRIBUTION AND REACTIVITY MONITOR (PDRM) AND PEAK CORE POWER DENSITIES

by J. M. Kallfelz and L. A. Belblidia

Annual Progress Report for ORNL Subcontract 7802-X01

October 1983

ABSTRACT

This annual progress report covers the activity of the Georgia Institute of Technology during the period October 1, 1982 - September 30, 1983, under Oak Ridge National Laboratory Subcontract 7802-X01.

The primary task of this activity, initiated in July 1983, is related to the development of a Power Distribution and Reactivity Monitor (PDRM) for a fast breeder reactor. This report contains a summary of these investigations, the conclusions that can be made based on the present status, and recommendations for further work.

Some effort was also expended to complete an article concerning the use of generalized perturbation theory for investigations of reactor power density distributions. This article has been published, and is included in this report as an appendix.

TABLE OF CONTENTS

1. Introduction

The studies discussed in this report have been described in more detail in our monthly progress reports[22-28] to Oak Ridge National Laboratory. The primary effort was related to the development of a Power Distribution and Reactivity Monitor (PDRM) for a fast breeder reactor. The studies related to the PDRM are discussed in Section 2. Section 3 and Appendix A concern the use of generalized perturbation theory for investigations of reactor power density distributions.

2. Power Distribution and Reactivity Monitor

2.1. General Comments on PDRM Development

The goal for development of an on-line power distribution and reactivity monitor (PDRM) is to provide a system which is "capable of providing a rapid assessment of the status of core parameters which are important for economical and safe reactor operation."[1] It is important to recognize the significant difference in the applicable experience for the two components of the monitor name, i.e. "power distribution" and "reactivity." There is considerable experience in the development and application of "reactivity balance meters" [2] in LMFBRs. However, development of power distribution monitoring capability in fast reactors is in a relatively early stage, partially because related experience in thermal reactors is not directly applicable. As discussed below, this is because of the difference in the location of neutron detectors in fast and thermal reactors.

2.1.1 Reactivity Balance Meters

Basically, a reactivity balance meter (RBM) compares on-line the "real" or "measured" reactivity with the "expected" or "theoretical" reactivity.[2-4] The measured reactivity is determined with a "reactivity meter" (RM), utilizing neutron detector readings and the inverse kinetics equations.[4] The theoretical reactivity is calculated, using reactivity feedback coefficients and various measured parameters, e.g. power, control rod positions, coolant T_{inlet}, coolant ΔT in core, etc.[2] Such a device is also called an anomalous-reactivity (ANOR) meter[4], and the associated

monitoring procedure has been referred to as "reactivity surveillance procedure-anomaly detection" (RSP-AD).[5]

Reactivity balance meters have been used in Rapsodie[2] and FFTF[5], and use of the CAROL RBM is planned for Super-Phenix.[3] An RBM was planned for the Fermi-1 "malfunction detection analyzer"[6], and a conceptual RBM design was performed for EBR-II.[4]

2.1.2 Power Distribution Monitor

For thermal reactors, several systems which include power shape monitoring have been developed.[7,8] Of particular interest is the BWR Hybrid Power Shape Monitoring System (PSMS) developed under EPRI sponsorship.[7] This system monitors the state of the core in real time, and allows for adjustment of a few parameters to mimimize the difference between measured and theoretical values for in-core detector readings.[7] A nodal[10] physics code coupled to a thermal hydraulics code is used for monitoring and predictive analysis.

The presence of in-core detectors is obviously a great advantage in power distribution monitoring. The readings from these monitors are used to check and adjust the calculated power distribution. The following performance parameter is minimized:[7]

$$J = \sum_{l,k} w(l,k) R^2(l,k) \qquad (1)$$

where l and k designated location, the residual R is the normalized difference between the measured and calculated detector readings, and w is a weighting factor.

Unfortunately, it is difficult to use in-core detectors in fast reactors, because of the core environmental conditions,[9] and most designs

call for ex-vessel detectors. For instance, the neutron detectors for Super-Phenix are located outside the safety vessel, which encloses the main containment vessel.[3] It is obvious that the information content of such detectors concerning the core power shape is relatively small, compared to that of in-core detectors.

This raises the obvious question:

> Are there any measurable parameters for an LMFBR which are appropriate for adjustment of data used for calculated power shapes?

Gamma scan data for fuel elements can be used, but only at end-of-cycle. For a BWR it has been shown that adjustment during the cycle is necessary to avoid a serious deterioration in the accuracy of calculated cycles.[7]

Possibly the best standard of comparison for on-line LMFBR calculational models is a detailed off-line 3D calculation, to be performed periodically. Sandra and Azekura[9] used detailed 3D calculations to validate results from an influence function method they propose for on-line LMFBR calculations.

2.2. Impact of PDRM on LMFBR Safety and Economics

In our August 1 meeting with John Lewellen, he requested a brief statement discussing the contribution of a PDRM to the safety and economics of an LMFBR. Following is a draft of this statement.

It is generally recognized that on-line core surveillance systems using special computers can have a significant impact on the safe and economic operation of both thermal and fast reactors.[1,3,7-9] The introduction of powerful mini-computers coupled to the surveillance process facilitates a significant improvement in on-line performance evaluation of a fast reactor core. The reactor state functions, e.g. reactivity and power distribution, can be estimated with increased accuracy using such systems.

The improvement in safety achieved by an on-line Power Distribution and Reactivity Monitor (PDRM) is accomplished in a variety of ways, including the following:

- o By the detection of incipient incidents as soon as possible. For instance, analysis has indicated that with a device to detect "anomalous reactivity" (the difference between predicted and measured reactivity) the Fermi-1 flow blockage incident would have been detected at a much smaller excess reactivity than for the actual case.[4]
- o By diagnosing any incipient incident promptly. Such diagnosis may be utilized to protect the core either by input to an automatic safety system, or by helping the operator to determine the proper action to control the incident.[3]
- o By insuring that various safety-related limits (e.g. peak clad temperature, peak fuel temperature) are not exceeded.

Many features of a PDRM contribute to improved economics of an LMFBR, e.g.

- o Prompt control of incipient incidents which have a potential for core damage obviously influences the reactor economics.
- o Early diagnosis of an incident may allow control thereof without scram. This avoids mechanical stresses which impact on the core life, and may allow continued operation at a reduced power, improving the plant load factor compared to that for a scram occurence.[3]
- o Increased knowledge of the reactor state aids in insuring that the design fuel life is reached.

- o Increased reliability of reactor state prediction also allows operation nearer the design limits, increasing the reactor power output.
- o Used to predict the influence of operator actions, the PDRM can assist in short-term operational strategy planning, considering economic criteria.

In summary, a PDRM can be a valuable tool to improve knowledge of the core state, to reduce the impact of incipient incidents, and to help the reactor staff to optimize reactor operation with regard to safety and economic criteria.

2.3. GPT Investigation of Ex-Core Detector Reading Sensitivity to Core Power Distribution

Generalized perturbation theory[11,12] (GPT) can be used to investigate the sensitivity of ex-core detector readings to the core power distribution. "Ex-core" is a very general expression, and apparently "ex-vessel" is a more appropriate term for most LMFBR designs. As mentioned in section 1.2, the neutron detectors for Super-Phenix are far from the core, under the safety vessel. For a realistic analysis of such a system, transport theory methods[13] are necessary.

2.3.1 Initial GPT Investigations

For initial calculations related to this problem, I have used diffusion theory GPT codes[12], the simple 1D slab model of an LMFBR described in Ref. 11, and an assumed detector location in the outer blanket, 10 cm from the core. This simple case is an appropriate starting point, and will yield some physical insight into the problem we are considering; definitive results will require gradual extension to a model approximating the realistic ex-vessel case, described above.

For these initial calculations, the response function is similar to that considered in our studies[11] of the core power density. Assuming the detector response is proportional to σ_f (U-235), the normalized response ratio is:

$$R(x_D) = \frac{Q_1(x_D)}{Q_2} \qquad (2)$$

where x_D is the detector location,

$$Q_1(x_D) = \int \sum_j \sigma_{fj} \phi_j(x') \delta(x'-x_D) dx' \qquad (3)$$

and Q_2, given by eqns. (11) and (12) of Ref. 11, is the total reactor power. Normalization with Q_2 represents the constraint of constant power for power density shape changes. It should be noted that R in eqn. (2) is of the same form as the response considered in our power density studies[11].

The generalized adjoint function, $\vec{\Gamma}^*(x)$, calculated for $R(x_D)$, gives the importance of neutrons at x in various energy groups to the ratio R.[11] The sensitivity of the core power density (PD) to the neutron flux distribution is given by the fixed source in the $\vec{\Gamma}^*$ eqn. for PD, as indicated by eqn. (5) of Ref. 11. Conversion from neutron flux sensitivity to that for the neutron density is trivial; thus the functions mentioned in this paragraph can be used to study the sensitivity of detector response to PD shape.

Figure 1 gives results for $\vec{\Gamma}^*$ for $R(x_D)$ of eqn. (2). The group cross section set is the same as that used in Ref. 11. Following are some aspects of interest, and their implications:

a. For obvious reasons, the importance curves are smooth in the core. Thus it seems unlikely that detection of <u>localized</u> flux perturba-

tions with ex-core detectors will be possible, even with a large number of detectors.

b. The importance curves have an appreciable space dependence over the core. Neutrons near the core edge have a larger probability of contributing to the detector reading, and thus have a positive importance, while those near the reactor center are more likely to contribute to the normalization denominator of $R(x_D)$, and have a negative importance. Thus for the case considered the ex-core detector could be useful in the determination of "core-wide" flux shape changes, e.g. "flux tilt". (Other information, e.g. total power and coolant ΔTs, would also be necessary.) This aspect should be investigated for detectors farther from the core.

c. If we are interested in sensitivity to <u>relative</u> changes in the flux shape, the curves in Fig. 1 should be multiplied by $\phi_g(x)$ to determine regions of significance. (The product $\phi\Gamma^*$ includes information on the location of neutrons which may contribute to R.) Since ϕ drops rapidly with distance from the core, this multiplication increases the significance of the core regions to $R(x_D)$.

At this point we are primarily interested in the sensitivity to changes in flux shape, rather than the cause of such changes. However, a perturbation calculation was performed for "Case 3" of Ref. 1, which replaces the inner blanket with driver. The impact on $R(x_D)$ was determined by GPT and "exactly" (by solving for ϕ for the base and perturbed cases.) The "exact" $\delta R/R$ is - 24.5%, while the GPT code result was -18.3% with by far the largest contribution from the "direct-effect" term[11]. As mentioned in Ref. 11, for this quite large perturbation second-and higher-order terms involving $\delta\Sigma$ and $\delta\phi$ are significant.

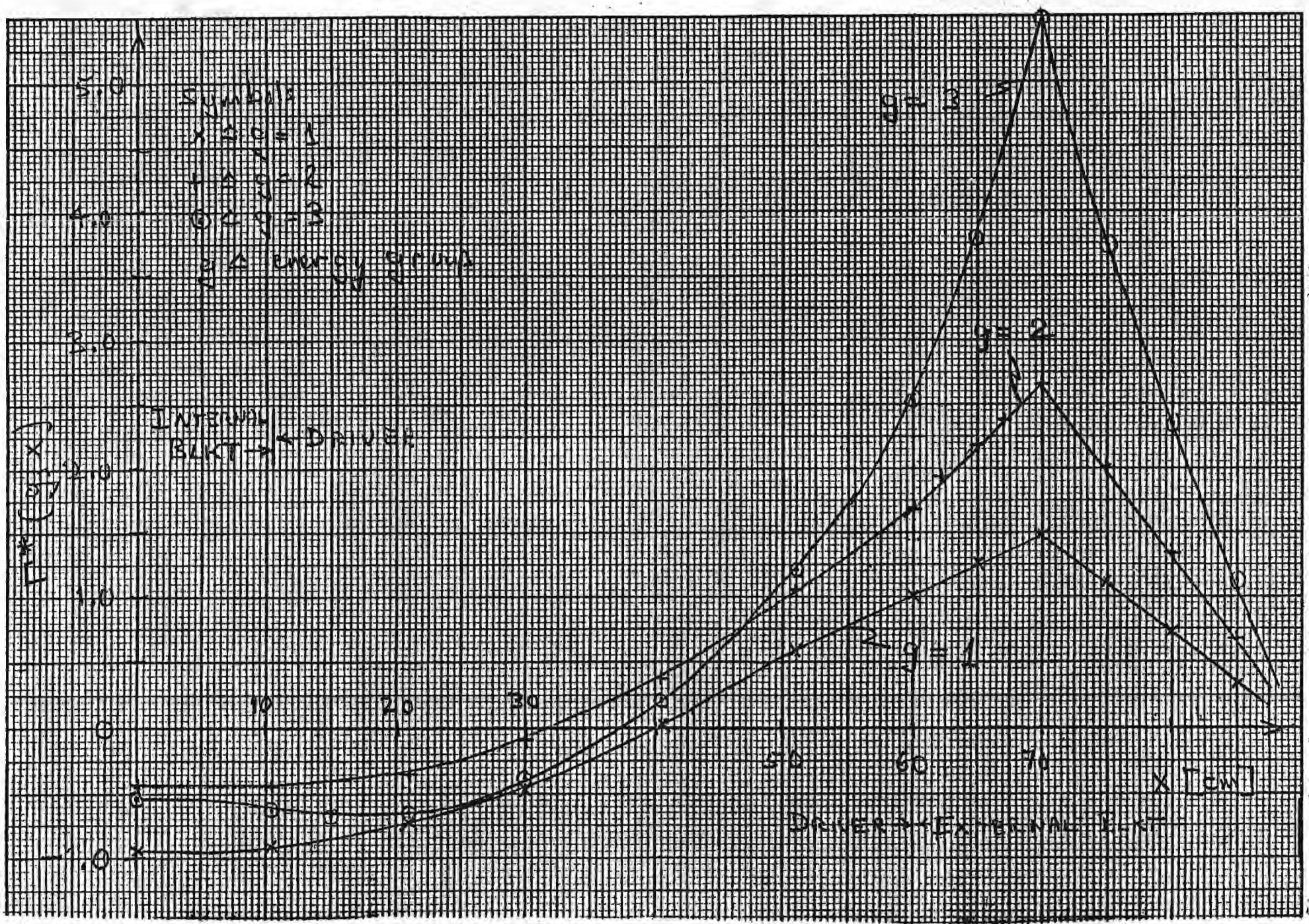

Figure 1. (From [28]. Γ^* for ex-core detector normalized response; (Detector at x = 70 cm; reactor model as in [11]).

2.3.2 Influence of Detector-Core Distance on Detector Information Content

In the previous section it was concluded that, while it seems unlikely that detection of localized flux perturbations with ex-core detectors will be possible, such detectors could be useful for the detection of "core-wide" flux shape changes For the studies described in the previous section the detector was assumed to be in the blanket 10 cm from the core. In the present section we describe investigations for detectors farther from the core.

Table 1 presents Γ^* results for detectors located in the blanket 10, 20, and 25 cm from the core. All results are for group 2 of the 3-group CITATION test case data set[14]. Several aspects of the results are significant:

a. Within the core the space-dependence of Γ^* for the three cases is nearly the same. At least for this aspect moving the detector farther from the core does not obviously decrease the information content of the detectors concerning core flux shape.

b. The relative importance to the detector response of neutrons near the detector compared to that for neutrons in the core does increase as the detector distance from the core is increased. This does not necessarily mean that the detector becomes less sensitive to the core flux behavior for such a move, however. As noted in the previous section, regions of significance for the detector response also depend on the neutron population distribution; thus $\phi_g \Gamma^*_g$ determines regions of significance. As can be seen in Table 1, the decrease in ϕ_2 as the core-detector distance increases more than compensates for the increase in Γ^* at the detector location.

For comparison of groups it should be noted that Γ^* gives the importance of neutrons, not flux. While ϕ_3 for the nuclear data set we used[14] is significantly smaller than ϕ_2, the ratio of the average velocities of these groups is roughly the same as that of the fluxes. Thus groups 2 and 3 have about the same value for neutron density.

In summary, for core-detector distance from 10 to 25 cm, the aspects considered yield no evidence that moving the detector farther from the core causes an appreciable decrease in the information content of the detectors concerning core flux shape.

Table 1. Comparison of Γ_2^* for Detector 10, 20, and 25 cm from Core, in Outer Blkt.[a,b]

x (dist. from core center)	$\Gamma^*(10)$	$\Gamma^*(20)$	$\frac{\Gamma^*(20)}{\Gamma^*(10)}$	$\Gamma^*(25)$	$\frac{\Gamma^*(25)}{\Gamma^*(10)}$	Φ_2	
0	-.435	-.473	1.09	-.481	1.11	2.18	Inner Blkt
10.5	-.444	-.484	1.09	-.492	1.11	2.22	
21.	-.345	-.384	1.11	-.392	1.14	2.25	Driver
30.	-.086	-.119	–[c]	-.128	–[c]	2.19	
40.5	+.400	+.379	.947	+.373	.932	2.01	
51.	1.05	1.05	1.00	1.05	1.00	1.72	
60.	1.69	1.72	1.02	1.73	1.02	1.41	
70.	2.66	2.79	1.05	2.81	1.06	0.91	Outer Blkt
80.	1.34	3.52	2.61	3.57	2.66	0.44	
85.	.673	1.77	2.64	3.85	5.71	0.22	

a. Core–outer Blkt. interface is at x = 60 cm, and blanket is 30 cm wide.

b. Γ^* values at detector location highlighted with rectangle.

c. Values excluded if proximity to location of Γ^* sign change makes ratio insignificant.

2.4 Method for On-Line Calculations of Reactor Parameters

For simple calculations of reactor parameters we have discussed three methods:

a. Nodal/Modal codes[10]. Such codes have extensive use for thermal reactor monitoring systems[7].

b. Influence function methods[9].

c. Eigenfunction expansion methods[16,30].

Felix di Fillipo is obtaining promising results from method c., for one-group calculations, with eigenfunctions of the Laplace-transformed equation.

Since one-group calculations are generally not adequate for fast reactors, we should consider the fact that for the multigroup case of the Boltzmann equation, it is "generally assumed that the eigenfunctions ϕ_n associated to eigenvalues λ_n —— do not form a complete set" except under special conditions[18]. This topic is further discussed in various references[17-21]. However, it is shown in Reference 18 that an expension in such eigenfunctions is applicable for functionals of the fission source, such as the reactor power. A recent paper by Gilai[31] substantiates this conclusion.

2.5 Recommendations for Further Work

2.5.1 Information Content of Ex-Vessel Detectors

Relevant to the sensitivity of ex-vessel neutron detectors to core power distributions, the following is recommended:

Lacking definitive information to the contrary, we should assume that the U.S. LMFBR will use a ex-vessel neutron monitor system similar to that of Super-Phenix[3]. Thus we should investigate the information content of neutron detectors located under the safety vessel, at the location of "neutron guides (themselves located in the first layer of the blanket)"[3]. Such investigations could involve at least two steps:

a. Calculations of Γ^* for the normalized neutron density (rather than detector response) at a position in the blanket. This will yield information on the

sensitivity of this density (as a function of group) to the core flux distribution. For these calculations a cylindrical model should be used, to include the radial "geometrical effects" not contained in the slab model used until now.

b. 2D adjoint transport theory calculations, similar to those performed in Reference 13, should be performed to determine the importance of neutrons at the core midplane (in the neutron guide tube) the response of the ex-vessel detectors at the bottom of the guide tube. For these calculations perhaps we can use a reactor model approximating that of the "modular breeder"[15].

2.5.2 Methods of On-Line Calculations

Parallel to the development of eigenfunction expansion methods discussed in section 2.4, we should begin investigations to determine which nodal methods or already-developed codes might be employed for our power distribution and reactivity monitor.

2.5.3 Use of Measured Values for Adjustment of Parameters Used in On-Line Calculations

We should investigate further the question raised in section 2.1.2, to determine how reactor parameters measured during operation could be used to adjust data used for calculated power shapes.

3. Generalized Perturbation Theory with Derivative Operators for Power Density Investigations in Nuclear Reactors

The research related to this topic was performed almost entirely in the previous report year[32]. However, some effort was devoted to this topic in the present report year, in making revisions to the final version of the journal article[11] describing this work. This article, published in July 1983, is included as Appendix A.

REFERENCES*

1. "Cooperative Nuclear Data and Methods Development, Fiscal Year 1982," GEFR-14073-8, General Electric Co., September 1982.

2. B. Berthet et al., "Operation Experience of a Reactivity Balance Meter at Rapsodie" in Proc. Internat. Topical Meting on LMFBR Safety and Related Design and Operational Aspects, Lyon, July 19-23, 1982.

3. C. Berlin et al., "Super-Phenix Core Surveillance and Protection System," in same procedings as ref. 2.

4. H. A. Larson and B. R. Peterson, "The EBR-II Reactivity Meter: Conceptual Design," ANL-79-52, Argonne Nat. Lab.

5. R. A. Harris et al., "Reactivity Feedbacks in the FFTF: Predictions and Monitoring Techniques" in Trans. ANS 44, 513 (1983).

6. E. R. Volk et al., "Direct Connectin of the Femi-1 Malfunction Detection Analyzer with the Plant Safety System," in Proc. Internat. Conf. on Engineering of Fast Reactors for Safe and Reliable Operation, Karlsruhe, Oct. 9-13, 1972, Gesellschaft fur Kernforschung, Karlsruhe, 1973.

7. B. Frogner, A. Ipaktchi and A. B. Long, "Hydraulic Calibration Methods for the BWR Hybrid Power Shape Monitoring System," in Proc. ANS/ENS Internat. Topical Meeting on Advances in Mathematical Methods for Nuclear Engineering Problems, Munich, April 27-29, 1981.

8. OECD Halden Reactor Project, "Core Surveillance Systems: Development at the Halden Project and Within Signatory Organizations," HWR-32, Institutt for Energiteknikk, Halden, Norway.

9. T. Sandra and K. Azekura, "Calculational Model Based on Influence Function Method for Power Distribution and Control Rod Worth in Fast Reactors," Nucl. Sci. Engr. 85, 70 (1983).

10. H. W. Graves, Jr., "Power-Reactor Performance Evaluation Using Nodal/Modal Analysis, Ann. Nucl. Energy 10, 395 (1983).

11. L. A. Belblidia, J. M. Kallfelz, and D. G. Cacuci, "Generalized Perturbation Theory with Derivative Operators for Power Density Investigations in Nuclear Reactors" Nucl. Sci. Engr. 84, 206 (1983).

12. Refs. 16-18 of Ref. 11.

13. G. F. Flanagan et al., "Analysis of Stored Fuel, Control Rod and Inherent Source Effects on the CRBR Ex-Vessel Source Range Monitoring System" in J. M. Kallfelz and R. A. Karam, Eds., Advanced Reactors: Physics, Design and Economics, Pergamon Press, New York, 1975.

*Note that the appendix has a separate reference list.

14. T.B. Fowler, D.R. Vondy and G.W. Cunningham, "Nuclear Reactor Core Analysis Code: CITATION," ORNL-TM-2496, Rev. 2, Oak Ridge Nat. Lab., July 1971. (See p. 250-3).

15. C.L. Cowan, private communication to J.M. Kallfelz received September 6, 1983.

16. F. di Fillipo, private communication received September 1983.

17. A. Gandini, Nucl. Sci. Engr. 67, 347 (1978).

18. A. Gandini, "On the Standard Perturbation Theory," NSE preprint received September 1981.

19. A. Sargeni, "Studi sulla Fisica dei Reattori Veloci," Thesis, Universita degli Studi di Roma, August, 1981.

20. J.M. Kallfelz, Letter to John R. White, ORNL, dated October 13, 1981, (with partial translation of Reference 19 enclosed).

21. J. M. Kallfelz, and L. A. Belblidia, "Progress Report for ORNL Subcontract 7802, Period October - December 1981, " Memorandum to C. R. Weisbin, J. H. Marable, and D. G. Cacuci (ORNL), School of Nuclear Engineering and Health Physics, Georgia Institute of Technology, January 19, 1982.

22. L. A. Belblidia and J. M. Kallfelz, "Progress Report for ORNL Subcontract 7802, Month of July 1982", Memorandum to D. G. Cacuci, J. H. Marable and C. R. Weisbin, (ORNL), School of Nuclear Engineering and Health Physics, Georgia Institute of Technology, August 4, 1982.

23. J. M. Kallfelz and L. A. Belblidia, "Progress Report for ORNL Subcontract 7802, Months of August and September 1982", Memorandum to C. R. Weisbin and D. G. Cacuci, (ORNL), School of Nuclear Engineering and Health Physics, Georgia Institute of Technology, December 20, 1982.

24. J. M. Kallfelz and L. A. Belblidia, "Progress Report for ORNL Subcontract 7802, Months of October, November and December 1982", Memorandum to C. R. Weisbin and D. G. Cacuci, (ORNL), School of Nuclear Engineering and Health Physics, Georgia Institute of Technology, December 20, 1982.

25. J. M. Kallfelz and L. A. Belblidia, "Progress Report for ORNL Subcontract 7802, Months of January, February, and March, 1983", Memorandum to C. R. Weisbin and D. G. Cacuci, (ORNL), School of Nuclear Engineering and Health Physics, Georgia Institute of Technology, April 5, 1983.

26. J. M. Kallfelz and L. A. Belblidia, "Progress Report for ORNL Subcontract 7802, Months of April, May, and June, 1983", Memorandum to C. R. Weisbin and D. G. Cacuci, (ORNL), School of Nuclear Engineering and Health Physics, Georgia Institute of Technology, August 9, 1983.

27. J. M. Kallfelz, "Progress Report for ORNL Subcontract 7802, "Period July 1 - August 1, 1983", Memorandum to D. G. Cacuci, C. R. Weisbin, and B. A. Worley, (ORNL), School of Nuclear Engineering and Health Physics, Georgia Institute of Technology, August 9, 1983.

28. J. M. Kallfelz, "Progress Report for ORNL Subcontract 7802, Period August 2, - September 1, 1983", Memorandum to D. G. Cacuci, C. R. Weisbin and B. A. Worley (ORNL), School of Nuclear Engineering and Health Physics, Georgia Institute of Technology, September 7, 1983.

29. J. M. Kallfelz, "Progress Report for ORNL Subcontract 7802, Period September 1-30, 1983", Memorandum to D. G. Cacuci and C. R. Weisbin, (ORNL), School of Nuclear Engineering and Health Physics, Georgia Institute of Technology, October 28, 1983.

30. F. C. di Fillipo, "Application of the Theory of Random Matrices to a Reactor-Noise Problem" Anals of Nuclear Energy, 9, 525 (October 1982).

31. D. Gilai, "Eigenfunction Expansion of Perturbed Power Profiles in Multigroup Reactor Models", Trans ANS, San Francisco 1983 meeting.

32. J. M. Kallfelz and L. Z. Belblidia, "Generalized Perturbation Theory with Derivative Operators for Power Density Investigations", GITNE-82/1, School of Nuclear Engineering and Health Physics, Georgia Institute of Technology (Annual Progress Report for ORNL subcontract 7802), December 1982.

NUCLEAR SCIENCE AND ENGINEERING: 84, 206-225 (1983)

APPENDIX A

ORNL ANNUAL PROGRESS REPORT, OCTOBER 1983

Generalized Perturbation Theory with Derivative Operators for Power Density Investigations in Nuclear Reactors

L. A. Belblidia and J. M. Kallfelz*

Georgia Institute of Technology, School of Nuclear Engineering and Health Physics
Atlanta, Georgia 30332

and

D. G. Cacuci

Oak Ridge National Laboratory, Engineering Physics Division, P.O. Box X
Oak Ridge, Tennessee 37830

Received August 12, 1982
Accepted January 20, 1983

This paper presents an efficient method to analyze variations that nuclear data perturbations induce in one-dimensional power-density distributions. This method is called the Taylor-generalized perturbation theory (Taylor-GPT) method since it is based on (a) use of a Taylor series expansion of the response variation, and (b) use of generalized perturbation theory (GPT) to evaluate the derivative operators that appear as coefficients in this Taylor series. Equations satisfied by the importance functions for the derivatives of the response variations are derived and solved with existing GPT codes. The characteristics of these functions are highlighted analytically.

Particular attention is focused on the numerical value and location of the maximum power density. This is because perturbations in system parameters affect not only the value at the maximum, but also the location of this maximum. The Taylor-GPT method can efficiently assess such effects.

The practical usefulness of the Taylor-GPT method is illustrated by considering test cases involving a simplified heterogeneous liquid-metal fast breeder reactor model. The results indicate that this method is as accurate as the GPT method, yet requires fewer calculations when investigating space-dependent power density variations.

I. INTRODUCTION

Generalized perturbation theory[1-4] (GPT) has been used for many years to investigate[2-6] the influence of cross-section perturbations and design changes on integral performance parameters (customarily called responses) in reactors. The successful application of GPT to analysis of the power density response[5,6] provided a strong motivation to study in detail the effects of parameter perturbations on such space-dependent responses. (References appear on p. 225.) Thus, this paper presents an application of first-order GPT to efficiently evaluate the space derivatives of the response that appear as coefficients in a Taylor series expansion technique. This technique is henceforth referred to as the "Taylor-GPT"

*Present address: Kernforschungszentrum Karlsruhe, D-7500 Karlsruhe 1, Federal Republic of Germany.

method, and is used to investigate the space-dependent characteristics of variations in the power density response. The shift in the location of the maximum of this response is of particular interest.[5,7-10]

I.A. Generalized Perturbation Theory

In reactor design studies, "sensitivities" $\delta P/\delta\alpha$ of a response P to input data α (typically nuclide densities or cross sections) are of interest.[2-6] In particular, P can denote a ratio of linear functionals of the real flux $\Phi(r)$. For such a P, the use of GPT to calculate sensitivities requires that the following adjoint inhomogeneous Boltzmann equation be solved for Γ^*:

$$(\mathbf{A}^* - \lambda\mathbf{B}^*)\Gamma^* = S^* \ . \tag{1}$$

In Eq. (1), $\mathbf{A}^*$ is the adjoint loss and scattering operator, $\mathbf{B}^*$ is the adjoint fission operator, and λ is the system eigenvalue.

In multigroup formalism, $\Gamma^*(r)$ is the generalized adjoint function, whose component $\Gamma_j^*(r)$ gives the importance of neutrons at r in energy group j to the ratio P. Thus, Γ_j^* satisfies the following equation that, except for the S^* term,[2] is formally identical to the "normal" adjoint equation[11] for ϕ_j^*:

$$-D_j\nabla^2\Gamma_j^*(r) + \Sigma_{rem,j}\Gamma_j^*(r) = \sum_h \Sigma_{j\to h}\Gamma_h^*(r) + \lambda\nu\Sigma_{f,j}\sum_h \chi_h\Gamma_h^*(r) + S_j^*(r) \ . \tag{2}$$

In Eq. (2), all cross sections are functions of r. The boundary conditions associated with Eq. (2) are formally identical to those for the ϕ_j^* equation, e.g., $\Gamma_j^* = 0$ at the outer reactor boundary (or extrapolated boundary).

Consider a ratio P of functionals of the real flux defined as

$$P = \frac{a_1}{a_2} = \frac{\int_{V_1}\sum_j \sigma_{1,j}(r)\phi_j(r)\,dr}{\int_{V_2}\sum_j \sigma_{2,j}(r)\phi_j(r)\,dr} \ , \tag{3}$$

where V_1 and V_2 specify the volumes associated with the space integration over r. (In the sequel, lack of such specification implies integration over the entire reactor volume.) For P defined by Eq. (3), there corresponds the following fixed source for Eq. (2):

$$S_j^*(r) = \frac{\sigma_{1,j}}{a_1} - \frac{\sigma_{2,j}}{a_2} \ . \tag{4}$$

Typically, $\sigma_{i,j}$ is some microscopic or macroscopic cross section.

In previous works[3,4] that used the concepts of GPT, the expression for the fixed source S^* was generally written as

$$S^* = \frac{1}{P}\frac{\partial P}{\partial\Phi} \ . \tag{5}$$

The expression $\partial P/\partial\Phi$, though, was used in a formal sense and did not have a precise mathematical meaning. Based on the rigorous and comprehensive sensitivity theory[7,8] for nonlinear systems that has recently been developed, it can be shown that $\partial P/\partial\Phi$ is in fact the partial Gateaux-derivative of P with respect to Φ, i.e., $\partial P/\partial\Phi$ is the operator defined via the relationship

$$\frac{d}{d\epsilon}\,[P(\Phi + \epsilon h)]_{\epsilon=0} = \frac{\partial P}{\partial\Phi}h \ , \tag{6}$$

where ϵ is a real scalar and h is an arbitrary vector of "increments" around Φ. Having thus specified its precise mathematical meaning, the notation $\partial P/\partial\Phi$ will be retained, for convenience, in the sequel.

In the first-order GPT method, the relative response variation is given by[4]

$$\frac{\delta P}{P} = \int \Phi\delta G\,dr + \int \Gamma^*\delta\mathbf{L}\Phi\,dr \ , \tag{7}$$

where Φ and Γ^* are, respectively, the real flux and generalized adjoint function, $\delta\mathbf{L}$ represents the perturbation in the Boltzmann operator, and the component of δG for energy group j is defined as

$$\delta G_j(r) = \frac{\delta\sigma_{1,j}(r)}{a_1} - \frac{\delta\sigma_{2,j}(r)}{a_2} \ . \tag{8}$$

The first term on the right side of Eq. (7) arises from changes in the cross sections that appear explicitly in Eq. (3), and is customarily referred to as the "direct-effect" term. The second term on the right side of Eq. (7) is customarily referred to as the "indirect-effect" term, and arises from the change in the flux corresponding to the perturbation $\delta\mathbf{L}$ of the Boltzmann operator.

I.B. Power Density and Related Spatial Shifts

In studies of uncertainties in calculated responses, P, for the heterogeneous core of a large liquid-metal fast breeder reactor[5,6] (LMFBR), GPT has been employed to determine the sensitivities $\delta P/\delta\sigma$ to variations in the cross sections. The responses studied included, for each driver zone, the ratio $R_M(r_m)$ of the zonal maximum power density to the total reactor power, defined as

$$R_M(r_m) = \frac{Q_1(r_m)}{Q_2} \ , \tag{9}$$

where r_m is the location at which the zonal maximum power density occurs in the unperturbed case (i.e., the "base case"). The terms in the above equation are defined by the following expressions:

$$Q_1(r_m) = \int \sum_j \Sigma_{1,j}(r')\phi_j(r')\delta(r' - r_m)\,dr' \ , \tag{10}$$

and

$$Q_2 = \int \sum_j \Sigma_{2,j}(r)\phi_j(r)\,dr \ . \tag{11}$$

The quantities $\Sigma_{i,j}$ have identical forms for $i = 1$ and 2; considering only fission energy and assuming localized energy deposit, their explicit expression is

$$\Sigma_{i,j}(r) = \sum_k p^k \Sigma^k_{f,j}(r) \ , \tag{12}$$

where p^k is the total recoverable energy release per fission in the k'th isotope.

The power density $R(r)$ is defined as in Eq. (9), except that r is not necessarily the location where a maximum occurs. Furthermore, to facilitate the subsequent presentation of the Taylor-GPT method, and to clearly highlight its most important characteristics, a one-dimensional (x) model is henceforth considered, with the power density defined as

$$R(x) = \frac{Q_1(x)}{Q_2} \ . \tag{13}$$

Such one-dimensional models are frequently used for scoping calculations; of course, detailed power-density studies require the use of multidimensional models.

Reference 5 discussed "far-range" shifts in the location of the reactor peak (i.e., maximum) of the power density (e.g., shifts between driver zones) and "near-range" shifts around the location of the initial maximum R in a particular driver zone. There, the influence of near-range shifts in the location of the zonal peak power density on the sensitivities $\delta R_M/R_M$ was estimated to be small. Note, though, that the nature of these spatial shifts was not rigorously analyzed.

The theory of Cacuci,[7,8] which uses Gateaux differentials, can be applied to problems involving such maxima. This theory has successfully been applied[12] to obtain sensitivities for the numerical values of the maximum power response and the maximum fuel temperature response, and for the sensitivities of the phase-space locations for these maxima, for a reactor safety problem describing a protected transient with scram on high power level in the Fast Flux Test Facility.

Recently, Gandini suggested the application of GPT to functionals involving derivative operators (see footnote 26 of Ref. 13). References 9 and 10 reported preliminary investigations that used GPT in conjunction with a Taylor series expansion for a simple response function. These investigations indicated that this method appears promising for explicitly investigating near-range, or localized, spatial shifts.

The purpose of this paper is to present new developments and results regarding response variations that involve localized spatial shifts. Included are first examples in reactor physics of importance functions associated with derivative operators,[14] and a detailed discussion of the characteristics of these functions. To analyze both direct and indirect effects caused by cross-section perturbations, this paper considers a more general response than previously considered in Refs. 9 and 10. The basics of the Taylor-GPT method are described in Sec. II, and the application of GPT to space derivatives of the response $R(x)$ is discussed in Sec. III. A theoretical analysis that highlights the main characteristics of the importance functions for these derivatives is presented in Sec. IV. Section V describes the use of the Taylor-GPT method for predicting effects of cross-section variations on the power density and on the spatial shifts in the maximum power density. In addition, this section discusses several indicators that can be used to assess the accuracy of the Taylor-GPT method. Comparison of results given by exact calculations, GPT, and Taylor-GPT have been performed for several test cases involving a simplified model of a heterogeneous LMFBR core. These test cases are described in Sec. VI, and the numerical results and specific comparisons are presented in Sec. VII. Finally, the summary and conclusions presented in Sec. VIII highlight the usefulness of the Taylor-GPT method for assessing effects of variations in nuclide densities and/or nuclear data on the maximum of the power density and on the spatial location of this maximum.

II. TAYLOR SERIES EXPANSION WITH GENERALIZED PERTURBATION THEORY (TAYLOR-GPT)

II.A. Taylor Series Expansion for Response Variation

The variation $\delta R(x)$ in the power density $R(x)$, caused by perturbations in cross sections, can be determined by using a Taylor series expansion about an arbitrary spatial point x_k. Retaining the first three terms only, this Taylor series is

$$\delta R(x) = \delta R(x_k) + (x - x_k)\delta R^{(1)}(x_k) + \frac{1}{2}(x - x_k)^2 \delta R^{(2)}(x_k) \ , \tag{14}$$

where $\delta R^{(i)}(x_k)$ denotes the i'th spatial derivative of the response variation $\delta R(x)$, evaluated at x_k.

Two alternative approaches can be used to calculate the derivatives $\delta R^{(i)}$. One approach is to use the finite difference approximations of the derivatives $\delta R^{(i)}$ at x_k, while an alternative approach is to use the adjoint solution that corresponds to $\delta R^{(i)}/R^{(i)}$ at x_k. As subsequent developments will show, either of these approaches can be implemented by using existing GPT codes,[16-18] thereby avoiding

any additional programming. This inherent implemental expendiency enhances the practical usefulness of the Taylor-GPT method.

II.B. Finite Difference Implementation of the Taylor-GPT Method

The values of the derivatives $\delta R^{(1)}(x)$ and $\delta R^{(2)}(x)$ can be approximated at $x = x_k$ by using the finite difference expressions

$$\delta R_k^{(1)} = \frac{\delta R_{k+1} - \delta R_{k-1}}{2\Delta} , \tag{15}$$

and

$$\delta R_k^{(2)} = \frac{\delta R_{k+1} - 2\delta R_k + \delta R_{k-1}}{\Delta^2} . \tag{16}$$

In Eqs. (15) and (16), Δ denotes the mesh spacing, and subscripts $k-1$, k, and $k+1$ refer to values at x_{k-1}, x_k, and x_{k+1}, respectively; for example, $\delta R_k = \delta R(x_k)$.

III. GPT FOR RESPONSES INVOLVING DERIVATIVE OPERATORS

Equation (1) represents a "fixed-source" problem, and, due to linearity, such problems are known to possess the so-called "additivity" property. That is, if Γ_1^* is a solution of Eq. (1) with source S_1^*, and Γ_2^* is a solution with S_2^*, then $(\Gamma_1^* + \Gamma_2^*)$ is a solution corresponding to $(S_1^* + S_2^*)$. In the finite difference approximation, the derivatives $\delta R^{(i)}$ are linear combinations of δR evaluated at x_k and at its neighboring mesh points. Therefore, it is possible, in principle, to find a source $S^{*(i)}$ so that the corresponding adjoint equation and boundary conditions would yield the $\Gamma^{*(i)}$ necessary to calculate $\delta R^{(i)}$. The actual procedure is detailed below.

III.A. Adjoint Functions for Calculating Spatial Derivatives of Response Variations

The ratio $\delta R^{(i)}/R^{(i)}$ at $x = x_k$ can be computed most efficiently by using adjoint functions. These adjoint functions, denoted by $\Gamma_k^{*(i)}$, are solutions of

$$(A^* - \lambda B^*)\Gamma_k^{*(i)} = S_k^{*(i)} , \tag{17}$$

where, by analogy with Eq. (5), the adjoint source is

$$S_k^{*(i)} = \frac{1}{R_k^{(i)}} \frac{\partial R_k^{(i)}}{\partial \Phi} . \tag{18}$$

In the above equations, the operator $\partial R_k^{(i)}/\partial\Phi$ is defined in the same way as $\partial R_k/\partial\Phi$ [see Eq. (6)]; $\Gamma_k^{*(i)}$ is subject to the same boundary conditions as Γ_k^*; and $R_k^{(i)}$ denotes the i'th derivative at x_k, of $R(x)$ with respect to x.

Changing the order of differentiation, Eq. (18) becomes

$$S_k^{*(i)} = \frac{1}{R_k^{(i)}} \left(\frac{\partial R}{\partial \Phi}\right)_{x=x_k}^{(i)} . \tag{19}$$

Recalling Eq. (5), Eq. (19) is finite differenced for $i = 1$ and 2 to obtain

$$S_k^{*(1)} = \frac{1}{R_k^{(1)}} \frac{R_{k+1}S_{k+1}^* - R_{k-1}S_{k-1}^*}{2\Delta} \tag{20}$$

and

$$S_k^{*(2)} = \frac{1}{R_k^{(2)}} \frac{R_{k+1}S_{k+1}^* - 2R_kS_k^* + R_{k-1}S_{k-1}^*}{\Delta^2} , \tag{21}$$

respectively.

For calculational purposes, Eqs. (20) and (21) can be further simplified by using the expression

$$R_k = \frac{Q_{1,k}}{Q_2} = \frac{Q_1(x_k)}{Q_2} , \tag{22}$$

and using similar expressions for R_{k-1} and R_{k+1}. Replacing these expressions in Eqs. (20) and (21), and using Eq. (5) yields, for energy group j,

$$S_{k,j}^{*(1)} = \frac{\Sigma_{1,j}(x)\delta(x - x_{k+1}) - \Sigma_{1,j}(x)\delta(x - x_{k-1})}{Q_{1,k+1} - Q_{1,k-1}} - \frac{\Sigma_{2,j}(x)}{Q_2} , \tag{23}$$

and

$$S_{k,j}^{*(2)} = \frac{\Sigma_{1,j}(x)\delta(x - x_{k+1}) - 2\Sigma_{1,j}(x)\delta(x - x_k) + \Sigma_{1,j}(x)\delta(x - x_{k-1})}{Q_{1,k+1} - 2Q_{1,k} + Q_{1,k-1}} - \frac{\Sigma_{2,j}(x)}{Q_2} , \tag{24}$$

respectively. Equations (23) and (24) can be used with existing GPT codes to calculate the corresponding $\Gamma_k^{*(i)}$, thereby avoiding any additional programming. The procedure is described in Appendix A for the Italian GPT package.[16-18]

For the finite difference approximations given by Eqs. (20) and (21), the functions $\Gamma_k^{*(i)}$ can be related to the generalized adjoint fluxes (i.e., importances) for the response sensitivities at x_{k-1}, x_k, and x_{k+1} by making use of the previously mentioned additivity property of fixed-source problems. For the sources given by Eqs. (20) and (21), the use of this property gives, for $i = 1$ and 2,

$$\Gamma_k^{*(1)} = \frac{1}{R_k^{(1)}} \frac{R_{k+1}\Gamma_{k+1}^* - R_{k-1}\Gamma_{k-1}^*}{2\Delta} \tag{25}$$

and

$$\Gamma_k^{*(2)} = \frac{1}{R_k^{(2)}} \frac{R_{k+1}\Gamma_{k+1}^* - 2R_k\Gamma_k^* + R_{k-1}\Gamma_{k-1}^*}{\Delta^2} , \tag{26}$$

respectively. The adjoint functions $\Gamma_k^{*(1)}$ and $\Gamma_k^{*(2)}$ are used to determine the values of $\delta R^{(1)}/R^{(1)}$ and $\delta R^{(2)}/R^{(2)}$ at x_k, respectively.

III.B. Calculation of Direct Effects

From the definition of the power density at x_k, the expression giving the direct-effect component of the response sensitivity is obtained as

$$\frac{\delta R_{k,D}}{R_k} = \frac{\sum_j \delta\Sigma_{1,j}(x_k)\phi_j(x_k)}{Q_{1,k}} - \frac{\int \sum_j \delta\Sigma_{2,j}(x)\phi_j(x)\,dx}{Q_2} . \tag{27}$$

Multiplying Eq. (27) by R_k gives

$$\delta R_{k,D} = \frac{1}{Q_2}\left[\sum_j \delta\Sigma_{1,j}(x_k)\phi_j(x_k) - R_k Q_3\right] , \tag{28}$$

where

$$Q_3 = \int \sum_j \delta\Sigma_{2,j}(x)\phi_j(x)\,dx . \tag{29}$$

Using a uniform mesh spacing about x_k, the first spatial derivative at x_k of the direct-effect component can be approximated as

$$\delta R_{k,D}^{(1)} = \frac{1}{2\Delta}\frac{1}{Q_2}\left[\sum_j \delta\Sigma_{1,j}(x_{k+1})\phi_j(x_{k+1}) - R_{k+1}Q_3 - \sum_j \delta\Sigma_{1,j}(x_{k-1})\phi_j(x_{k-1}) + R_{k-1}Q_3\right] . \tag{30}$$

Dividing Eq. (30) by $R_k^{(1)}$ and simplifying the resulting expression gives

$$\frac{\delta R_{k,D}^{(1)}}{R_k^{(1)}} = \frac{1}{Q_2}\frac{1}{R_{k+1} - R_{k-1}}\sum_j [\delta\Sigma_{1,j}(x_{k+1})\phi_j(x_{k+1}) - \delta\Sigma_{1,j}(x_{k-1})\phi_j(x_{k-1})] - \frac{Q_3}{Q_2} . \tag{31}$$

Using the fact that

$$Q_2(R_{k+1} - R_{k-1}) = \sum_j [\Sigma_{l,j}(x_{k+1})\phi_j(x_{k+1}) - \Sigma_{l,j}(x_{k-1})\phi_j(x_{k-1})] ,$$

and replacing Q_2 and Q_3 by their respective expressions, Eq. (31) becomes

$$\frac{\delta R_{k,D}^{(1)}}{R_k^{(1)}} = \frac{\sum_j [\delta\Sigma_{1,j}(x_{k+1})\phi_j(x_{k+1}) - \delta\Sigma_{1,j}(x_{k-1})\phi_j(x_{k-1})]}{\sum_j [\Sigma_{1,j}(x_{k+1})\phi_j(x_{k+1}) - \Sigma_{1,j}(x_{k-1})\phi_j(x_{k-1})]} - \frac{\int \sum_j \delta\Sigma_{2,j}(x)\phi_j(x)\,dx}{\int \sum_j \Sigma_{2,j}(x)\phi_j(x)\,dx} . \tag{32}$$

The procedure that has led to Eq. (32) is repeated to derive the expression for the second spatial derivative at x_k of the direct-effect component. The final result is

$$\frac{\delta R_{k,D}^{(2)}}{R_k^{(2)}} = \frac{\sum_j [\delta\Sigma_{1,j}(x_{k+1})\phi_j(x_{k+1}) - 2\delta\Sigma_{1,j}(x_k)\phi_j(x_k) + \delta\Sigma_{1,j}(x_{k-1})\phi_j(x_{k-1})]}{\sum_j [\Sigma_{1,j}(x_{k+1})\phi_j(x_{k+1}) - 2\Sigma_{1,j}(x_k)\phi_j(x_k) + \Sigma_{1,j}(x_{k-1})\phi_j(x_{k-1})]} - \frac{\int \sum_j \delta\Sigma_{2,j}(x)\phi_j(x)\,dx}{\int \sum_j \Sigma_{2,j}(x)\phi_j(x)\,dx} . \tag{33}$$

The expressions given by Eqs. (32) and (33) can be calculated with existing GPT codes[18] as described in Appendix A.

IV. THE FUNCTIONS Γ^* AND $\Gamma^{*(i)}$: A THEORETICAL ANALYSIS OF THEIR PROPERTIES

For each $i = 0, 1, \ldots$, the adjoint functions $\Gamma_k^{(i)}$ satisfy Eq. (17), and thus are functions of both x and x_k, i.e., $\Gamma_k^{*(i)} = \Gamma^{*i}(x, x_k)$. The responses $R_k^{(i)} \equiv R^{(i)}(x_k)$, though, depend on x_k only. Therefore, the equations and boundary conditions satisfied by the adjoint functions Γ_k^* and $\Gamma_k^{*(i)}$ are recast in the form

$$\left.\begin{aligned} A^*(R_k\Gamma_k^*) - \lambda B^*(R_k\Gamma_k^*) &= R_k S_k^* \ , \\ (R_k\Gamma_k^*) &= 0 \quad \text{at } x = L \ , \\ d(R_k\Gamma_k^*)/dx &= 0 \quad \text{at } x = 0 \ , \end{aligned}\right\} \tag{34}$$

and

$$\left.\begin{aligned} A^*[R_k^{(i)}\Gamma_k^{*(i)}] - \lambda B^*[R_k^{(i)}\Gamma_k^{*(i)}] &= R_k^{(i)} S_k^{*(i)} \ , \\ [R_k^{(i)}\Gamma_k^{*(i)}] &= 0 \quad \text{at } x = L \ , \\ d[R_k^{(i)}\Gamma_k^{*(i)}]/dx &= 0 \quad \text{at } x = 0 \ , \end{aligned}\right\} \tag{35}$$

where L denotes the outer (or the extrapolated) boundary of the reactor system, and all other quantities have the same meanings as before.

Equations (34) and (35) are the basis for establishing and analyzing relationships among the adjoint functions $\Gamma_k^{*(i)}$, $i = 1, 2, \ldots$, and Γ_k^*. Of course, the functions $\Gamma_k^{*(0)}$ and Γ_k^* are identical, since Eq. (35) reduces to Eq. (34) when $i = 0$.

Differentiating Eq. (35) with respect to x_k gives

$$\left.\begin{aligned} A^*\{\partial[R_k^{(i)}\Gamma_k^{*(i)}]/\partial x_k\} - \lambda B^*\{\partial[R_k^{(i)}\Gamma_k^{*(i)}]/\partial x_k\} \\ = \partial[R_k^{(i)} S_k^{*(i)}]/\partial x_k \ , \\ \partial[R_k^{(i)}\Gamma_k^{*(i)}]/\partial x_k = 0 \quad \text{at } x = L \ , \\ d\{\partial[R_k^{(i)}\Gamma_k^{*(i)}]/\partial x_k\}/dx = 0 \quad \text{at } x = 0 \ . \end{aligned}\right\} \tag{36}$$

Using the definition of $S_k^{*(i)}$ [i.e., Eq. (19)], the quantity $R_k^{(i)} S_k^{*(i)}$ can be expressed as

$$R_k^{(i)} S_k^{*(i)} = \int [d^i(\partial R/\partial \Phi)/dx^i]\,\delta(x - x_k)\,dx \ . \tag{37}$$

Differentiating Eq. (37) with respect to x_k, and using the definition[19] of the δ' functional, i.e.,

$$\int f(x)\delta'(x - a)\,dx = -\int f'(x)\delta(x - a)\,dx \ , \tag{38}$$

leads to

$$\begin{aligned} &\partial[R_k^{(i)} S_k^{*(i)}]/\partial x_k \\ &= -\int [d^i(\partial R/\partial \Phi)/dx^i]\,\delta'(x - x_k)\,dx \\ &= \int [d^{i+1}(\partial R/\partial \Phi)/dx^{i+1}]\,\delta(x - x_k)\,dx \ . \end{aligned} \tag{39}$$

Writing Eq. (37) for $i + 1$, and comparing the result with Eq. (39) shows that

$$\partial[R_k^{(i)} S_k^{*(i)}]/\partial x_k = R_k^{(i+1)} S_k^{*(i+1)} \ . \tag{40}$$

Using Eq. (40) to replace the corresponding source term in Eq. (36), and comparing the resulting system of equations to the system obtained by writing Eq. (35) for $(i + 1)$ leads to the conclusion that

$$\partial[R_k^{(i)}\Gamma_k^{*(i)}]/\partial x_k = R_k^{(i+1)}\Gamma_k^{*(i+1)} \ , \quad i = 0, 1, 2, \ldots \ . \tag{41}$$

A simple inductive reasoning can now be used in conjunction with Eq. (41) to conclude that

$$R_k^{(i)}\Gamma_k^{*(i)} = \partial^i[R_k\Gamma_k^*]/\partial x_k^i \ . \tag{42}$$

The qualitative behavior of Γ_k^*, $\Gamma_k^{*(1)}$, and $\Gamma_k^{*(2)}$ as functions of x can be studied analytically by considering a one-group, one-region representation[20] of the adjoint diffusion equations given by Eqs. (34) and (35). For clarity, the functions satisfying the corresponding simplified adjoint diffusion equations are denoted by Γ_1^*, $\Gamma_1^{*(1)}$, and $\Gamma_1^{*(2)}$, where the subscript 1 now refers to the one-group model rather than to the location of x_k. The respective equations can be written explicitly as follows:

$$\left.\begin{aligned} d^2\Gamma_1^*/dx^2 + B^2\Gamma_1^* &= -S^*/D \ , \\ \Gamma_1^* &= 0 \quad \text{at } x = L \ , \\ d\Gamma_1^*/dx &= 0 \quad \text{at } x = 0 \ , \end{aligned}\right\} \tag{43}$$

$$\left.\begin{aligned} d^2\Gamma_1^{*(1)}/dx^2 + B^2\Gamma_1^{*(1)} &= -S^{*(1)}/D \ , \\ \Gamma_1^{*(1)} &= 0 \quad \text{at } x = L \ , \\ d\Gamma_1^{*(1)}/dx &= 0 \quad \text{at } x = 0 \ , \end{aligned}\right\} \tag{44}$$

and

$$\left.\begin{aligned} d^2\Gamma_1^{*(2)}/dx^2 + B^2\Gamma_1^{*(2)} &= -S^{*(2)}/D \ , \\ \Gamma_1^{*(2)} &= 0 \quad \text{at } x = L \ , \\ d\Gamma_1^{*(2)}/dx &= 0 \quad \text{at } x = 0 \ . \end{aligned}\right\} \tag{45}$$

In Eqs. (43), (44), and (45), B^2 and D represent the customary one-group, one-region buckling and diffusion coefficient, respectively. The analytical expressions for S^*, $S^{*(1)}$, and $S^{*(2)}$ are obtained by using Eqs. (9), (10), and (11) in conjunction with Eq. (19) and with the definitions[19] of the δ' and δ'' functionals. Also, for simplicity, the constants $\Sigma_{i,j}$ [see Eq. (12)] are arbitrarily set to unity. Under these conditions, the following analytical expressions are obtained:

$$R_k = Q_{1,0}/Q_2 \ , \tag{46}$$

$$R_k^{(1)} = Q_{1,1}/Q_2 \ , \tag{47}$$

$$R_k^{(2)} = Q_{1,2}/Q_2 \ , \tag{48}$$

$$S^* = \frac{\delta(x - x_k)}{Q_{1,0}} - \frac{1}{Q_2} \quad , \tag{49}$$

$$S^{*(1)} = -\frac{\delta'(x - x_k)}{Q_{1,1}} - \frac{1}{Q_2} \quad , \tag{50}$$

$$S^{*(2)} = \frac{\delta''(x - x_k)}{Q_{1,2}} - \frac{1}{Q_2} \quad , \tag{51}$$

where

$$Q_{1,0} = \phi(x_k) \quad , \tag{52}$$

$$Q_{1,1} = (d\phi/dx)_{x=x_k} \quad , \tag{53}$$

$$Q_{1,2} = (d^2\phi/dx^2)_{x=x_k} \quad , \tag{54}$$

and

$$Q_2 = \int \phi(x)\, dx \quad . \tag{55}$$

The adjoint diffusion equations given by Eqs. (43), (44), and (45), with the source terms given by Eqs. (49), (50), and (51), respectively, can be solved analytically to determine Γ_1^*, $\Gamma_1^{*(1)}$, and $\Gamma_1^{*(2)}$. For this purpose, it is convenient to use the Laplace transform method, as illustrated in Appendix B where Eq. (45) is solved in detail. The following analytical expressions for the solutions of Eqs. (43), (44), and (45) are thus obtained:

$$\Gamma_1^* = \frac{1}{B^2DQ_2} + \left[\frac{1}{BDQ_{1,0}}\left(\frac{\cos Bx_k}{BL} - \frac{L - x_k}{L}\sin Bx_k\right) - \frac{2}{LB^3DQ_2}\right]\cos Bx - \frac{1}{BDQ_{1,0}} H(x - x_k)\sin B(x - x_k) \quad , \tag{56}$$

$$\Gamma_1^{*(1)} = \frac{1}{B^2DQ_2} - \left(\frac{L - x_k}{DLQ_{1,1}}\cos Bx_k + \frac{2}{LB^3DQ_2}\right)\cos Bx + \frac{1}{DQ_{1,1}} H(x - x_k)\cos B(x - x_k) \quad , \tag{57}$$

$$\Gamma_1^{*(2)} = \frac{1}{B^2DQ_2} + \left[\frac{\cos Bx_k + B(L - x_k)\sin Bx_k}{LDQ_{1,2}} - \frac{2}{DB^3LQ_2}\right]\cos Bx + \frac{B}{DQ_{1,2}} H(x - x_k)\sin B(x - x_k) - \frac{\delta(x - x_k)}{DQ_{1,2}} \quad , \tag{58}$$

where $H(x)$ represents the customary[19] Heaviside (unit-step) functional.

In view of Eqs. (56), (57), and (58), the behavior of the functions Γ_1^*, $\Gamma_1^{*(1)}$, and $\Gamma_1^{*(2)}$ as x approaches x_k becomes of particular interest. Thus, Γ_1^* is continuous at x_k, where

$$\Gamma_1^*(x_k) = \frac{1}{B^2DQ_2} + \left[\frac{1}{BDQ_{1,0}}\left(\frac{\cos Bx_k}{BL} - \frac{L - x_k}{L}\sin Bx_k\right) - \frac{2}{LB^3DQ_2}\right]\cos Bx_k \quad , \tag{59}$$

but the first and second derivatives of Γ_1^* with respect to x have a Heaviside and a Dirac delta-type discontinuity, respectively, at $x = x_k$, since

$$(d\Gamma_1^*/dx)_{x=x_k} = \left[\frac{2}{LB^2DQ_2} - \frac{1}{DQ_{1,0}}\left(\frac{\cos Bx_k}{BL} - \frac{L - x_k}{L}\sin Bx_k\right)\right]\sin Bx_k - \frac{1}{DQ_{1,0}} H(x - x_k) \quad , \tag{60}$$

and

$$(d^2\Gamma_1^*/dx^2)_{x=x_k} = \left[\frac{2}{LBDQ_2} - \frac{B}{DQ_{1,0}}\left(\frac{\cos Bx_k}{BL} - \frac{L - x_k}{L}\sin Bx_k\right)\right]\cos Bx_k - \frac{\delta(x - x_k)}{DQ_{1,0}} \quad . \tag{61}$$

At $x = x_k$, the function $\Gamma_1^{*(1)}$ has a Heaviside-type discontinuity, since

$$[\Gamma_1^{*(1)}]_{x=x_k} = \frac{1}{B^2DQ_2} - \left(\frac{L - x_k}{DLQ_{1,1}}\cos Bx_k + \frac{2}{LB^3DQ_2}\right)\cos Bx_k + \frac{1}{DQ_{1,1}} H(x - x_k) \quad , \tag{62}$$

while the first derivative of $\Gamma_1^{*(1)}$ with respect to x has a Dirac delta discontinuity, since

$$[d\Gamma_1^{*(1)}/dx]_{x=x_k} = \left[\frac{B(L - x_k)}{DLQ_{1,1}}\cos Bx_k + \frac{2}{LB^2DQ_2}\right]\sin Bx_k + \frac{\delta(x - x_k)}{DQ_{1,1}} \quad . \tag{63}$$

Finally, $\Gamma_1^{*(2)}$ has a Dirac delta-type discontinuity at $x = x_k$, since

$$[\Gamma_1^{*(2)}]_{x=x_k} = \frac{1}{B^2DQ_2} + \left[\frac{\cos Bx_k + B(L - x_k)\sin Bx_k}{LDQ_{1,2}} - \frac{2}{DB^3LQ_2}\right]\cos Bx_k - \frac{\delta(x - x_k)}{DQ_{1,2}} \quad . \tag{64}$$

When x_k is close to the exact location x_m of the maximum, but such that $x_k < x_m$, $Q_{1,0}$ and $Q_{1,1}$ are positive, while $Q_{1,2}$ is negative. In this case, Eqs. (59) through (64) indicate that

1. The functions $\Gamma_1^{*(1)}$ and $d\Gamma_1^*/dx$ both undergo step jumps at $x = x_k$, but the former function undergoes a *positive* step jump, while the latter undergoes a *negative* step jump

2. The functions $\Gamma_1^{*(2)}$, $d\Gamma_1^{*(1)}/dx$, and $d^2\Gamma_1^*/dx^2$ all display "spikes," i.e., Dirac delta-type discontinuities at $x = x_k$. These delta functionals cause positive spikes in $\Gamma_1^{*(2)}$ and $d\Gamma_1^{*(1)}/dx$, but cause a negative spike in $d^2\Gamma_1^*/dx^2$.

Since Eqs. (43), (44), and (45) are particular forms of Eqs. (34), (35), and (36), respectively, the functions Γ_1^*, $\Gamma_1^{*(1)}$, and $\Gamma_1^{*(2)}$ should also satisfy the relationships given by Eqs. (41) and (42). This fact can readily be verified by using Eqs. (56), (57), and (58) and Eqs. (46), (47), and (48) to show that

$$\partial(R_k\Gamma_1^*)/\partial x_k = R_k^{(1)}\Gamma_1^{*(1)} \tag{65}$$

and

$$\partial^2(R_k\Gamma_1^*)/\partial x_k^2 = \partial[R_k^{(1)}\Gamma_1^{*(1)}]/\partial x_k = R_k^{(2)}\Gamma_1^{*(2)} \ . \tag{66}$$

V. RESPONSE VARIATIONS AND SPATIAL SHIFTS: CALCULATIONAL PROCEDURES AND ACCURACY OF PREDICTIONS

V.A. Response Variations and Accuracy of Predictions

The effects on the power density of variations in the macroscopic cross sections can be evaluated by three methods:

1. direct calculations

2. use of GPT

3. use of Taylor series expansion method with GPT (Taylor-GPT).

The first method consists of calculating the response (in this case, the point-power density) for the unperturbed case (denoted by the subscript 0), the response for the perturbed case (denoted by the subscript 1), and subtracting the two to determine the change. The result of this process gives

$$\Delta R_e(x) = R_1(x) - R_0(x) \ . \tag{67}$$

This method will henceforth be called "exact."

For the first-order GPT method, the response variation, denoted by $R_p(x)$, is considered to be given by

$$\delta R_p(x) = R(x)\left(\frac{\delta R}{R}\right)_x \ , \tag{68}$$

where $\delta R/R$ has the same expression as $\delta P/P$ in Eq. (7), except that P is replaced by the particular response $R(x)$ defined by Eq. (13).

For the Taylor-GPT method, the response variation at x, denoted by $\delta R_{tp}(x)$, is considered to be given by the following three-term Taylor series expansion about x:

$$\delta R_{tp}(x) = \delta R_p(x_k) + (x - x_k)\delta R_p^{(1)}(x_k) + \frac{1}{2}(x - x_k)^2\delta R_p^{(2)}(x_k) \ . \tag{69}$$

In Eq. (69), the variation in the power density at x_k and its first two derivatives at x_k are determined from GPT calculations.

The accuracy of the Taylor-GPT method can be assessed by comparing the left side of Eq. (69) to the result of a GPT sensitivity calculation at x, i.e., Eq. (68). A relative error, denoted by TAP and defined as

$$TAP = \frac{\delta R_{tp}(x) - \delta R_p(x)}{\delta R_p(x)} \tag{70}$$

can be used to assess this accuracy.

On the other hand, the relative error that results from (a) the inaccuracy of GPT, and (b) the differences between Eq. (68) and the Taylor series expansion of $\delta R(x)$ about x_k is found by taking the direct calculations as the basis for comparison. This relative error is henceforth denoted by TAE and is defined as

$$TAE = \frac{\delta R_{tp}(x) - \Delta R_e(x)}{\Delta R_e(x)} \ . \tag{71}$$

V.B. Spatial Shifts in the Maximum Power Density

Numerically, a discrete set $R_i = R_0(x_i)$, $i = 1, 2, \ldots, N$ is obtained when the unperturbed power density $R_0(x)$ is calculated as a function of x. Consider now that x_k represents the discrete point at which the largest discrete value R_k is obtained. In general, x_k does not coincide with the spatial location, denoted by x_{m0}, at which $R_0(x)$ attains its *actual* maximum. The location x_{m0} can approximately be determined by expanding $R_0(x)$ in a Taylor series around x_k, i.e.,

$$R_0(x) = R_0(x_k) + (x - x_k)R_0^{(1)}(x_k) + \frac{1}{2}(x - x_k)^2R_0^{(2)}(x_k) + \ldots \tag{72}$$

and by evaluating the first spatial derivative of this expansion at x_{m0}. Retaining only terms up to $O[(x - x_k)^3]$ in Eq. (72), and noting that $dR_0(x)/dx$ vanishes at x_{m0} [since $R_0(x)$ attains its maximum there] gives

$$x_{m0} - x_k = -\frac{R_0^{(1)}(x_k)}{R_0^{(2)}(x_k)} . \quad (73)$$

When the system parameters are perturbed, the perturbed response, denoted by $R_1(x)$, attains its actual maximum at a location x_{m1}, which, in general, will not coincide with x_{m0}. The location x_{m1} can be determined by expanding the perturbed response $R_1(x)$ in a Taylor series analogous to Eq. (72), and following the same procedure as that leading to Eq. (73). This gives

$$x_{m1} - x_k = -\frac{R_1^{(1)}(x_k)}{R_1^{(2)}(x_k)} . \quad (74)$$

The spatial shift $(x_{m1} - x_{m0})$ in the peak power density can now be estimated by subtracting Eq. (72) from Eq. (74). This gives

$$x_{m1} - x_{m0} = -\frac{R_0^{(1)} + \delta R^{(1)}}{R_0^{(2)} + \delta R^{(2)}} + \frac{R_0^{(1)}}{R_0^{(2)}} , \quad (75)$$

where all $R^{(i)}$ and $\delta R^{(i)}$, $i = 1,2$, are understood as being evaluated at $x = x_k$. When $\delta R^{(2)}/R^{(2)}$ is much less than unity, Eq. (75) reduces to

$$x_{m1} - x_{m0} \simeq -\frac{\delta R^{(1)}}{R_0^{(2)}} . \quad (76)$$

Within the framework of first-order GPT, the perturbed response can be written as the sum of the unperturbed response and the response variation δR_p, where the latter term consists of a direct-effect component, δR_d, and an indirect-effect component, δR_i, i.e.,

$$\begin{aligned} R_1 &= R_0 + \delta R_p \\ &= R_0 + \delta R_d + \delta R_i . \end{aligned} \quad (77)$$

Similar expressions can be written for the spatial derivatives of the perturbed response:

$$\left.\begin{aligned} R_1^{(1)} &= R_0^{(1)} + \delta R_d^{(1)} + \delta R_i^{(1)} \\ R_1^{(2)} &= R_0^{(2)} + \delta R_d^{(2)} + \delta R_i^{(2)} \end{aligned}\right\} . \quad (78)$$

If, on the one hand, the direct-effect components vanish, then Eqs. (74) and (78) give

$$(x_{m1} - x_k)_i = -\frac{R_0^{(1)} + \delta R_i^{(1)}}{R_0^{(2)} + \delta R_i^{(2)}} . \quad (79)$$

If, on the other hand, the indirect-effect components vanish, then Eqs. (74) and (78) give

$$(x_{m1} - x_k)_d = -\frac{R_0^{(1)} + \delta R_d^{(1)}}{R_0^{(2)} + \delta R_d^{(2)}} . \quad (80)$$

Adding Eqs. (79) and (80), and neglecting second-order terms of the form $\delta R_d^{(i)} \delta R_i^{(j)}$, gives

$$\begin{aligned} &(x_{m1} - x_k)_d + (x_{m1} - x_k)_i \\ &\quad = -\frac{R_0^{(1)} + \delta R_d^{(1)} + \delta R_i^{(1)}}{R_0^{(2)} + \delta R_i^{(2)} + \delta R_i^{(2)}} - \frac{R_0^{(1)}}{R_0^{(2)}} . \end{aligned} \quad (81)$$

In view of Eqs. (74) and (78), the first term on the right side of Eq. (81) is the expression for $(x_{m1} - x_k)$ when both direct and indirect effects are present. The second term on the right side of Eq. (81) corresponds to the unperturbed case, i.e., to $(x_{m0} - x_k)$ as given by Eq. (73). Therefore, Eq. (81) becomes

$$(x_{m1} - x_k)_d + (x_{m1} - x_k)_i = (x_{m1} - x_k) + (x_{m0} - x_k) . \quad (82)$$

Noting that x_k is a fixed point, and subtracting twice the quantity $(x_{m0} - x_k)$ from Eq. (82) gives

$$(x_{m1} - x_{m0})_d + (x_{m1} - x_{m0})_i = x_{m1} - x_{m0} . \quad (83)$$

Equation (83) shows that the spatial shift in the peak location can be expressed as the sum of a spatial shift due solely to direct effects and a spatial shift due solely to indirect effects.

V.C. Influence of the Spatial Shift on the Sensitivity of the Peak-Power Density

When a macroscopic cross section is perturbed, the resulting variation in peak power density is given by

$$\Delta R_{es} = R_1(x_{m1}) - R_0(x_{m0}) . \quad (84)$$

Note that Eq. (84) is *exact*, i.e., it contains no approximations.

If the shift in the location of the peak is neglected, the variation in the response is given by Eq. (67) evaluated at x_{m0}; that is,

$$\Delta R_{e0} = R_1(x_{m0}) - R_0(x_{m0}) . \quad (85)$$

In view of Eqs. (84) and (85), the effect of the spatial shift on the sensitivity of the peak power density can be assessed by using the expression

$$SE = \frac{\Delta R_{es} - \Delta R_{e0}}{\Delta R_{e0}} . \quad (86)$$

Since Cacuci[8] has shown that

$$|R_1(x_{m1}) - R_1(x_{m0})| = O[(\delta\sigma)^2] , \quad (87)$$

where $\delta\sigma$ represents variations in the system parameters, it follows that the numerator of Eq. (86) is also of second order in these variations. Figure 1 illustrates the near-range spatial shift and its influence on the sensitivity of the extremum.

VI. DESCRIPTION OF TEST CASES

VI.A. Model and Cross Sections

A simplified three-region model, which has some of the significant characteristics[10] of a heterogeneous LMFBR, has been chosen to test the theoretical developments outlined in the previous sections. This model consists of an infinite slab, finite in the x direction, with internal blanket (IB), driver (D),

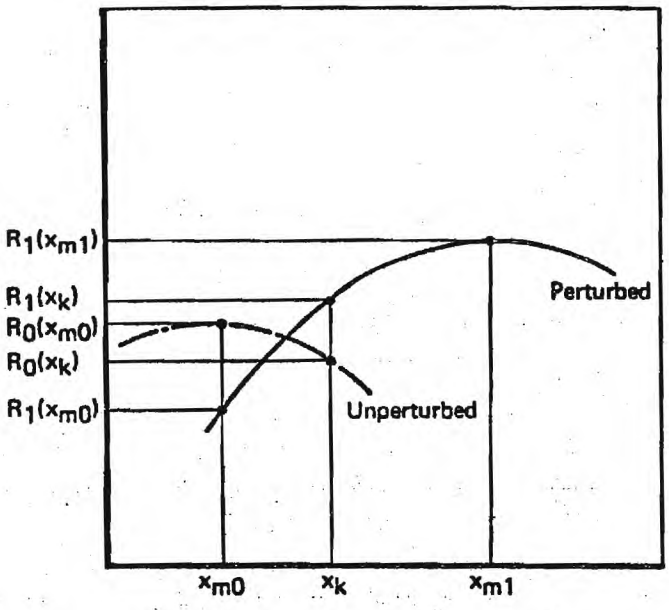

Fig. 1. Influence of spatial shift on peak response [after Cacuci (Ref. 8)].

and external blanket (EB). The concentrations of sodium, ^{238}U, and ^{239}Pu are given in Table I, and are the same as for the beginning-of-life LMFBR model considered in Ref. 22. The three-group cross sections used are from the CITATION test case.[23]

The outer boundaries of regions IB, D, and EB are located at 10.5, 60, and 90.0 cm from the reactor center ($x = 0$), respectively. A driver zone mesh spacing of 1.5 cm is used for all reported results; however, this spacing was varied in some of the test calculations discussed in Sec. VII.B.

VI.B. Selection of Perturbations

Perturbations of nuclide densities or microscopic cross sections cause changes in the macroscopic cross sections, Σ, and thus in the Boltzmann operator, L. To choose perturbations appropriate for testing the proposed method, several desirable, and sometimes conflicting, conditions should be considered:

1. To test the Taylor series method, $\delta\Sigma$ should cause a response variation $\delta R(x)$ that appreciably depends on x. This implies that the change in at least one of the derivatives $\delta R^{(i)}(x_k)$ should be appreciable.

2. To check the GPT method [see Eq. (7)], the indirect-effect component of the total perturbation $\delta R^{(i)}(x)$ should be appreciable.

3. To allow useful comparisons with exact (i.e., direct calculation) results, the perturbation $\delta\Sigma$ should not be so large that second- and higher order terms in $\delta\Sigma$, which are ignored in the first-order GPT applied herein, become overwhelmingly large.

In view of the conditions described above, four test cases, as described in Table II, have been devised. In general, these cases meet the above conditions adequately, but the following exceptions should be noted:

a. Case 1 does not satisfy condition 1 above well, but is a good test for predicting a small spatial shift in the peak power density.

b. Case 3 does not satisfy condition 3 above well, but is an interesting example of a very large perturbation that effectively transforms the heterogeneous core into a homogeneous one.

TABLE I

Nuclide Concentrations for Test Model

Nuclide	Concentration (10^{24} atom/cm^3)	
	Driver	Internal and External Blankets
^{238}U	0.006	0.012
^{239}Pu	0.001	0.0
Sodium	0.010	0.007

TABLE II

Selected Perturbations and Corresponding Test Cases

Case	Zonal Perturbation[a]		
	Internal Blanket	Driver	External Blanket
1		$\frac{\delta N^{49}}{N^{49}} = -3\%$	$\delta N^{49} = +0.045 N_D^{49}$
2	$\frac{\delta N^{28}}{N^{28}} = +5\%$	$\frac{\delta N^{49}}{N^{49}} = -5\%$	$\frac{\delta N^{28}}{N^{28}} = +5\%$
3	Replaced with driver	Inner boundary extended to core center ($x = 0$)	
4	Outer 3 cm replaced with driver	Inner boundary extended to $x = 7.5$ cm	

[a]Here, N_x^{yz} is the number density in zone x of the nuclide with the last digits in its atomic number and weight of y and z, respectively. If no x appears, N is for the zone designated by the column heading; N values are given in Table I.

VII. RESULTS FOR TEST CASES

VII.A. $\Gamma_k^{*(i)}$ *Results*

Various characteristics of the functions $\Gamma_k^{*(i)}$ are illustrated by the results presented in Figs. 2 through 5. All numerical results discussed in this and the following sections are for x_k = 22.5 cm, the mesh point at which the maximum value of R_k occurred in the unperturbed (i.e., "base case") calculation of the power density $R(x)$. The spatial shape of Γ_k^* is illustrated in Figs. 2 and 3. The neutron importance to $R(x_k)$ is greatest near x_k; there, a neutron is more likely to contribute to the numerator rather than the denominator of Eq. (13). As a function of x, $\Gamma_k^*(x)$ is negative over a wide range due to the neutron contributions to the denominator of Eq. (13).

The shape of the curves for $\Gamma_k^{*(1)}$ and $\Gamma_k^{*(2)}$ can be discussed in terms of the expressions derived in Sec. IV. For this purpose, recall that Γ_k^* depends both on x_k and x, and that the associated response $R_k \equiv R(x_k)$ depends on x_k but not on x. In the following, the dependence of $\Gamma^{*(i)}(x,x_k) \equiv \Gamma_k^{*(i)}(x)$ on each of the two independent variables x and x_k will be addressed separately.

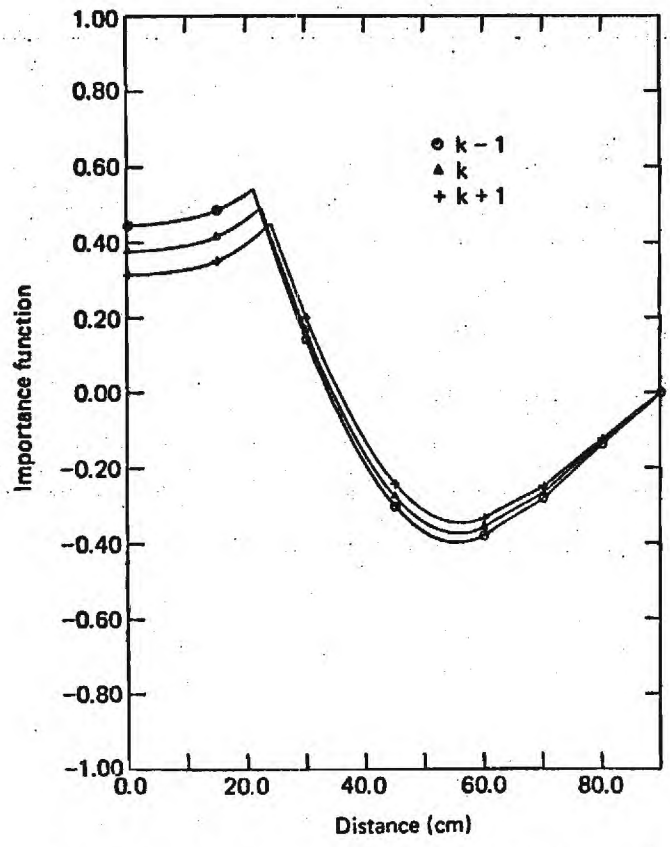

Fig. 2. Spatial behavior of Γ_{k-1}^*, Γ_k^*, and Γ_{k+1}^* for energy group 2, and x_{k-1} = 21.0 cm, x_k = 22.5 cm, and x_{k+1} = 24.0 cm.

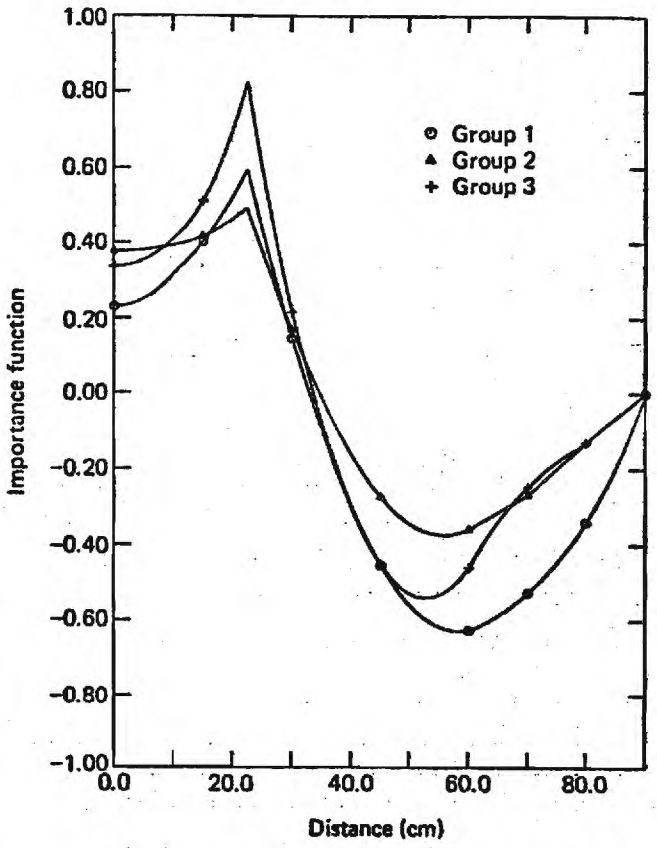

Fig. 3. Spatial behavior of Γ_k^* for energy groups 1, 2, and 3, and x_k = 22.5 cm.

As functions of x_k, the relationships between the $\Gamma_{k,j}^{*(i)}$ for the j'th energy group have been generally given, in vector form, by Eq. (42), i.e.,

$$R_k^{(i)}\Gamma_k^{*(i)} = \partial^i[R_k\Gamma_k^*]/\partial x_k^i \ . \qquad [(42)]$$

Qualitatively, this behavior is illustrated in Fig. 4, which presents $\Gamma_k^{*(1)}(x)$ as a function of x. For group 2, for example, given the fact that $R_k^{(1)}$ is positive, the shape shown in Fig. 4 can be obtained by considering various fixed, but successively larger, values of x on the set of curves for $\Gamma^*(x,x_k)$ shown in Fig. 2.

As functions of x, the qualitative behavior of $\Gamma_{k,j}^{*(i)}$, shown in Figs. 2 through 5, can be supported by considering the analytic results for Γ_1^*, $\Gamma_1^{*(1)}$, and $\Gamma_1^{*(2)}$ obtained in Sec. IV for a simple one-group, one-region case. Although the results shown in Figs. 2 through 5 are for a multiregion, multigroup case, the predominant features of these results near x_k are expected to be similar to those of the simpler one-group, one-region model. This is because

1. fixed point x_k is well within the interior of the driver region, and hence is neutronically

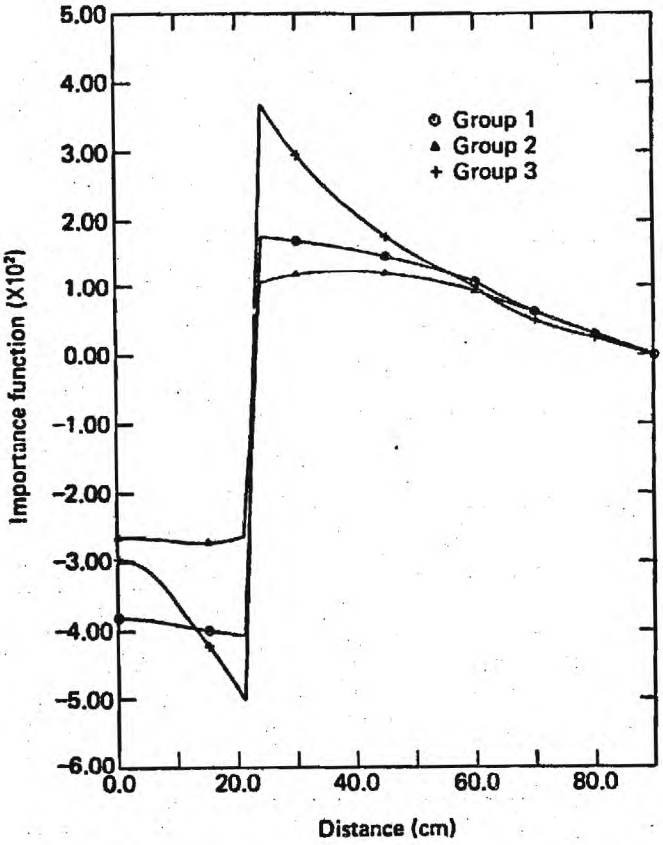

Fig. 4. Spatial behavior of $\Gamma_k^{*(1)}$ for energy groups 1, 2, and 3, and $x_k = 22.5$ cm.

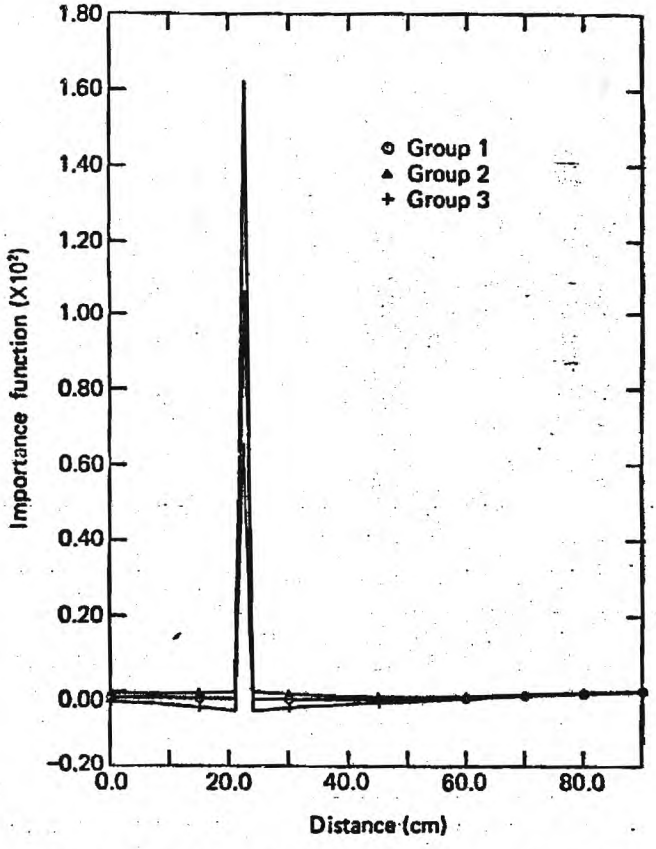

Fig. 5. Spatial behavior of $\Gamma_k^{*(2)}$ for energy groups 1, 2, and 3, and $x_k = 22.5$ cm.

"far" (several mean-free-paths) from other regions

2. the x dependence of $\Gamma_{k,j}^{*(i)}(x)$ is strongly influenced by the spatial form of the fixed sources, $S_k^{*(i)}(x)$; for our test cases, these sources are space-energy separable in the driver region
3. coupling between groups for the multigroup case does not change the predominant features of the x dependence of $\Gamma_{k,j}^{*(i)}(x)$, since this dependence is similar for all groups. This similarity, illustrated in Fig. 3, is principally due to item 2 above.

The discussion that followed Eqs. (59) through (64), and that focused on the predominant features of the x dependence of the functions $\Gamma_1^{*(1)}$ and $\Gamma_1^{*(2)}$, also provides a good description of the predominant features of the x dependence of the derivative importance functions shown in Figs. 4 and 5.

The values of $\Gamma_k^{*(2)}$ for $x \neq x_k$ are significantly smaller than the value at x_k, and are sensitive to the "fundamental harmonic correction"[2,4,24] that must be used to eliminate fundamental harmonic contamination when calculating $\Gamma^{*(i)}$. Although the CIAP-INO version of CIAP-ID (Ref. 17) that was employed to calculate the adjoint functions performs this correction, the correction was numerically inadequate to determine $\Gamma_k^{*(2)}$. This situation was resolved by noting that the functions $\Gamma_k^{*(i)}$ satisfy the orthogonality property

$$\langle \Gamma_k^{*(i)}, B\Phi \rangle = 0 \ , \qquad (88)$$

where B is the fission operator. As a result of applying this orthogonality property to eliminate fundamental harmonic contamination, the values for $\Gamma_k^{*(2)}$ obtained by using the fixed source $S_k^{*(2)}$ [see Eq. (24)] agreed well with the corresponding values obtained by using Eq. (26).

The numerical accuracy of calculating $\Gamma_k^{*(1)}$ was verified in a similar manner: On the one hand, $\Gamma_k^{*(1)}$ was calculated by using the fixed source $S_k^{*(1)}$ [see Eq. (23)] and, on the other hand, $\Gamma_k^{*(1)}$ was calculated by using Eq. (25). These calculations gave essentially identical results.

A mesh spacing of 1.5 cm, which is a typical value specified for benchmark calculations of critical assemblies with LMFBR characteristics, e.g., ZPR-3-48 (Ref. 25), was initially chosen for both forward and adjoint calculations. The results for the functions

$\Gamma_k^{*(i)}$ were obtained by using this mesh spacing. The sharp variations displayed by these functions provided a strong motivation to investigate whether this mesh spacing, which is adequate for calculating the comparatively smooth forward fluxes, is indeed adequate for accurately calculating the adjoint functions. This adequacy was investigated by performing several calculations with a finer mesh, obtained by reducing the 1.5-cm mesh spacing to 0.5 cm in a region around x_k. Although the shapes of $\Gamma_k^{*(i)}$ changed slightly due to the additional mesh points (an expected outcome considering the sharp variations involved), the use of the two meshes yielded essentially identical results for $\delta R_k^{(i)}$. This gives confidence that the 1.5-cm mesh spacing is indeed adequate. All numerical results reported here were obtained by using the 1.5-cm mesh spacing.

VII.B. Comparison of Results for $\delta R^{(i)}(x_k)$ Obtained from GPT and Direct Calculations

The accuracy of values for $\delta R_k^{(i)}$ obtained from GPT calculations was verified by performing two direct TAIM calculations.[16] As discussed in Sec. V.A, the results of these direct calculations are termed exact. The convergence criteria for these direct calculations were adequately stringent to ensure that the exact results retained sufficient significant figures for comparisons with perturbation-theory results. As indicated in Tables III through VI, the exact and GPT results for $\delta R_k^{(i)}$ generally agreed within ~5%. Note that for all four cases, the indirect component of $\delta R_k^{(i)}$ is greater than the direct component for at least two of the three i values. Thus, condition 2 of Sec. VI.B is largely satisfied.

The results shown in the last columns of Tables IV and V indicate that GPT and exact results do not agree well for $\delta R_k^{(2)}$ of cases 2 and 3, respectively. For case 3, the disagreement between GPT and exact results indicates that the nonlinear terms disregarded by first-order GPT are not small. This is not surprising since, as discussed in Sec. VI.B, case 3 represents a very large perturbation. The disagreement between GPT and exact results for $\delta R_k^{(2)}$ of case 2 can be analyzed by comparing the results for $\delta R_k^{(2)}/R_k^{(2)}$ presented in the fourth columns of Tables III through

TABLE III

GPT and Exact $\delta R^{(i)}(x_k)$ Results for Case 1*

Derivative Order, i	GPT Results for $\delta R^{(i)}/R^{(i)}$			$\delta R_p^{(i)}$ (GPT)	$\Delta R_e^{(i)}$ (Exact)[b]	$\frac{\text{GPT} - \text{Exact}}{\text{Exact}}$ (%)
	Direct[a]	Indirect[a]	Total			
0	−9.16−3[c]	−2.25−3	−1.14−2	−3.56−4	−3.69−4	−3.7
1	+2.26−1	+2.97−1	+5.23−1	+2.71−6	+2.88−6	−5.8
2	−3.59−3	−1.16−2	−1.52−2	+2.86−7	+3.04−7	−5.8

*All values are for x_k = 22.5 cm. Because of the characteristics of CIAP, R has a ΔVol factor of 1.5 cm³ in the numerator, which is not contained in Eq. (9). Read $(\pm x - y)$ as $\pm x \cdot 10^{-y}$; see Table II for description of perturbation cases. The values presented in the last three columns are calculated with more significant figures than shown.

[a]See discussion of Eq. (7).

[b]The exact value was determined from two direct calculations [see Eq. (67)].

[c]Read as -9.16×10^{-3}.

TABLE IV

GPT and Exact $\delta R^{(i)}$ Results for Case 2*

Derivative Order, i	GPT Results for $\delta R^{(i)}/R^{(i)}$			$\delta R_p^{(i)}$ (GPT)	$\Delta R_e^{(i)}$ (Exact)	$\frac{\text{GPT} - \text{Exact}}{\text{Exact}}$ (%)
	Direct	Indirect	Total			
0	5.41−4[a]	2.59−3	3.13−3	9.77−5	9.09−5	7.4
1	3.93−1	−2.17+0	−1.78+0	−9.21−6	−9.05−6	7.7
2	9.82−3	−7.26−3	2.55−3	−4.80−8	−3.4−8	39

*See footnotes for Table III.

[a]Read as 5.41×10^{-4}.

TABLE V

GPT and Exact $\delta R^{(i)}$ Results for Case 3*

Derivative Order, i	GPT Results for $\delta R^{(i)}/R^{(i)}$			$\delta R_p^{(i)}$ (GPT)	$\Delta R_e^{(i)}$ (Exact)	$\frac{\text{GPT} - \text{Exact}}{\text{Exact}}$ (%)
	Direct	Indirect	Total			
0	−1.59−1[a]	3.78−2	−1.21−1	−3.79−3	−3.79−3	−0.14
1	−1.59−1	−5.44+1	−5.46+1	−2.83−4	−2.14−4	32
2	−1.59−1	−4.52−1	−6.11−1	1.15−5	1.00−5	14

*See footnotes for Table III.
[a]Read as -1.59×10^{-1}.

TABLE VI

GPT and Exact $\delta R^{(i)}$ Results for Case 4*

Derivative Order, i	GPT Results for $\delta R^{(i)}/R^{(i)}$			$\delta R_p^{(i)}$ (GPT)	$\Delta R_e^{(i)}$ (Exact)	$\frac{\text{GPT} - \text{Exact}}{\text{Exact}}$ (%)
	Direct	Indirect	Total			
0	−4.54−2[a]	1.14−2	−3.39−2	−1.06−3	−1.05−3	0.75
1	−4.54−2	−1.58+1	−1.58+1	−8.19−5	−7.64−5	7.2
2	−4.54−2	−1.31−1	−1.76−1	3.32−6	3.22−6	3.1

*See footnotes for Table III.
[a]Read as -4.54×10^{-2}.

VI. This comparison shows that $\delta R_k^{(2)}/R_k^{(2)}$ is smallest for case 2, being about an order of magnitude smaller than for case 1 and about two orders of magnitude smaller than for cases 3 and 4. Note now that the effects of the nonlinear terms disregarded by first-order GPT are measured by $\epsilon(x)$ defined as

$$\epsilon(x) = \delta R_p(x) - \Delta R_e(x) \ , \qquad (89)$$

where ΔR_e and δR_p are given by Eqs. (67) and (68), respectively. Recalling that $\delta R_k^{(2)}$ for case 2 is a very small quantity that is calculated by using Eq. (16), it is expected that even a weak dependence of $\epsilon(x)$ on x would cause appreciable differences between exact and GPT results. Calculations of $\epsilon(x)$ have indicated that this is indeed true for case 2. Note, though, that if $\delta R_k^{(2)}$ is small compared to δR_k and/or $\delta R_k^{(1)}$, then inaccuracies in $\delta R_k^{(2)}$ will influence results for $\delta R(x)$ appreciably only if $(x - x_k)$ is large. This follows from the use of Eq. (14).

VII.C. Comparison of Taylor-GPT, GPT, and Exact Results for $\delta R(x)$

The use of the Taylor-GPT method raises questions concerning the accuracy of both the GPT and Taylor series features. Tc investigate these questions, two series of comparisons were performed:

1. First, results obtained for $\delta R_{tp}(x)$ were compared to exact values $\Delta R_e(x)$ [see Eqs. (69) and (67), respectively]. As discussed in Sec. V.A, this comparison assesses the composite accuracy of both features (i.e., second-order Taylor expansion around x_k and use of first-order GPT) of the Taylor-GPT method.
2. Second, results for $\delta R_{tp}(x)$ were compared to results for $\delta R_p(x)$ [see Eqs. (69) and (68), respectively]. As discussed in Sec. V.A, this comparison assesses the accuracy of solely the Taylor series expansion feature of the Taylor-GPT method. (The inaccuracies due to the use of GPT are eliminated in this comparison.)

Tables VII, VIII, and IX present the comparisons mentioned in item 1 above. These comparisons show that for values of $(x - x_k)$ varying from −10 to 20 cm, $\delta R_{tp}(x)$ and $\Delta R_e(x)$ agree within ~5%. This generally good agreement worsens only when $(x - x_k)$ becomes large (in absolute value), or when $\delta R(x)$ is about to change sign while going smoothly through a zero (e.g., case 4, $x = 10.5$ cm, in Table IX).

Although case 1 does not generally satisfy condition 1 of Sec. VI.B, the values of $\delta R_{tp}(x)$ obtained by using all three terms in Eq. (69) agree well, within

TABLE VII

Taylor-GPT and Exact $\delta R(x)$ Results* for Case 1;† $x_k = 22.5$ cm

x (cm)	$x - x_k$ (cm)	Exact[a] ΔR_e	Taylor-GPT[b] δR_{tp}	$\frac{\delta R_{tp} - \Delta R_e}{\Delta R_e}$ (%)[b]	
				Three Term[c]	Two Term[d]
13.5	-9	-3.84-4[e]	-3.69-4	-4.0	-1.0
16.5	-6	-3.82-4	-3.67-4	-3.9	-2.5
25.5	+3	-3.60-4	-3.46-4	-3.7	-3.3
28.5	+6	-3.47-4	-3.34-4	-3.6	-2.1
34.5	+12	-3.13-4	-3.02-4	-3.3	+3.2
40.5	+18	-2.68-4	-2.61-4	-2.9	+14
52.5	+30	-1.53-4	-1.46-4	-4.9	+79

*Read $(\pm x - y)$ as $\pm x \cdot 10^{-y}$.
†See Table II for description of test cases.
[a]The exact value was determined from two direct calculations [see Eq. (67)].
[b]The values presented in the last three columns are calculated with more significant figures than shown.
[c]The values for δR_{tp} were obtained by using all three terms in Eq. (69).
[d]The values for δR_{tp} were obtained by using only the first two terms in Eq. (69).
[e]Read as -3.84×10^{-4}.

5%, with the exact values $\Delta R_e(x)$. Notably, this good agreement persists even at distances $(x - x_k)$ as large as 30 cm. As will be discussed in Sec. VII.D, the perturbation considered in case 1 causes only a small spatial shift in the location of the maximum power density. Thus, the good overall agreement between $\delta R_{tp}(x)$ and $\Delta R_e(x)$ obtained in this case represents an additional positive verification of the adequacy of the numerical methods used in this work.

The results presented in the last two columns of Tables VII, VIII, and IX also indicate that the use of only the first two terms in the Taylor expansion given by Eq. (69) is adequate when x is not very far from x_k. The generally good agreement between $\Delta R_e(x)$ and the values of $\delta R_{tp}(x)$ obtained by using this two-term expansion indicates that, in certain cases, the number of adjoint calculations may be reduced; for example, calculation of $\Gamma_k^{*(2)}$ may not be necessary if only small to moderately

TABLE VIII

Taylor-GPT and Exact Results* for Case 2; $x_k = 22.5$ cm

x (cm)	$x - x_k$ (cm)	Exact ΔR_e	Taylor-GPT δR_{tp}	$\frac{\delta R_{tp} - \Delta R_e}{\Delta R_e}$ (%)	
				Three Term	Two Term
10.5	-12	+1.93-4[a]	+2.05-4	+6.0	+8
13.5	-9	+1.69-4	+1.79-4	+5.4	+7
16.5	-6	+1.44-4	+1.52-4	+5.5	+6
19.5	-3	---	+1.25-4	---	---
25.5	+3	---	+6.98-5	---	---
28.5	+6	+3.64-5	+4.16-5	+14	+17
34.5	+12	-1.71-5	-1.63-5	-4.9	-25
40.5	+18	-6.79-5	-7.59-5	+12	+0.3
52.5	+30	-1.57-4	-2.00-4	+27	+13

*See footnotes for Table VII.
[a]Read as 1.93×10^{-4}.

TABLE IX

Taylor-GPT and Exact Results* for Case 4, $x_k = 22.5$ cm

x (cm)	$x - x_k$ (cm)	Exact ΔR_e	Taylor-GPT δR_{tp}	$\frac{\delta R_{tp} - \Delta R_e}{\Delta R_e}$ (%)	
				Three Term	Two Term
10.5	−12	+8.32-5[a]	+1.63-4	+96	+190
13.5	−9	−2.38-4	−1.87-4	−21	+35
16.5	−6	−5.36-4	−5.07-4	−5	+6
19.5	−3	---	−7.98-4	---	---
25.5	+3	---	−1.29-3	---	---
28.5	+6	−1.45-3	−1.49-3	+3	+7
34.5	+12	−1.73-3	−1.80-3	+4	+18
40.5	+18	−1.88-3	−2.00-3	+6	+34
52.5	+30	−1.81-3	−2.02-3	+12	+94

*See footnotes for Table VII.
[a]Read as 8.32×10^{-5}.

large distances $(x - x_k)$ are of interest. Of course, the adequacy of using a two-term expansion for calculating $\delta R_{tp}(x)$ also depends on the size of the perturbation. Cases 1 and 2 involve small perturbations, but cases 3 and 4 involve larger ones. For the latter cases, the importance of the term containing $\delta R_k^{(2)}$ in Eq. (69) is illustrated in Fig. 6.

Results for the second set of comparisons, i.e., those mentioned in item 2 at the beginning of this section, are presented in Table X. For completeness, this table presents not only comparisons of $\delta R_{tp}(x)$ versus $\delta R_p(x)$, but also includes comparisons with the exact values $\Delta R_e(x)$. Note the selection of particular combinations of perturbation cases (i.e., cases 3 and 4 of Table II) and values of x: Each combination simutaneously involves a large perturbation and a large absolute value of $(x - x_k)$. The reason for selecting such combinations is to deliberately accentuate the space-dependent inaccuracies, expressed by $\epsilon(x)$ defined by Eq. (89), of using first-order GPT.

The outcome of comparing $\delta R_{tp}(x)$, $\delta R_p(x)$, and $\Delta R_e(x)$ is concisely expressed in Table X by presenting the values for *TAP* and *TAE* obtained from Eqs. (70) and (71), respectively. As expected, the nonlinear effects ignored by the Taylor-GPT method are important in these cases; this importance is clearly indicated by the large values obtained for the quantity *TAE*. The main contribution to these nonlinear effects, though, arises from the GPT component of the Taylor-GPT method. This fact is indicated by the small values obtained for the quantity *TAP*, which show that the Taylor-GPT results agree closely with the GPT results. These characteristics are further highlighted in Fig. 6, which shows that, even though the GPT results differ from the exact ones by as much as 50%, the Taylor-GPT and GPT results agree within 4% for a large range of distances x. This indicates that whenever the GPT method is sufficiently accurate, the use of the Taylor-GPT method could substantially reduce the number of calculations for investigations of space-dependent response variations.

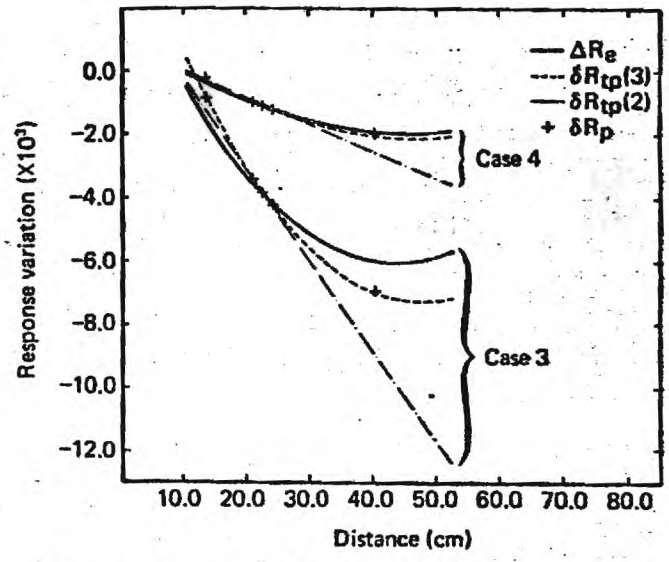

Fig. 6. Comparisons of exact, GPT, two-term Taylor-GPT [$\delta R_{tp}(2)$], and three-term Taylor-GPT [$\delta R_{tp}(3)$] results for cases 3 and 4.

TABLE X

Comparisons of $\Delta R_e(x)$, $\delta R_p(x)$, and $\delta R_{tp}(x)$ for Large Perturbations and Large $|x - x_k|$

Perturbation Case	x (cm)	TAP[a] (%)	TAE[b] (%)
4	13.5	−3.7	−22
4	40.5	+1.9	+6.3
3	13.5	−3.3	−47
3	40.5	+2.0	+17

[a]See Eq. (70).
[b]See Eq. (71).

VII.D. Spatial Shifts and Their Influence on Peak-Power Density Sensitivities

Perturbations in nuclear data alter not only the maximum value taken on by the power density, but also cause spatial shifts in the location of this maximum. To calculate these shifts by using the Taylor-GPT method, it is convenient to rewrite Eq. (75) as

$$x_{m1} - x_{m0} = -\frac{R_0^{(1)}}{R_0^{(2)}} \cdot \frac{\delta R^{(1)}/R^{(1)} - \delta R^{(2)}/R^{(2)}}{1 + \delta R^{(2)}/R^{(2)}} . \quad (90)$$

Table XI presents numerical values for the spatial shifts (i.e., $x_{m1} - x_{m0}$) caused by the perturbations described in cases 1 through 4. Direct, indirect, and total contributions were calculated by using the Taylor-GPT method. The respective contributions are denoted in Table XI by $S_{tp,D}$, $S_{tp,I}$, and $S_{tp,T}$, and were obtained by replacing the quantity $\delta R^{(i)}$ in Eq. (90) with $\delta R_D^{(i)}$, $\delta R_I^{(i)}$, and $[\delta R_D^{(i)} + \delta R_I^{(i)}]$, respectively.

TABLE XI

Spatial Shifts in Location of Peak Power

Shifts[a]	Case 1 (cm)	Case 2 (cm)	Case 3 (cm)	Case 4 (cm)
$S_{e,T}$	+0.160	−0.482	−22.8	−4.85
$S_{tp,T}$[b]	+0.151	−0.490	−38.2	−5.23
$S_{tp,I}$	+0.086	−0.601	−27.1	−4.96
$S_{tp,D}$	+0.064	+0.105	0.0	0.0
$S_{tp,I} + S_{tp,D}$	+0.150	−0.496	−27.1	−4.96
$\frac{S_{tp,T} - S_{e,T}}{S_{e,T}}$	−5.6%	+1.7%	+67.8%	+8.0%

[a]Shifts are defined in Sec. VII.D.
[b]The quantity $S_{tp,T}$ differs slightly from $(S_{tp,I} + S_{tp,D})$ because the sum neglects the second-order terms mentioned immediately after Eq. (80).

Recall that Eq. (90) has inaccuracies stemming from the use of both first-order GPT and second-order Taylor expansion in x. Inaccuracies due to the use of first-order GPT in Eq. (90) can be assessed by using perturbed data to recalculate the response $R_1(x)$. The numerical values of $R_1(x)$ thus obtained have been examined to determine the grid location x_{k1} at which the largest discrete value of $R_1(x)$ occurred. Except for very small shifts, x_{k1} is not generally expected to coincide with x_k. (Recall that x_k denotes the location where the largest discrete value of the unperturbed response occurred.)

Using now the same procedure as that leading to Eq. (74) but with x_{k1} replacing x_k gives

$$x_{m1} - x_{k1} = -\frac{R_1^{(1)}(x_{k1})}{R_1^{(2)}(x_{k1})} . \quad (91)$$

Equation (91), rather than Eq. (74), is now used to determine x_{m1}; this is because, although both equations stem from Taylor series truncated at the third-order terms, the truncation errors in Eq. (91) are smaller than those in Eq. (74) since, in general, $|x_{m1} - x_{k1}| < |x_{m1} - x_k|$. Furthermore, it is expected that this procedure will, in general, allow determination of x_{m1} within an accuracy comparable to that of determining x_{m0} from Eq. (73).

The results shown in Table XI in the row labeled $S_{e,T}$ are the numerical values of $(x_{m1} - x_{m0})$, where x_{m1} and x_{m0} are obtained from Eqs. (91) and (73), respectively. A comparison between these results and the corresponding results shown in the row labeled $S_{tp,T}$ indicates the magnitude of effects arising from the use of first-order GPT in Eq. (90).

The indirect contributions (i.e., $S_{tp,I}$) are generally preponderant; the direct contributions $S_{tp,D}$ are zero for cases 3 and 4, and are still much smaller than $S_{tp,I}$ for case 2. Only for case 1, which involves a very small shift, are the values of $S_{tp,I}$ and $S_{tp,D}$ comparable.

The results presented in the last row of Table XI show that shifts predicted by the Taylor-GPT method agree well with the exact ones for distances between ~0.15 and 5 cm. For case 3, which represents a perturbation so large that it effectively transforms the heterogeneous core into a homogeneous one, the shift predicted by the Taylor-GPT method substantially overestimates the actual shift. This highlights the importance of the nonlinear terms that are neglected by first-order GPT.

The influence of spatial shifts on the sensitivity of peak-power density has been discussed in Sec. V.C. This influence is characterized by the quantity SE defined by Eq. (86). Note that the results for SE are subject to inaccuracies associated with Eqs. (73) and (91), which are used to determine the locations

x_{m0} and x_{m1}, respectively. Table XII shows that the error caused by the shift in the location of the maximum power is small for cases 1 and 2. For larger perturbations, e.g., cases 3 and 4, the effect of the spatial shift on the sensitivity is appreciable and cannot be neglected.

VIII. SUMMARY AND CONCLUSIONS

This paper has presented an efficient method to investigate one-dimensional, space-dependent variations $\delta R(x)$ in the power density $R(x)$. This method has been called the Taylor-GPT method in order to highlight its two main characteristics:

1. use of a Taylor series expansion of $\delta R(x)$ in the spatial variable x
2. use of first-order GPT (Refs. 1 through 4) to efficiently evaluate the derivative operators that appear as coefficients in this Taylor series.

Equations satisfied by the importance (i.e., adjoint) functions for the i'th spatial derivative of $\delta R(x)$ have been derived within the framework of GPT. Using finite differences, it has been shown that these equations can be solved in a straightforward manner with existing GPT codes to obtain the importance functions. The main characteristics of these importance functions have been highlighted analytically by deriving certain relationships that they satisfy. A deeper understanding of these characteristics has been facilitated by deriving the complete analytical expressions of the importance functions for an illustrative (one-region, one-group) reactor model.

It has been shown that the Taylor-GPT method is efficient not only for estimating space-dependent variations in the power density, but also for estimating spatial shifts that parameter perturbations induce in the peak power density. To illustrate its usefulness, this method has been applied to four test cases involving a simplified three-region, one-dimensional model of a heterogeneous LMFBR. The results given by the Taylor-GPT method have been compared to those produced by the standard GPT method, and both have been verified by comparisons to exact results (obtained by actual recalculations with altered parameter values).

These comparisons indicate that the results given by the Taylor-GPT method are practically as accurate as those given by the standard GPT method. The Taylor-GPT method includes all the advantages offered by adjoint methods, e.g., the same importance functions are used to assess the effects on the response of many parameter perturbations. In addition, the Taylor-GPT method could substantially reduce (even by comparison to standard GPT) the number of calculations for investigations of space-dependent variations in the power density. Note, though, that the Taylor-GPT method does not account for second- and higher order effects of parameter variations. Nevertheless, the Taylor-GPT method provides detailed information regarding specific contributions (e.g., due to leakage, absorption) to the overall variation in the response. The availability of such detailed information is valuable for systematic and efficient reactor design studies.

TABLE XII

Influence of the Spatial Shift on the Peak-Power Density

Case	SE[a] (%)
1	0.009
2	−0.029
3	−63.5
4	−17.0

[a]See Eq. (86).

APPENDIX A

APPLICATION OF THE ITALIAN GPT CODE PACKAGE TO CALCULATE SPATIAL DERIVATIVES OF $\delta R(x)$

A.I. Calculation of $\Gamma^{*(i)}$

In general, the solution to the adjoint problem is computed by CIAP (Ref. 17) for ratios of the form

$$R_0 = \frac{\int_{V_1} \sum_j \Sigma_{1,j}(x)\phi_j(x)\,dx}{\int_{V_2} \sum_j \Sigma_{2,j}(x)\phi_j(x)\,dx} \qquad \text{(A.1)}$$

Equation (A.1) can be cast in a form amenable to calculate $\delta R^{(i)}/R^{(i)}$ by simply preparing, as indicated below, the input data for the adjoint source.

The energy production cross sections in the numerator and denominator of Eq. (A.1) are written as

$$\Sigma_{1,j}(x) = \sum_k p^k N_1^k(x)\sigma_{f,j}^k \qquad \text{(A.2)}$$

and

$$\Sigma_{2,j}(x) = \sum_k p^k N_2^k(x)\sigma_{f,j}^k\,, \qquad \text{(A.3)}$$

respectively, where N_i^k denotes densities for nuclide k. Subscripts 1 and 2 in N_1^k and N_2^k, respectively, allow for potentially distinct spatial behavior of the energy production cross sections. With these

specifications, CIAP computes the desired $\Gamma^{*(i)}$ if the densities are chosen in the following manner:

1. $N_2^k(x) = N_m^k$ for all x in region m, $m = 1$ through M

2. for $\Gamma^{*(1)}$ calculations,

$$N_1(x) = \begin{cases} +N_{m0}\ , & \text{for } x = x_{k+1} \text{ and } x \in m0 \\ -N_{m0}\ , & \text{for } x = x_{k-1} \text{ and } x \in m0 \\ 0.0\ , & \text{elsewhere} \end{cases}$$

3. for $\Gamma^{*(2)}$ calculations,

$$N_1(x) = \begin{cases} +N_{m0}\ , & \text{for } x = x_{k+1}, x_{k-1}, \text{ and } x \in m0 \\ -2N_{m0}\ , & \text{for } x = x_k \text{ and } x \in m0 \\ 0.0\ , & \text{elsewhere}\ . \end{cases}$$

Here, m and M refer, respectively, to the region number and the number of regions; $m0$ denotes the number of the region where the peak power occurs; and N_m^k and N_{m0}^k are the densities of nuclide k in regions m and $m0$, respectively.

Note that CIAP includes the volumes associated with the mesh points in the integrations over space. But, as long as the mesh spacing is uniform in the vicinity of x_k, this does not affect the values of the fractional variation of the derivatives. Note also that CIAP attaches a factor of 0.5 to the contribution of a point to the integral value if the contribution of the point preceding it or the point following it is zero. To guard against this, one must use a very small value for the input density (of the order of 10^{-14}) at x_{k-2} and x_{k+2}.

A.II. Direct-Effect Calculations

The code GLOBPERT-1D (Ref. 18) can be used to calculate the direct-effect component of $\delta R^{(i)}/R^{(i)}$. For this purpose, the input data for the direct-effect calculations must be prepared as follows:

1. for $\delta R^{(1)}/R^{(1)}$ calculations,

$$\delta N = \begin{cases} +\delta N_i\ , & x = x_{k+1} \\ -\delta N_i\ , & x = x_{k-1} \\ 0.0\ , & \text{elsewhere} \end{cases}$$

2. for $\delta R^{(2)}/R^{(2)}$ calculations,

$$\delta N = \begin{cases} +\delta N_i\ , & x = x_{k+1} \text{ or } x = x_{k-1} \\ -2\delta N_i\ , & x = x_k \\ 0.0\ , & \text{elsewhere}\ . \end{cases}$$

Here, δN_i denotes the density change for nuclide i and effected in the quantity $Q_{1,k}$ [see Eq. (22)].

Also note that GLOBPERT-1D was modified to treat more accurately the interfaces between regions. In addition, an algorithm was implemented to calculate δD (i.e., the perturbation in the diffusion coefficient) exactly, rather than via a first-order expansion in $\delta\Sigma_{tr}$ as done in the original version of this code.

APPENDIX B

DETERMINATION OF $\Gamma_1^{*(2)}$

In view of Eqs. (45) and (51), the function $\Gamma_1^{*(2)}$ is the solution of

$$\left.\begin{aligned} \frac{d^2\Gamma_1^{*(2)}}{dx^2} + B^2\Gamma_1^{*(2)} &= \frac{1}{DQ_2} - \frac{1}{DQ_{1,2}}\delta''(x - x_k) \\ \Gamma_1^{*(2)} &= 0 \quad \text{at } x = L \\ \frac{d\Gamma_1^{*(2)}}{dx} &= 0 \quad \text{at } x = 0 \end{aligned}\right\}. \tag{B.1}$$

Applying a Laplace transform to Eq. (B.1), and defining

$$U(p) = \int_0^\infty \exp(-px)\Gamma_1^{*(2)}\,dx \tag{B.2}$$

gives

$$U(p) = K\frac{p}{p^2 + B^2} - \frac{1}{DQ_{1,2}}\frac{p^2\exp(-px_k)}{p^2 + B^2} + \frac{1}{DQ_2}\frac{1}{p(p^2 + B^2)}\ , \tag{B.3}$$

where K is, at this stage, an unknown constant to be determined.

Taking the inverse Laplace transform of Eq. (B.3) gives

$$\Gamma_1^{*(2)} = K\cos Bx + \frac{1}{B^2DQ_2}(1 - \cos Bx) - \frac{1}{DQ_{1,2}}[\delta(x - x_k) - BH(x - x_k)\sin B(x - x_k)]\ . \tag{B.4}$$

For a critical reactor, the boundary conditions given in Eq. (B.1) are automatically satisfied; thus, the constant K is determined by using the orthogonality condition given in Eq. (88). This leads to

$$K = \frac{1}{B^2DQ_2}\left(1 - \frac{2}{BL}\right) + \frac{B}{DQ_{1,2}} \times \left(\frac{\cos Bx_k}{BL} + \frac{L - x_k}{L}\sin Bx_k\right)\ . \tag{B.5}$$

Replacing Eq. (B.5) in Eq. (B.4) yields

$$\Gamma_1^{*(2)} = \frac{1}{B^2 DQ_2} + \left[\frac{\cos Bx_k + B(L - x_k) \sin Bx_k}{LDQ_{1,2}} - \frac{2}{DB^3 LQ_2} \right] \cos Bx + \frac{B}{DQ_{1,2}} H(x - x_k) \sin B(x - x_k) - \frac{\delta(x - x_k)}{DQ_{1,2}} . \quad \text{(B.6)}$$

ACKNOWLEDGMENTS

Stimulating discussions with A. Gandini and V. Perone are gratefully acknowledged. We thank Jim Marable for his critical review of the manuscript, which led to some modifications in the presentation. Special thanks are due to Lynne Messenger and Sharon Reeves for their expert typing of this manuscript.

This research was sponsored by the U.S. Department of Energy with the Georgia Institute of Technology and with the Union Carbide Corporation.

REFERENCES

[1]A. GANDINI, *J. Nucl. Energy*, **21**, 755 (1967).

[2]G. P. CECCHINI and M. SALVATORES, *Nucl. Sci. Eng.*, **46**, 304 (1971).

[3]J. H. MARABLE, C. R. WEISBIN, and G. de SAUSSURE, *Nucl. Sci. Eng.*, **75**, 30 (1980).

[4]C. R. WEISBIN et al., *Sensitivity and Uncertainty Analysis of Reactor Performance Parameters, Advances in Nuclear Science and Technology*, Vol. 14, J. LEWINS and M. BECKER, Eds., Plenum Press, New York (1982); see, in particular, Chap. 5 by E. GREENSPAN.

[5]J. M. KALLFELZ, D. BISWAS, C. L. COWAN, J. H. MARABLE, M. L. WILLIAMS, C. R. WEISBIN, J. D. DRISCHLER, T. B. FOWLER, and J. R. WHITE, "Design and Sensitivity Analysis of a CDS-Type LMFBR Heterogeneous Core," *1980 Advances in Reactor Physics and Shielding*, p. 467, American Nuclear Society, La Grange Park, Illinois (1980).

[6]J. H. MARABLE, D. G. CACUCI, C. R. WEISBIN, J. R. WHITE, D. BISWAS, J. M. KALLFELZ, C. L. COWAN, and R. PROTSIK, "Sensitivities and Uncertainties of a Large LMFBR Using Adjusted Cross Section Library ORACLE-1," *Proc. Topl. Mtg. Advances in Reactor Physics and Core Thermal Hydraulics*, Kiamesha Lake, New York, September 22-24, 1982, NUREG/CP-0034, Vol. 2, p. 1120, U.S. Nuclear Regulatory Commission (1982).

[7]D. G. CACUCI, *J. Math. Phys.*, **22**, 2794 (1981).

[8]D. G. CACUCI, *J. Math. Phys.*, **22**, 2803 (1981).

[9]V. A. PERONE, J. M. KALLFELZ, and L. A. BELBLIDIA, *Nucl. Sci. Eng.*, **79**, 326 (1981).

[10]L. A. BELBLIDIA, A. GANDINI, J. M. KALLFELZ, and V. A. PERONE, *Trans. Am. Nucl. Soc.*, **39**, 957 (1981).

[11]A. F. HENRY, *Nuclear-Reactor Analysis*, MIT Press, Cambridge, Massachusetts, (1975).

[12]D. G. CACUCI, P. J. MAUDLIN, and C. V. PARKS, *Nucl. Sci. Eng.*, **83**, 112 (1983).

[13]A. GANDINI, *Nucl. Sci. Eng.*, **77**, 316 (1981).

[14]In Ref. 15, Cacuci et al. considered the heat conduction equation and gave examples of the importance function for the first derivative of the temperature.

[15]D. G. CACUCI, C. F. WEBER, E. M. OBLOW, and J. H. MARABLE, *Nucl. Sci. Eng.*, **75**, 88 (1980).

[16]I. DAL BONO, "TAIM-Multigroup Diffusion Code," CEC(66)12, Comitato Nazionale per l'Energia Nucleare (1966).

[17]I. DAL BONO, V. LEPRONI, and M. SALVATORES, "The CIAP-1D Code," RT/FI(68)9, Comitato Nazionale per l'Energia Nucleare (1968).

[18]I. DAL BONO, V. LEPRONI, and M. SALVATORES, "The GLOBPERT-1D Code," RT/FI(68)10, Comitato Nazionale per l'Energia Nucleare (1968).

[19]A. H. ZEMANIAN, *Distribution Theory and Transform Analysis*, McGraw-Hill Book Company, Inc., New York (1965).

[20]Such a model has also been used by Pomraning (Ref. 21) to analyze, via a variational approach, the behavior of the peak-to-average power density. Note, though, that this quantity is not the same as our R_k.

[21]G. C. POMRANING, *J. Nucl. Energy*, **21**, 285 (1967).

[22]J. M. KALLFELZ, G. B. BRUNA, G. PALMIOTTI, and M. SALVATORES, *Nucl. Sci. Eng.*, **62**, 304 (1977).

[23]T. B. FOWLER and D. R. VONDY, "Nuclear Reactor Analysis Code: CITATION," ORNL-TM-2496, Rev. 2, Oak Ridge National Laboratory (1971).

[24]E. M. OBLOW, "Reactor Cross-Section Sensitivity Studies in Critical Reactors Using Transport Theory," ORNL-TM-4437, Oak Ridge National Laboratory (1974).

[25]W. G. DAVEY and A. L. HESS, "Additional Fast Reactor Benchmarks for Phase II Data Testing of ENDF/B," *CSEWG Newsletter 18*, Cross Section Evaluation Working Group (Mar. 1969).